Biscayne Bay Turbidity Study

Prepared for the U.S. Army Corps of Engineers

Atlantic Oceanographic and Meteorological Laboratory
Miami, Florida

February 2013

Biscayne Bay Turbidity Study

S. Jack Stamates[1]
Patricia L. Blackwelder[2]
Cheryl J. Brown[1,3]
Thomas P. Carsey[1]
Charles M. Featherstone[1]
Maribeth L. Gidley[1,3]
Christopher R. Kelble[1]
Rachel M. Kotkowski[1]
Robert J. Roddy[1,3]

[1]Atlantic Oceanographic and Meteorological Laboratory
Miami, Florida

[2]University of Miami/Rosenstiel School of Marine and Atmospheric Science
Miami, Florida

[3]University of Miami/Cooperative Institute of Marine and Atmospheric Studies
Miami, Florida

February 2013
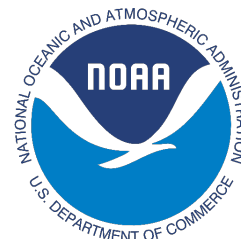
This page intentionally left blank.

Table of Contents

Table of Contents (continued)

List of Tables

This page intentionally left blank.

List of Figures

List of Figures (continued)

List of Figures (continued)

List of Figures (continued)

Acronyms

ADCP	Acoustic Doppler current profiler
CDOM	Colored dissolved organic matter
CFU	Colony-forming units
CT	Conductivity and temperature
DRER	Department of Regulatory and Economic Resources
EDS	Energy dispersive spectroscopy
EDT	Eastern Daylight Time
EST	Eastern Standard Time
MPL	Millions of particles per liter
NTU	Nephelometric turbidity units
PAR	Photosynthetically-active radiation
QSU	Quinine sulfate units
SEM	Scanning electron microscopy
TSS	Total suspended solids
UT	Universal Time

This page intentionally left blank.

1. Introduction

Biscayne Bay is a large subtropical estuary that extends from Broward County in the north to Barnes Sound in the south. While average depths are shallow, the Bay also includes portions of the Intracoastal Waterway, the Port of Miami, and numerous dredged channels to support commercial and recreational boating. The highly developed and economically vibrant urban areas of Miami and Miami Beach reach to the shoreline in many parts of the Bay, especially in the north. To the south, undeveloped coastline can be found on both the east and west sides of the Bay. Overall, Biscayne Bay is widely regarded as a highly valued marine ecosystem with considerable natural value. All areas of the Bay have some level of protected status at either the national or state level (e.g., http://www.dep.state.fl.us/coastal/sites/biscayne/info.htm; http://www.nps.gov/bisc/index.htm; and http://floridakeys.noaa.gov/).

In an area where the services provided by a natural marine ecosystem are so diverse, it is inevitable that projects are required for economic development, ecosystem restoration, and the maintenance of navigable waterways. When dredging is required, at least a temporary increase in the suspended sediment load is expected, thus projecting an increase in turbidity. Protocols for monitoring turbidity levels during construction operations sometimes reference background turbidity levels which are not expected to be influenced by the operations. It has been observed that these background turbidity levels naturally fluctuate due to winds, the presence of marine plankton, high concentrations of particles from land-based sources, and other environmental factors. While other investigators have studied turbidity in Biscayne Bay, there is scant information that is highly resolved in time. In this study, moored underwater instruments were used to monitor turbidity and related parameters continuously at three selected sites in Biscayne Bay for more than a year.

1.1 Objectives

The principal goal of this study was to estimate the expected value of turbidity at selected study sites in Biscayne Bay during times when no major construction or dredging activities were taking place, using methods that allowed for observations at high temporal resolution, and to examine how these turbidity levels were perturbed and modulated by environmental factors. A second goal was to examine the natural variability in factors influencing the overall clarity of the water, notably the concentration of colored dissolved organic matter (CDOM), which attenuates solar radiation used for photosynthesis by seagrasses. The final goal was to collect data on the sources and nature of naturally-occurring suspended material in the Bay using scanning electron microscopy (SEM).

2. Study Design and Methods

2.1 Overview

The geographic focus of this study was the northern region of Biscayne Bay where anthropogenic influences are the greatest. Data on turbidity, chlorophyll fluorescence, current speed and direction, temperature, and fluorescence from CDOM were collected continuously using sensors mounted on platforms affixed to the Bay bottom at three sites (Figures 1 and 2, Table 1). Additional data requiring discrete water samples were collected at 14-21 day intervals when the bottom-mounted instruments were serviced. The data from these discrete samples were used to estimate chlorophyll concentration, the concentration of total suspended sediments (TSS), and characterization of particulate material in the water via SEM. Furthermore, attenuation of photosynthetically-active radiation (PAR) was measured via two 4pi spherical quantum sensors at almost every site visit. A time-lapse camera system was mounted atop the Four Seasons Hotel in downtown Miami to collect photographic images of the study area between the Rickenbacker Causeway and Port of Miami. A small boat equipped with down-looking Doppler sonar and a flow-through water sampling system was used to examine the spatial variability of turbidity in the selected areas. Data were gathered from weather stations at Virginia Key (VAKF1) and Miami International Airport so that other measurements could be placed in the context of prevailing meteorological conditions.

Table 1. Locations and water depths of study sites.

Site	Latitude	Longitude	Mean Water Depth (m)
1	25°49.126′N	80°09.722′W	2.16
2	25°45.831′N	80°09.729′W	2.35
3	25°44.949′N	80°10.823′W	3.31
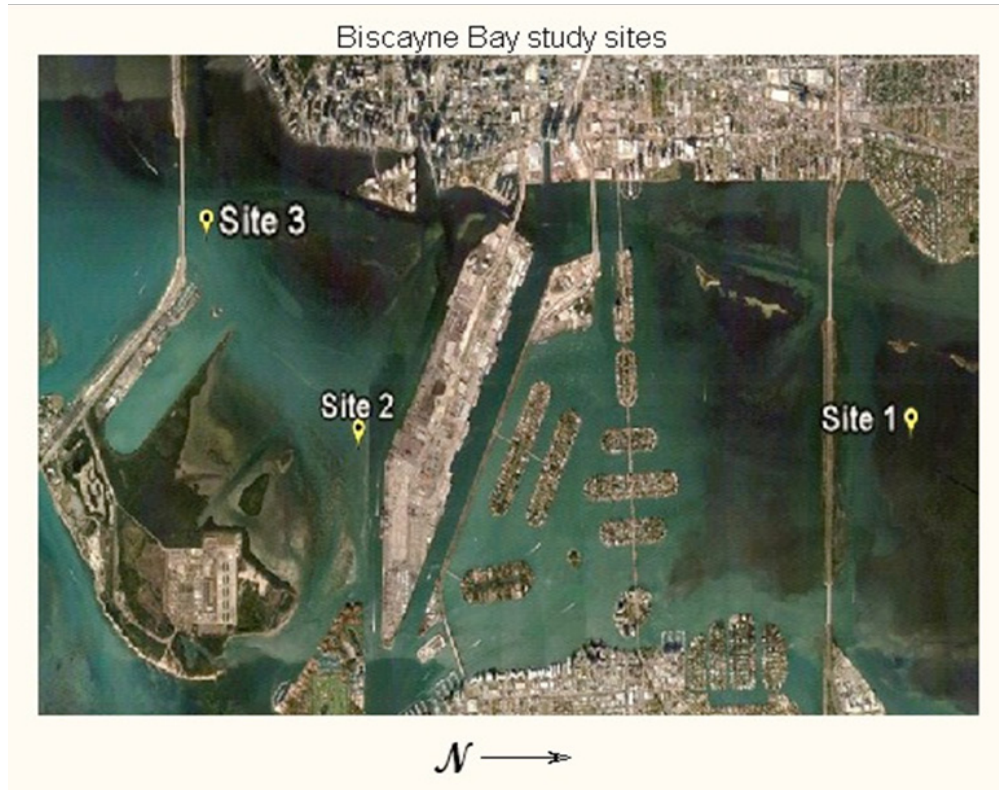
Figure 1. Location of the three Biscayne Bay study sites.
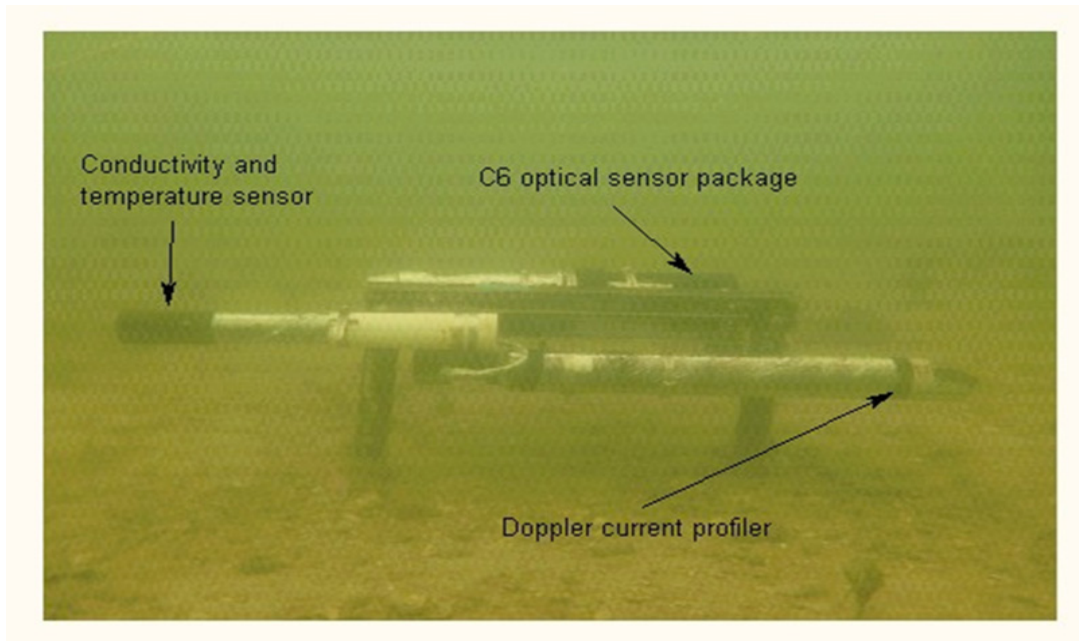
Figure 2. Instrument platform mounted on the Biscayne Bay bottom with the C6 multi-sensor platform, Aquadopp current profiler, and Valeport conductivity and temperature sensor attached.

2.1.1 Site 1

The Biscayne Bay site 1 study area is bounded by mainland Miami on the west, the 79th Street Causeway on the north, Miami Beach on the east, and the Julia Tuttle Causeway on the south (Figure 3). This basin is considered to be a part of the North Bay. The average water depth is 1.1 m (Van de Kreeke and Wang, 1984). There is no direct linkage between the basin that includes site 1 and the ocean, but the mouth of Little River, located at the northwest corner of this basin, can be a source of freshwater runoff. The basin where site 1 is located is sometimes referred to in literature as Unit 3 (Van de Kreeke and Wang, 1984). The instrument site is located 850 m north of the Julia Tuttle Causeway inside a large seagrass meadow. Manatee grass (*Syringodium filiforme*) is the dominant species at this site (Figure 4).

2.1.2 Sites 2 and 3

Sites 2 and 3 are located in a basin bounded by Dodge Island (the Port of Miami) on the north, mainland Miami to the west, the Rickenbacker Causeway to the south, and Virginia Key and Fisher Island to the east. The basin where sites 2 and 3 is located is sometimes referred to as Unit 7 (Van de Kreeke and Wang, 1984). This basin is a transitional region between the North Bay (north of the Port of Miami) and the Central Bay (south of the Rickenbacker Causeway). Linkages to the Atlantic Ocean are via Government Cut and Norris Cut. The mouth of the Miami River is located in the northwest corner of this basin and is a major source of fresh water into the basin. This basin exchanges water with Bay waters to the south via the Rickenbacker Causeway Bridge and the small channel at the westernmost end of the causeway. This basin exchanges water with Bay waters to the north via the Intracoastal Waterway located at the west end of the Port of Miami. The water depth in this basin averages 1.7 m (Van de Kreeke and Wang, 1984).

Site 2 is located between Fisherman's Channel and the Bill Sadowski Critical Wildlife Area (CWA) and is close to the marker that indicates the northwest boundary of the CWA (Figure 5). The site is approximately 135 m from the shipping channel and approximately 400 m from the port bulkhead. The bottom at site 2 is comprised of sand and shell. In the vicinity of the instrument are patches of turtle grass (*Thalassia testudinum*) mixed with manatee grass (*S. filiforme*) and patches of calcareous algae, principally *Udotea flabellum* and *Halimeda* sp. (Figure 6).

Figure 3. Location of the site 1 study.

Figure 4. Bottom-mounted instrument package deployed at site 1. Site 1 is located inside a dense meadow of manatee grass (*Syringodium filiforme*).

Figure 5. Location of the site 2 study.
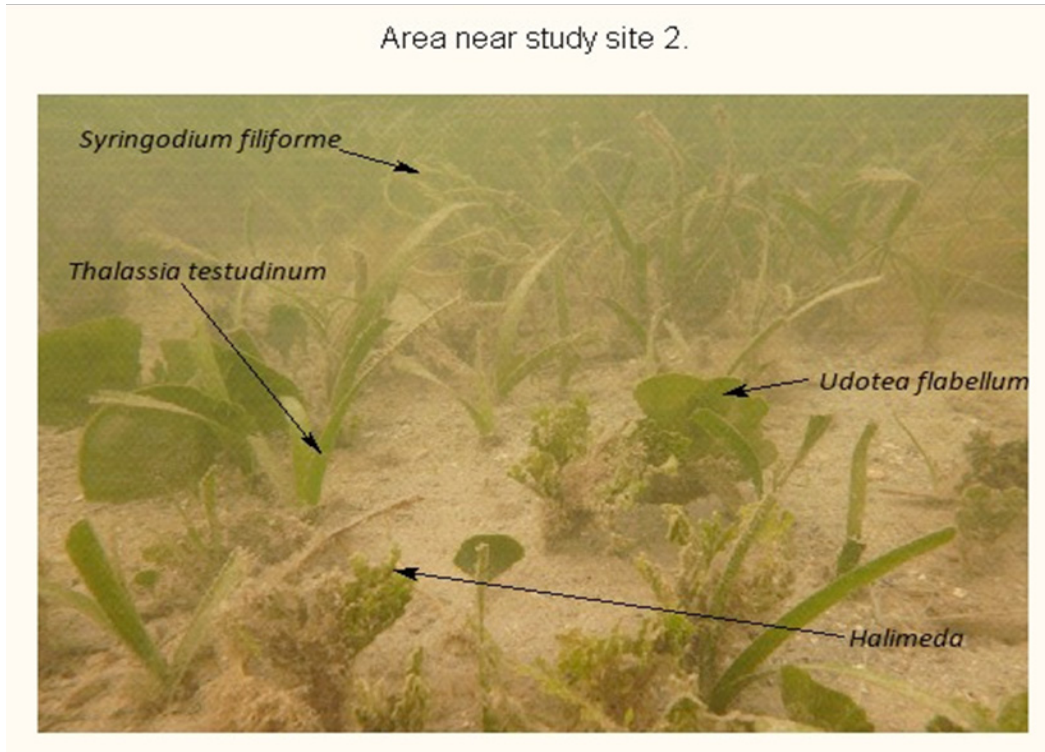
Figure 6. Area near study site 2 with flora typically observed in this area. *Thalassia testudinum*, *Syringodium filiforme*, *Udotea flabellum,* and *Halimeda* are shown with arrows.

Site 3 is the deepest of the sites with an average water depth of 3.3 m. This site is located 330 m north of the William Powell Bridge (Figure 7). The bottom is comprised of sand and shell, and the benthic species composition near site 3 is similar to that at site 2 but with sparser coverage (Figure 8).

2.2 Bottom Mountings

At the three measurement locations (Table 1), instrument mounting platforms were secured to the Bay bottom (Figure 2). These mountings were designed to securely and repeatably position the instruments at the same height relative to the Bay bottom. Table 2 lists the sensors that were attached to the bottom mounting. Table 3 gives the height above the bottom for each of the sensors that were attached to the bottom mountings.

2.3 Turner C6 and Associated Sensors

The Turner C6 multi-sensor platform (C6) provides a platform to which the Cyclops-7 series of optical sensors may be attached (Turner Designs, Sunnyvale, CA). The C6

provides power, data logging and command, and control of the attached sensors. The C6 also has a wiper mechanism that cleans the optical surfaces of the attached sensors before each measurement. In addition to the attached Cyclops-7 sensors, the C6 has integral temperature and pressure sensors. Data from these sensors are recorded with each measurement. For this project, the Cyclops-7 optical sensors attached to each of the C6 platforms were turbidity, chlorophyll, and CDOM.

2.3.1 Turbidity Sensor

The Turner Cyclops-7 turbidity sensor measures turbidity using an 850-nm light source and a detector that receives scattered light at a 90-degree angle relative to the direction of light transmission. This type of instrument is also referred to as a nephelometer (Davis-Colley and Smith, 2001). The turbidity sensor was calibrated using commercial standards to convert the measurements to Nephelometric Turbidity Units (NTU). The Turner turbidity sensor has a minimum detection limit of 0.05 NTU and a range of 03000 NTU. Performing turbidity measurements in this manner conforms to ISO 7027 standards.

Figure 7. Location of the site 3 study.
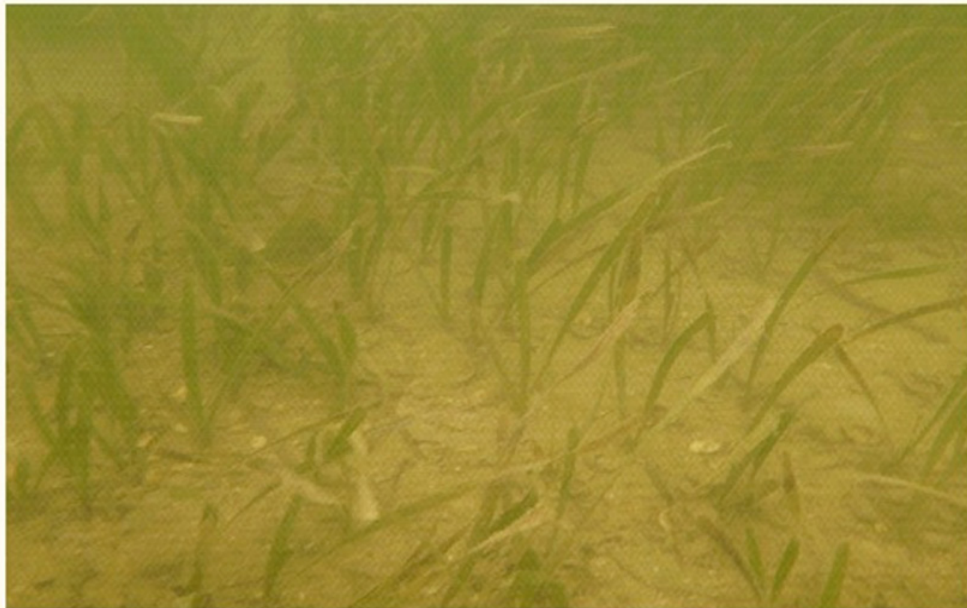
Figure 8. Site 3 bottom with flora typically observed in this area.

Table 2. Bottom-mounted instruments.

Instrument	Manufacturer	Measurements
C6 Multi-Sensor Platform	Turner Designs 845 W. Maude Avenue Sunnyvale, CA 94085	Turbidity, chlorophyll, CDOM, temperature, and pressure
Nortek 2 MHz Aquadopp Current Profiler	Nortek USA 27 Drydock Avenue Boston, MA 02210	Current velocity and direction, acoustic backscatter, temperature, and pressure
Valeport Model 620 CT	Valeport, Ltd. St. Peter's Quay Totnes TQ9 5EW Devon United Kingdom	Conductivity and temperature (data are digitized and logged on the Aquadopp current profiler)

2.3.1.1 Turbidity sensor calibration

The turbidity sensor (attached to the C6 platform) was calibrated by immersing it into commercial turbidity standard solutions (AMCO CLEAR, GFS Chemical, Powell, OH) or standards made from diluting the commercial turbidity standard solutions. Initially, standard solutions were prepared at concentrations of 0, 5, 10, 50, and 100 NTU. After determining that the values of turbidity observed in the field were almost always less than 20 NTU, it was decided to use concentrations of 0, 1, 5, 10, and 20 NTU to better match the range of expected measurements. While the sensor was immersed in each of the solutions, data from the turbidity sensor were logged onto the C6 for one minute at a sampling rate of one sample per second. After data were collected for all the standards, the data were retrieved from the C6, and the mean of the data collected

Table 3. Distance from bottom to sensor.

Instrument	Height Above Bottom (cm)
Turbidity	34
Chlorophyll	30
CDOM	30
C6 temperature and pressure	31
Aquadopp profiler pressure and temperature	23
CT conductivity and temperature	31

for each of the standards was calculated. A linear regression was calculated using these means and the stated value of the turbidity standards. The coefficient of determination (R^2) for the linear regression was calculated, and the calibration was considered acceptable if this value was greater than 0.99.

In a separate procedure, before any equation was applied to the raw data to calculate turbidity in NTU, the calibration equation was examined to determine if any of the data points used to generate the calibration equation deviated from the linear regression line significantly. In the very few cases where a data point was identified as suspect, that point was eliminated and the equation was recalculated using the remaining data. During the course of the project and at the completion of data collection, the slope and intercept from each of the instrument calibrations were examined and compared to one another to determine if any systematic changes were occurring in the instruments (evident by a systematic shift in the calibration equations). In one instance, such a shift was noted. It was further noted that the data values calculated from this calibration appeared offset from the deployments that occurred before and after this deployment. This was corrected by applying the post-deployment calibration equation rather than the standard use of applying the pre-deployment calibration equation. In all cases, upon recovery of a data set, the turbidity data were plotted and compared with the data from the deployments that preceded it to look for inconsistencies and signs of instrument fouling or malfunction.

2.3.2 Chlorophyll Sensor

The Turner Cyclops-7 chlorophyll-*a* sensor uses fluorescence to estimate *in vivo* chlorophyll concentrations. The excitation wavelength is 460 nm. The emission detector is sensitive to light with wavelengths between 620 and 715 nm. The sensor is specified to have a minimum detection limit of 0.03 µg/l of chlorophyll and a linearity of 0.99 R^2 throughout its range of 0500 µg/l. The C6 platform has the ability to compensate for the chlorophyll sensor's response to temperature using a factory set correction of 1.4% per °C. This feature was enabled for all chlorophyll data collection.

2.3.2.1 Chlorophyll sensor calibration

To calibrate the chlorophyll sensor, the raw (temperature compensated) fluorescence output value of the chlorophyll sensor was regressed against the chlorophyll concentration measured in the laboratory from water samples collected at the sensor location. These values were used to generate a calibration equation for the chlorophyll sensor (see section 2.6.1 for a description of the methods used to process the water samples).

2.3.3 CDOM Sensor

The Turner Cyclops-7 CDOM sensor uses an ultraviolet light-emitting diode with an excitation filter for maximum sample excitation. The emission filter is designed to detect the fluorescence of many different sources of CDOM, as naturally-occurring CDOM is variable. The CDOM sensor is specified and calibrated using quinine sulfate. It is specified to have a minimum detection limit of 0.2 parts per billion (ppb) of quinine sulfate and a linearity of 0.99 R^2 throughout its full range of 0-1000 ppb quinine sulfate.

2.3.3.1 CDOM sensor calibration

Quinine sulfate was used to calibrate the CDOM sensors. The following text is an excerpt from the Turner CDOM sensor manual (Turner Designs, 2012).

Quinine is a strongly fluorescent alkaloid that is extracted from the cinchona tree. Because it absorbs UV light and has a high quantum fluorescent yield, it has often been used as a standard in fluorometric analyses. Maximum fluorescence yield can be achieved if diluted in weak acids. It has an excitation wavelength of 350 nm and

emission wavelength of 450 nm, similar to many CDOM compounds. This is why it is primarily used as a proxy for CDOM when calibrating or determining fluorometer specifications.

The CDOM sensors were immersed into standard solutions prepared from quinine sulfate diluted with weak sulfuric acid (0.1 N) to represent concentrations of 0, 5, 10, 50, and 100 quinine sulfate units (QSU). To calibrate the CDOM sensors, the sensors (attached to the C6 platform) were immersed into each of the quinine sulfate standards. While the sensors were immersed, data from the CDOM sensor were logged onto the C6 platform for about one minute at a sampling rate of one sample per second. After data were collected for all the standards, the data were retrieved from the C6, and the mean value of the data collected for each of the standards was calculated. A linear regression equation was then calculated using these means and the stated values of the quinine sulfate standards. The coefficient of determination (R^2) from the linear regression was calculated and the calibration considered acceptable if this value was greater than 0.99.

In a separate procedure, before any equation was applied to the raw data to calculate CDOM in ppb, the calibration equation was examined to determine if any of the data points used to generate the calibration equation deviated from the linear regression line significantly. In the very few cases where a data point was identified as suspect, the point was eliminated, and the equation was recalculated using the remaining data. During the course of the project and at the completion of data collection, the slope and intercept of each of the CDOM sensor calibrations were examined and compared to one another to determine if any systematic changes were occurring in the instruments (evident by a shift in the calibration equations). On one occasion this was found to be the case, and the post-deployment calibration was used for that deployment to correct the discrepancy.

2.3.4 Turner C6 Temperature Sensor

The C6 platform is equipped with a temperature sensor. This sensor is integral to the C6 platform, and a measurement of temperature in degrees Celsius was logged along with the data from the attached sensors at each sampling interval. No attempts were made to calibrate this sensor.

2.3.5 Turner C6 Pressure Sensor

The C6 platform is equipped with a pressure sensor. A measurement of the C6 depth in meters was logged along with the data from the attached sensors at each sampling interval. Before each deployment, the pressure sensor was zeroed while the C6 unit was in the air.

2.4 Nortek 2 MHz Aquadopp Current Profiler

The Nortek 2 MHz Aquadopp current profiler (Nortek USA, Boston, MA) is a compact Doppler sonar capable of making measurements in shallow water. This device transmits acoustical energy at 2 MHz from three transducers equally spaced around the vertical axis of the instrument, and each transducer is angled 25° with respect to the vertical axis. The instrument was equipped with a flux gate compass and pitch and roll sensors to compensate for the orientation of the instrument in its mounting. After transmitting an acoustical "ping" from each of the transducers, acoustical energy is reflected (backscattered) from particles in the water. This backscattered energy is received and processed by the instrument. The radial Doppler velocity is extracted from the signal returned on each of the beams, and this information is used to calculate the three-dimensional velocity of the water flowing above the instrument.

It is important to note that there is an underlying assumption when using Doppler sonar systems that the particles causing the acoustic energy to be backscattered to the instrument are being advected by the water and, therefore, have the same velocity as the water. The relative intensity of the acoustical energy returned to each of the three transducers is recorded as a measure of acoustical backscatter strength. By partitioning the returned acoustical signal into "bins" or "cells," a profile of the water velocity and acoustic backscatter above the instrument is generated.

The instruments used in this study were programmed to make velocity and backscatter measurements in 15-cm cells with the first cell center located 20 cm above the transducers of the instrument. Table 4 gives the distance above the bottom and the depth relative to the mean water level for each of the cells for the three deployment sites. The

Table 4. Aquadopp current profiler measurement cell locations.

Cell Number	Site 1 Distance off Bottom	Site 1 Depth from Mean Water Level	Site 2 Distance off Bottom	Site 2 Depth from Mean Water Level	Site 3 Distance off Bottom	Site 3 Depth from Mean Water Level
1	0.41	1.75	0.41	1.935	0.415	2.895
2	0.56	1.6	0.56	1.785	0.565	2.745
3	0.71	1.45	0.71	1.635	0.715	2.595
4	0.86	1.3	0.86	1.485	0.865	2.445
5	1.01	1.15	1.01	1.335	1.015	2.295
6	1.16	1	1.16	1.185	1.165	2.145
7	1.31	0.85	1.31	1.035	1.315	1.995
8	1.46	0.7	1.46	0.885	1.465	1.845
9	1.61	0.55	1.61	0.735	1.615	1.695
10	1.76	0.4	1.76	0.585	1.765	1.545
11	1.91	0.25	1.91	0.435	1.915	1.395
12	2.06	0.1	2.06	0.285	2.065	1.245
13			2.21	0.135	2.215	1.095
14					2.365	0.945
15					2.515	0.795
16					2.665	0.645
17					2.815	0.495
18					2.965	0.345
19					3.115	0.195
20					3.265	0.045

instrument mountings and the Aquadopp configuration were designed so that the first measurement cell was located at the same height off the bottom as the optical turbidity sensor. This was done so that the data from the acoustical and turbidity sensors could be compared. Because water flow at the depth of the first cell was blocked by the C6 platform, this first cell was not used for estimating the water velocity.

In addition to acoustical sensors, the Aquadopp current profiler is equipped with temperature and pressure sensors. Data from these sensors were recorded with each acoustical profile. The instrument was configured to generate one measurement every 15 minutes; this measurement is an ensemble average of 250 acoustical "pings." The horizontal standard deviation of the Doppler velocity measurement for the instrument as configured is calculated to be 1.3 cm/sec. The Aquadopp current profiler has the ability to digitize two 0-5 Volt Direct Current (VDC) signals using a 16-bit analog to digital converters and to incorporate these data into its recorded data stream. These two ports were used to digitize the signals from the Valeport Model 620 conductivity and temperature sensors which are described in section 2.5.

2.4.1 Calibration of the Current Profiler

The ability of this instrument to make current velocity measurements is determined by the signal processing algorithms and the physical construction of the instrument. These parameters are fixed by the manufacturer. No user calibration was required.

To optimize the acoustical backscatter measurement for comparison with data from the optical turbidity sensor, each of the four units deployed in this study was subjected to a series of bench measurements where a test signal was injected into the instruments and the response of each instrument was recorded. These tests helped to identify the individual response characteristics of each instrument so that the acoustic backscatter return from the instruments could be intercompared between instruments and also compared with other data. The pressure sensor on the Aquadopp current profiler was zeroed in open air before each deployment. The local atmospheric pressure at that time was recorded in a log book. Before each deployment, the internal compass of the Aquadopp profiler was calibrated using the

manufacturer's compass calibration routine while rotating the instrument through a complete circle. Current data were corrected in post processing for a local magnetic variation of 6°W.

2.5 Valeport Model 620 Conductivity and Temperature Sensor

The Valeport Model 620 conductivity and temperature (CT) sensor outputs two 0-5 VDC signals that are proportional to the conductivity and temperature of the water in which the sensor is immersed. These voltages were digitized by the 16-bit analog to digital converters on the Aquadopp current profiler, and the resultant data were stored on the current profile. In post-deployment processing, salinity was calculated from the conductivity and temperature data from the CT probe with the addition of the pressure data from the Aquadopp current profiler. The conductivity measurement is specified to be accurate to ±0.01 mS/cm with a resolution of 0.002 mS/cm, and the temperature sensor is specified to be accurate to ±0.005°C with a resolution of 0.001°C.

2.5.1 Calibration of the Conductivity and Temperature Sensor

Extremely high precision temperature measurements were not required for this study. As the C6 multi-parameter platform and the Aquadopp current profiler were also equipped with temperature sensors, intercomparison of these three measurements gave assurance that none of the sensors was deviating significantly from the others. Two intercomparison methods were used to assess the accuracy of the conductivity sensor. First, the conductivity sensors were placed in a test tank containing saltwater. The salinities calculated from the conductivity sensor were compared with the salinity of water samples from the test tank as measured by a high precision salinometer. Secondly, samples of water were collected at the study sites during the instrument change-outs. These samples were analyzed with a precision salinometer and compared to the values recorded by the bottom-mounted CT sensor. Both of these intercomparison tests showed the conductivity sensor error to be typically less than 1 psu.

2.6 Discrete Water Sample Analysis

At each instrument service interval and during small boat surveys, water samples were collected at the surface via a sample bottle using gloved hands and at the depth of the bottom-mounted instruments via a swimmer and Niskin bottle water-sampling device. An advantage of using a swimmer to collect the bottom water samples is that the bottom water samples could be reliably gathered at the precise location and depth of the bottom-mounted sensor package. These water samples were stored on ice until they could be brought to the laboratory for processing.

2.6.1 Water Sample Chlorophyll

Water samples from the bottom were analyzed for chlorophyll-*a* concentration via a standardized filtration-extraction method using a 60:40 mixture of acetone and dimethyl sulfoxide (Shoaf and Lium, 1976). The fluorescence of each sample was measured on a Turner Designs model TD-700 fluorometer before and after acidification to correct for phaeophytin. These fluorescence values were calibrated using known concentrations of chlorophyll-*a* to yield chlorophyll-*a* concentrations in µg/l.

2.6.2 Water Sample Total Suspended Solids

Water samples from the surface and bottom were analyzed for TSS. The TSS concentration of the water samples was determined gravimetrically following Young *et al.* (1981). A sample volume of 1 liter was filtered through pre-weighed filters that were then dried and reweighed to calculate the TSS.

2.6.3 Scanning Electron Microscopy Water Sample Particulate Analysis

2.6.3.1 SEM/EDS imaging and elemental composition

Following field collection of 1 liter of sample water at the surface and bottom for each site, the particulate loading, concentration, and identification were evaluated by filtration of a fixed volume of water preserved in 2% gluteraldehyde in sodium cacodylate-buffered seawater. Two hundred milliliters of the collected water and preserved particulates were filtered through a 0.22 Nuclepore filter and rinsed in the filtration set-up with 50 ml of filtered fresh water. The

filters were prepared for SEM by cutting out a portion of each filter, mounting it on an aluminum stub covered with a carbon adhesive tab, and coating it with palladium in a plasma sputter coater.

To quantify particulate loading and the number per liter, a set number of images was taken at a fixed magnification in the SEM, which resulted in a known area, and examined. These images were then converted to drawings utilizing the NIH program Image-J (Figure 9). This program assigns each particle a number, and the surface areas and number of particles in each image are generated in tabular form. These data were then imported into Excel. The Excel data were collected in spreadsheet form for calculation of the total particulate number in millions of particles per liter (MPL) and surface area (mm^2) for each site and water depth.
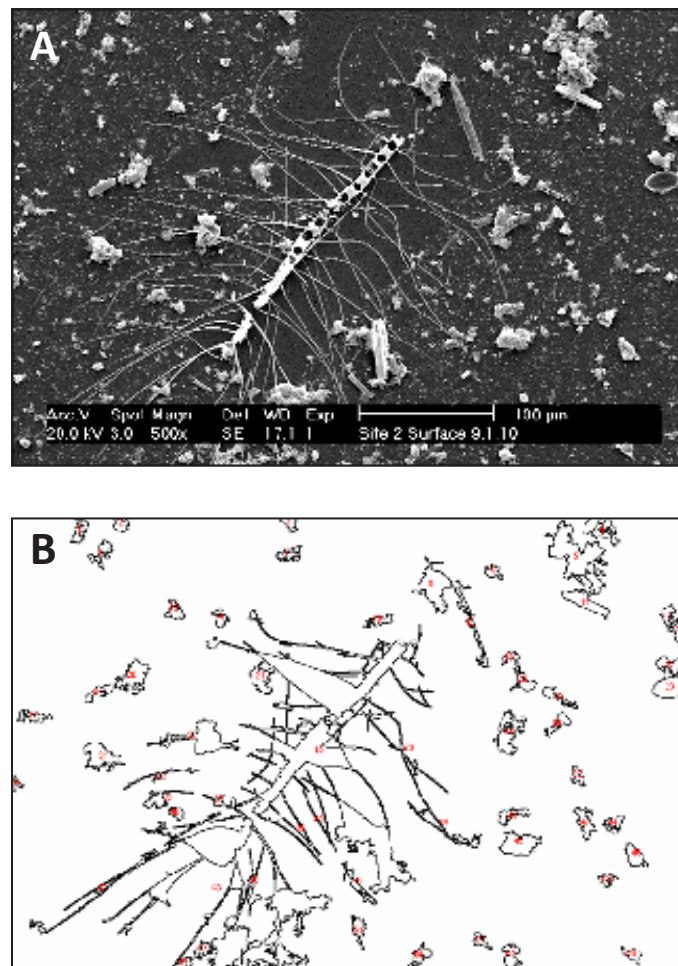
Figure 9. (A) SEM image of a water sample taken at 500x; and (B) Same image processed using Image-J software to calculate the surface area and number of particles present.

2.6.3.2 Particulate enumeration and surface area calculation

The average number and surface areas were calculated as per the following example protocol for the greater and less than 5 micron size fraction:

- Surface area of 47 mm filter = 1320 mm^2 (excluding filter edge)

- (>5 µ) Total area viewed per frame in the SEM at 500x = 0.175 mm^2

- (<5 µ) Total area viewed per frame at 5000x = 0.0175 mm^2

- 14 frames viewed of each sample at 500x = 2.45 mm^2

- 10 frames viewed at 5000x = 0.175 mm^2

- Number of particles/surface area examined in <5 µ and >5 µ size fraction × total surface area of the filter × 5 (200 ml filtered) = **number of particles/liter (MPL)**

- **Average particulate surface area = Sum of the individual particle surface areas obtained in Image-J/number of particles**

2.6.3.3 Particle size distribution

Data from the Image-J particle area results were further sorted into seven size categories: (1) particles with an area of <10 µ^2; (2) 10-20 µ^2; (3) 20-50 µ^2; (4) 50-100 µ^2; (5) 100-200 µ^2; (6) 200-500 µ^2; and (7) those with an area >500 µ^2.

2.6.3.4 Particle characterization

In addition to quantitative assessment of particulate loading and number, identification and comparison of the relative abundance of sample particulates were accomplished by examining 300 particles from each sample. Many of the particulates were phytoplankton, which were identified using appropriate keys and relevant articles (Tester and Steidinger, 1979; Tomas, 1997). The relative abundance of each component was calculated for each sample.

2.6.4 Water Sample Microbiological Analysis

During many of the site visits, a water sample was collected to assess the concentration of certain microbial agents that could potentially be present in the water. These samples were collected using the following protocol.

Surface water was collected from the side of the vessel, using gloved hands, into a sterilized 250-ml opaque bottle. To minimize potential personal flora contamination from the sampler, the bottle was filled and rinsed three times with site water up current and away from the sampler's hand, then was filled to the rim and sealed. All samples were placed on ice in a cooler for transport to the laboratory and refrigerated during the time interval before filtration for analysis. Samples were typically processed within two hours and within no more than six hours after their collection. One hundred milliliters of sample were filtered onto Whatman filters and plated on mEI media following EPA method 1600 for isolation and enumeration of enterococci. They were incubated at 41° for 24 hours and then assessed for positive colonies. Fifty milliliters of sample water were filtered onto Whatman filters and plated on Baird-Parker media for isolation and subsequent genetic characterization of methicillin-sensitive and methicillin-resistant *Staphylococcus aureus* populations. The plates were incubated at 37° for 24 hours and refrigerated until processed.

2.7 Light Attenuation Measurements

During site visits, light attenuation (K_t) was measured using two 4-pi spherical quantum sensors (LiCor model LI-193 SA) according to Kelble *et al.* (2005). These two sensors were placed 0.36 m apart on a polyvinyl chloride (PVC) pole with two perpendicular PVC lengths to mount the quantum sensors. This allowed the sensors to measure the intensity of PAR (400-700 nm) simultaneously at two depths. The light attenuation coefficient K_t was calculated according to following equation (Kirk, 1994):

$$K_t = \ln(E_{z1}/E_{z2})/(z_2-z_1) \qquad (1)$$

where (z_2-z_1) is the difference in depths between the two instruments, which is 0.36 m, and E_{z1} and E_{z2} are the light intensities at the two respective depths. At each station, we measured K_t at two depths below the surface. Moreover, we

recorded and calculated a minimum of two K_t values at each depth, enabling a rigorous estimation of the mean and standard deviation of K_t at each station for each site visit.

2.8 Meteorological Observations

Meteorological data used for analysis in this study were gathered from the National Data Buoy Center VAKF1 station located at the end of the Rosenstiel School of Marine and Atmospheric Science pier on the south side of Virginia Key in Miami, Florida. The data source was the quality controlled standard meteorological data that are available from the station's web site (http://www.ndbc. noaa.gov/station_history.php?station=vakf1). Wind speed, wind direction, and wind gust data were tabulated and then interpolated to match the sampling times of the bottom-mounted instruments. Data were available for the entire span of the project with the exception of the period February 2, 2010 15:00 UT through February 8, 2010 14:18 UT. Daily precipitation rates at Miami International Airport were acquired from the website of NOAA's National Weather Service Forecast Office in Miami (http://www.nws.noaa.gov/climate/index.php?wfo=mfl).

2.9 Visual Observations

The site 2-3 basin is located directly north of the Rickenbacker Causeway. The William Powell Bridge (part of the Rickenbacker Causeway) and the old bridge that the Powell Bridge replaced provide a vantage point for visually observing the site 2-3 basin. On a number of occasions, visual observations of conditions in the site 2-3 basin were made and noted in a log. These observations provided a point of reference for later examining the data record for events of interest.

2.10 Photographic Observations

To capture photographic images of the site 2-3 basin, a camera surveillance package was obtained from Harbortronics (Time Lapse Package), which included a Pentax K200 SLR camera with a time-lapse controller (DigiSnap2000), battery pack, and solar panel recharger. A support mount for the system was built and installed on the southeast corner of the roof of the Four Seasons Hotel, 1435 Brickell Avenue, Miami, Florida (Figure 10). This location, approximately 700 feet above the ground, provided an excellent view of Biscayne Bay. The mount positioned the camera at an angle of 16° from the horizon. The resulting view covered the Port of Miami to the east end of the William Powell Bridge. The field of view also included sites 2 and 3. Photographs were taken every five minutes. The camera's memory allowed the system to record continuously for 14 days. To calibrate times recorded with each image by the camera, the camera was directed to photograph a cell phone clock during each memory swap-out. A regression of the file creation time against the clock time for these calibration photographs resulted in a calibration correction formula. This formula was employed to provide the correct time for all of the pictures.

Location and Field of View of Biscayne Bay Camera System
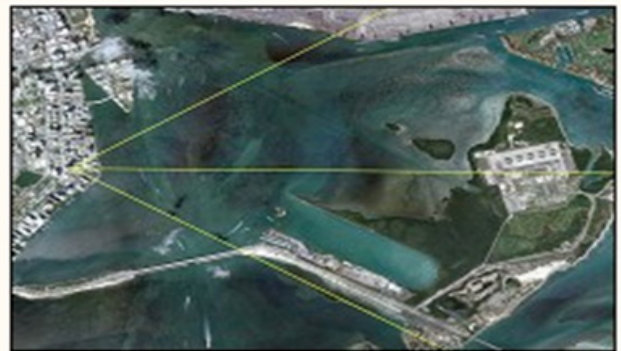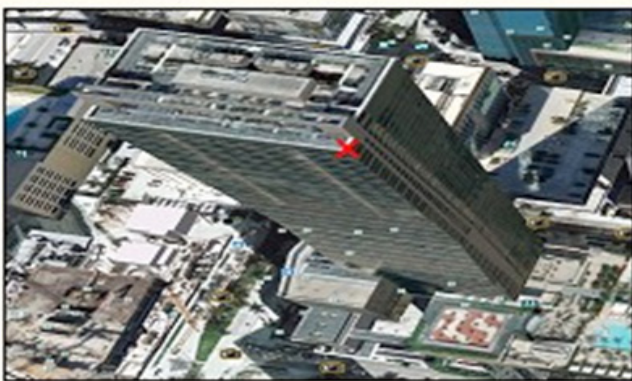
Figure 10. Location of the photographic system on the Four Seasons Hotel and the field of view of this system.

2.11 Small Boat Observations

In an attempt to capture the spatial variability of the turbidity levels in the site 2-3 basin, a small boat equipped with a down-looking 1.2 MHz Doppler sonar and a flow-through water sampling system was operated while the vessel transected a predefined course. The flow-through system continuously made measurements of water temperature, salinity, turbidity, and chlorophyll-*a* concentrations. On all days, discrete water samples were collected at selected points on the survey course. These samples were returned to the laboratory to be analyzed for chlorophyll and TSS. The goals of the small boat effort were reformulated during the course of the study to reflect what was learned from analysis of the data collected and the desire to study the turbidity levels present in the shipping channel proper.

3. Results

A principal goal of this study was to estimate the expected value of turbidity at each of the study sites and to examine how that expected value was perturbed and modulated by other environmental factors during a one-year study period.

Data were collected for somewhat longer periods than one year at the sites. The one-year interval that contained the highest quality and most continuous period of data was selected for analysis. For site 1, this period was September 17, 2010 through September 16, 2011; for sites 2 and 3 this was August 4, 2010 through August 3, 2011. An analysis of meteorological and current data is presented for the same time intervals for the respective sites. The meteorological, current, and chlorophyll-*a* data sets are discussed prior to the turbidity data so that the variability observed in the turbidity data may be examined in the context of these variables.

3.1 Meteorological and Climatic Data

Figure 11 gives histograms of wind speed and direction for the period August 4, 2010 through August 3, 2011. The mean wind speed is 3.9 m/s. The median wind speed is 3.8 m/s, and the most prevalent wind direction is from the east. Figure 12 compares the wind velocity plotted as a function of wind direction for the site 2-3 analysis year (August 4, 2010 through August 3, 2011) with data from the entire time span available from that weather station (April 1, 2005 through November 2008 and April 2009
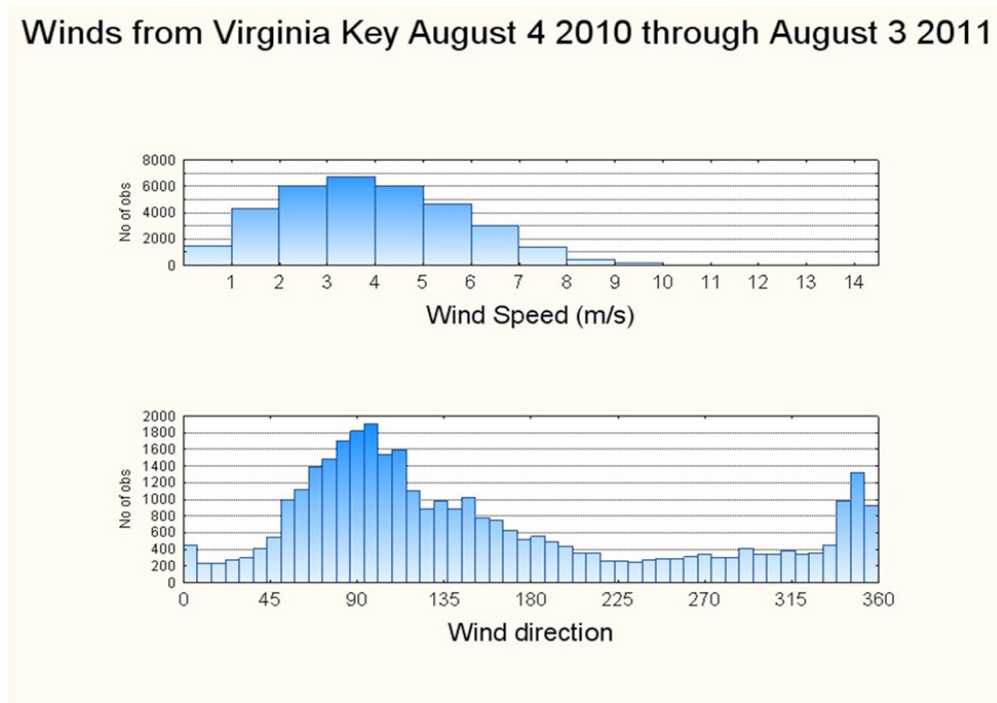
Figure 11. Histograms of wind speed and wind direction from the Virginia Key (VAKF1) weather station. Data presented are from the site 2-3 study period (August 4, 2010 through August 3, 2011).
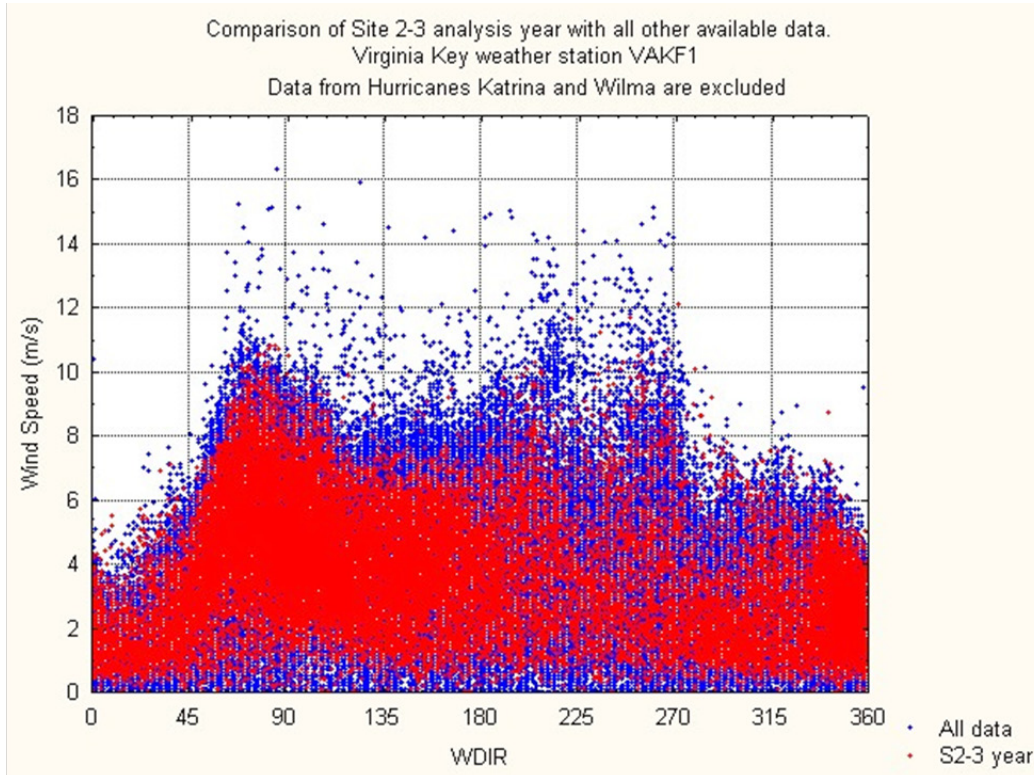
Figure 12. Wind speed plotted as a function of wind direction for the site 2-3 analysis year (August 4, 2010 through August 3, 2011). All available data from this station are also plotted (April 1, 2005 through November 2008 and April 2009 through September 15, 2011). Data from hurricanes Katrina and Wilma have been excluded.

through September 15, 2011). Data that were influenced by hurricanes Katrina and Wilma were excluded in this analysis. Figure 13 shows the wind speed averages by month for three time intervals: all data from this station (excluding data from hurricanes Katrina and Wilma), the site 2-3 analysis year, and the site 1 analysis year. From Figure 13 it can be seen that while there are seasonal changes in the wind speed averages, those changes were not extreme. Figure 14 shows histograms of the north and east components of the wind for the period August 4, 2010 through August 3, 2011. Table 5 gives the mean wind velocities for the north and east wind components for all data in the year that correspond to the analysis year for site 1 (September 17, 2010 through September 16, 2011) and sites 2 and 3 (August 4, 2010 through August 3, 2011). Table 5 also gives the mean velocities of those components when segregated into categories of velocities below -5 m/s, velocities between -5 m/s and +5 m/s, and velocities above 5 m/s. The 75th percentile of the wind speed for the site 1 analysis year was 5.1 m/s and for the sites 2-3 year it was 5.2 m/s.

From Table 5, it can be seen that the mean statistics of the wind velocities are similar for the site 1 and sites 2 and 3 analysis years. The Biscayne Bay area receives an average of 127-165 cm of rainfall per year with the majority of rain falling between May and October (Wanless *et al.*, 1984). During the site 1 analysis year, Miami International Airport received 143 cm of precipitation, and for the sites 2-3 analysis year, Miami International Airport received 155 cm of precipitation. The study period encompassed a significant La Niña phase, as determined by the multivariate El Niño Southern Oscillation (ENSO) Index (http://www.esrl.noaa.gov/psd/enso/mei/). In fact, the period from June 2010 through March 2011 constituted the strongest La Niña since 1988. The La Niña significantly weakened in March 2011 and remained moderate, but was present for the study duration. ENSO effects are minimal in south Florida during the summer, but La Niña events are typically associated with warmer, dryer winters, while El Niño events bring cooler, wetter winters (http://www.srh.noaa.gov/mfl/?n=winteroutlookforsouthflorida).
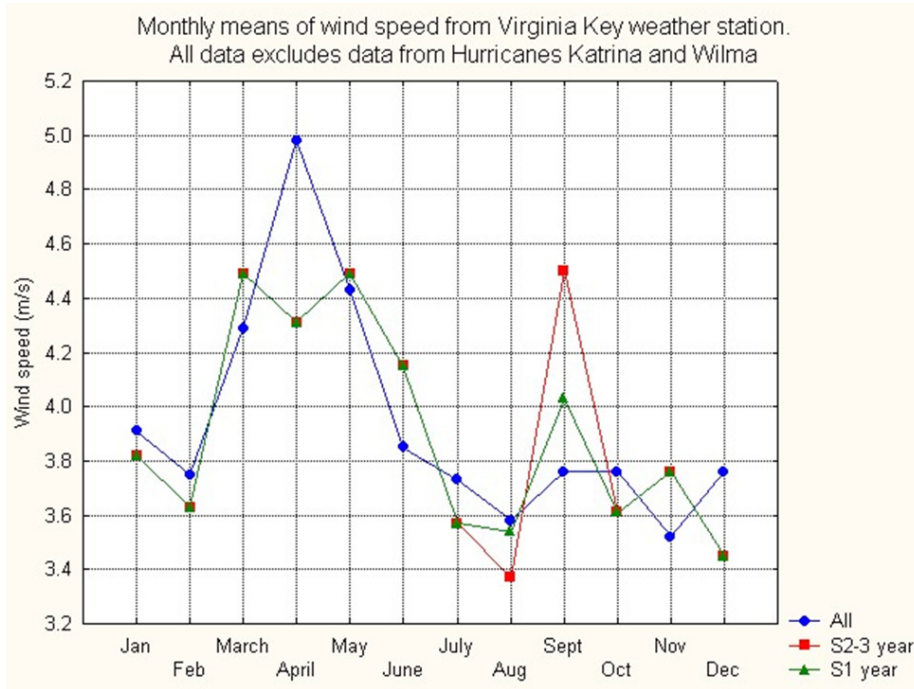
Figure 13. Monthly wind speed averages from the Virginia Key (VAKF1) weather station for all available data from the station (April 1, 2005 through November 2008 and April 2009 through September 15, 2011) excluding data from hurricanes Wilma and Katrina, the site 2-3 analysis year, and the site 1 analysis year.
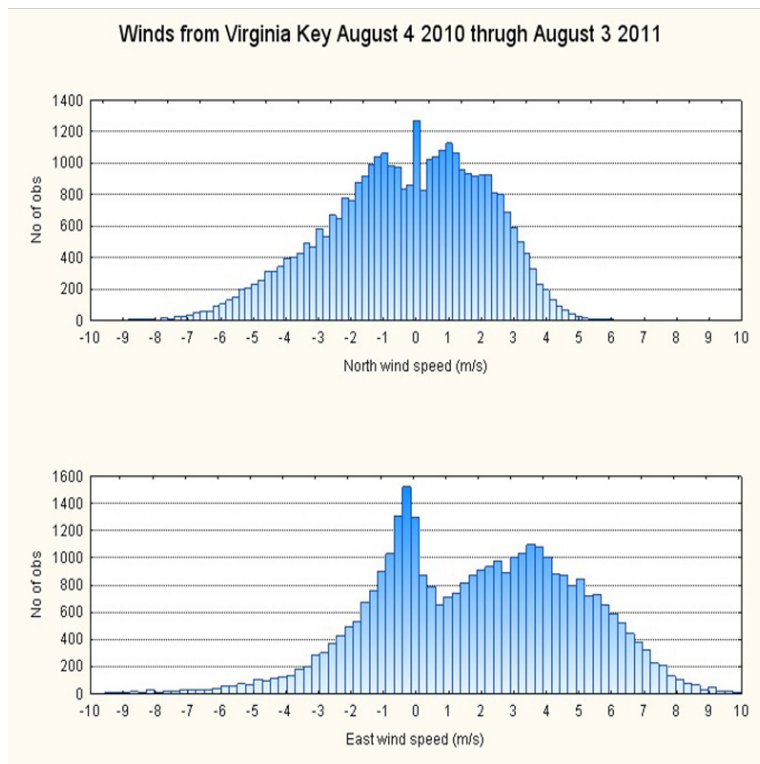
Figure 14. Histograms of the north and east wind velocities reported by the Virginia Key (VAKF1) weather station for the site 2-3 analysis year (August 4, 2010 through August 3, 2011). Data from hurricanes Katrina and Wilma have been excluded.

Table 5. North and east wind velocities. The mean north and east wind velocities with the number of observations (N) are given in four categories: All observations; those less than -5 m/s; those between -5 m/s and 5 m/s; and those above 5 m/s.

Velocity bounds	East All Velocities	East <-5	East >-5 and <5	East >5	North All Velocities	North <-5	North >-5 and < 5	North >5
Site 1 year mean velocity (m/s)	1.7	-6.5	1.0	6.2	-0.3	-6.0	-0.1	5.6
N	34294	667	28281	5349	34294	1260	32969	66
Sites 2 and 3 year mean velocity (m/s)	2.0	-6.6	1.1	6.3	-0.3	-5.9	-0.1	5.6
N	34464	534	28059	5844	34464	1274	33128	63

3.2 Currents

This section presents data from the Aquadopp current profiler meters at each of the sites. For this analysis, the same one-year interval used for the analysis of the turbidity data was used. Statistics are given for the near bottom and near surface. The near bottom measurement is 0.7 m from the bottom. The distance of the near surface measurement with respect to the water surface varies with changing water level. This near-surface cell was selected so that the measurement contained valid data for all water levels. For all the sites, statistics are given for the near bottom and near surface velocity during flood and ebb tides. Direction versus velocity plots of the near bottom and near surface data are presented in polar and rectangular form. Plots of the vertical profile of velocities are presented for flood and ebb tides. Tides in Biscayne Bay are semidiurnal. The mean tidal range is 0.77 m, the spring tidal range is 0.92 m, and the neap tidal range is 0.60 m. There exists a tidal nodal point just north of the 79th Street Causeway (near site 1) (Van de Kreeke and Wang, 1984). Wind-generated currents are also of major importance in Biscayne Bay circulation and water residence time (Wanless *et al.*, 1984).

3.2.1 Site 1 Currents

Site 1 is located well away from any of the channels that connect this basin to the basins to the north and south (Figure 3). Current speeds are quite low. There is a tidally-directed flow with the ebb tide directed approximately 182° and the flood tide directed approximately 23° (Figures 15B

and 15C). The vertical velocity profiles show a linear increase in mean speed from the bottom to the surface (Table 6, Figure 15D).

3.2.2 Site 2 Currents

At the location of site 2, it would be expected that flow characteristics are influenced by the proximity of Government Cut, Fisherman's Channel, and Norris Cut (Figure 16). Table 7 gives statistics for the current velocities during the flood and ebb tides. The flood tide is directed approximately 265° from the north. The ebb tide is directed approximately 68°. Note that the near-surface current takes a slightly different trajectory and has more variance in its direction (Figures 17B and Figure 17C). The ebb tide direction is roughly aligned with the axis of the basin, while the flood tide axis is more aligned with the inlet channels.

3.2.3 Site 3 Currents

Figure 7 shows the location of site 3. Table 8 gives statistics for the current velocities during the flood and ebb tides. There is a significant difference in the current velocities between the flood and ebb tides at site 3 (Figure 18D). A possible explanation is that during the ebb tide the water moving north is pushed up against the south side of Virginia Key Causeway Beach and is then forced under the east side of the Rickenbacker Causeway Bridge. This contrasts with the flood tide where the water moves more uniformly southward across the basin and more uniformly under the
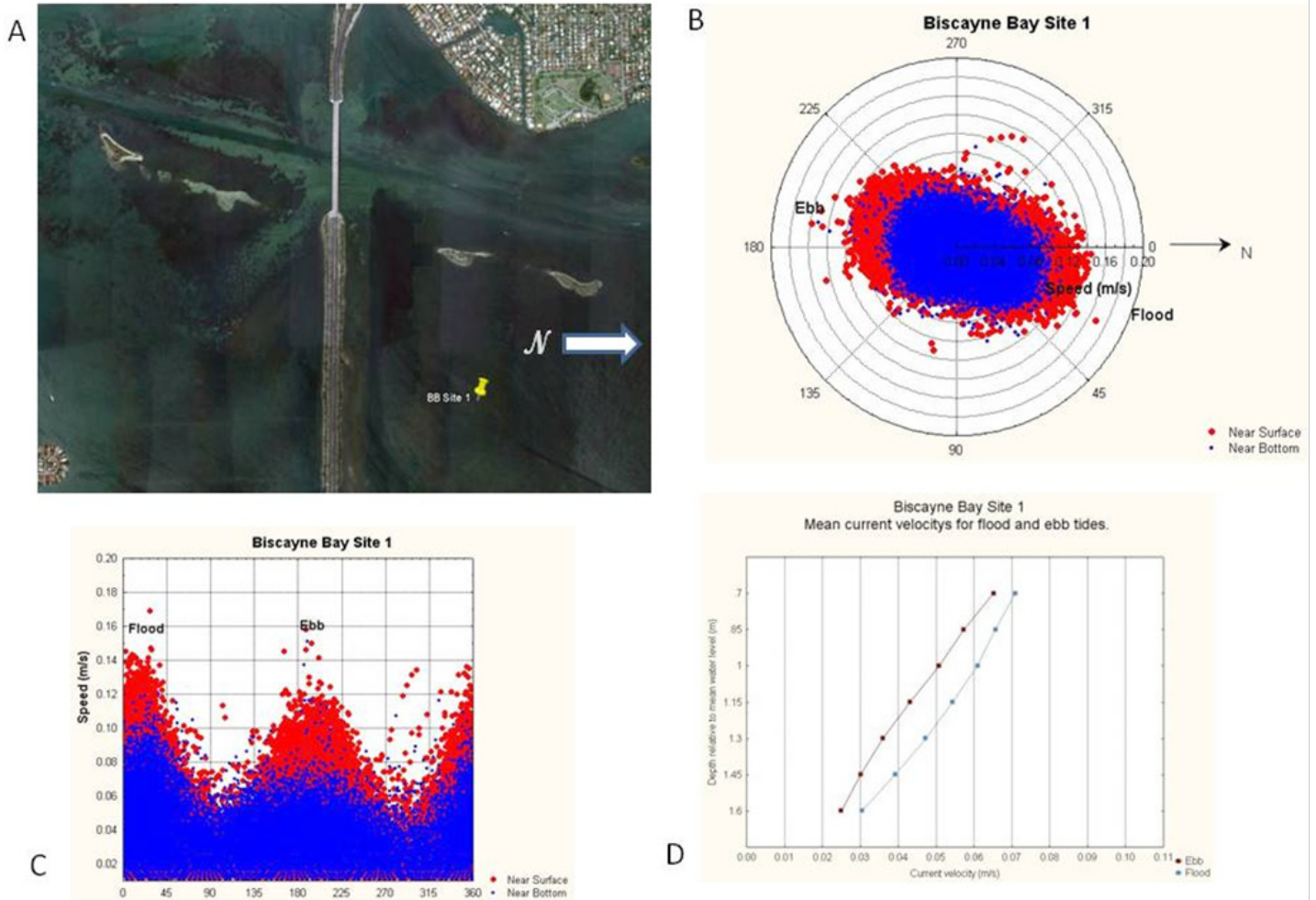
Figure 15. Currents at site 1: (A) the location of site 1; (B) a polar plot showing the velocity versus direction for near-bottom and near-surface currents; (C) a rectangular plot of current velocity versus direction for near-bottom and near-surface currents; and (D) a profile of average velocities with depth for the flood and ebb tides.

Table 6. Site 1 current velocities.

Site 1	Near Bottom	Near Surface
Ebb tide—average speed (m/s)	0.04	0.06
Ebb tide—typical maximum speed (m/s)	0.06	0.11
Flood tide—average speed (m/s)	0.04	0.06
Flood tide—typical maximum speed (m/s)	0.09	0.13

Figure 16. Location of sites 2 and 3.

bridge. Compared to sites 1 and 2, there is less variation in the current direction. The flood tide is directed approximately 225°, and the ebb tide is directed approximately 45° (Figures 18B and 18C).

3.3 Chlorophyll Data

Chlorophyll levels at site 1 are typically below 1 µg/l. However, during diatom bloom events, chlorophyll-*a* concentrations were significantly elevated (Figure 19). The most intense bloom occurred in April 2012, had chlorophyll-*a* concentrations greater than 7 µg/l, and was present for more than a month. The other two blooms both lasted approximately one week. An in-depth analysis of the blooms is presented in section 3.9.

At sites 2 and 3, "background" chlorophyll-*a* levels were greater than at site 1, but were still typically less than 2 µg/l (Figure 20). The blooms in this basin were not as distinct from "background" levels as observed in site 1. The phytoplankton blooms were also not as intense, with peaks rarely exceeding 4 µg/l. The chlorophyll-*a* measurements at sites 2 and 3 were very similar, as would be expected given

their proximity within the same small basin. When processed with a five-point smoothing filter, the chlorophyll-*a* data from sites 2 and 3 are correlated with a Pearson-R coefficient of 0.64. The chlorophyll*a* values from these measurements are similar to those reported for long-term monitoring programs that take monthly grab samples for chlorophyll-*a* in this area of Biscayne Bay (Boyer *et al.*, 2009).

3.4 Turbidity

In preparing the turbidity data for analysis, one calendar year was selected for the analysis period. For site 1, this period was September 17, 2010 through September 16, 2011, and for sites 2 and 3 the period was August 4, 2010 through August 3, 2011. These dates were selected to use the best available continuous data for one year. The data were examined to detect evidence of sensor fouling or other factors that would cause the data to be considered invalid (see section 3.4.1). These data were flagged in the data set and are excluded from the analysis. Turbidity values over 25 NTU were considered to be outliers and were eliminated from the analysis. These data-screening procedures resulted
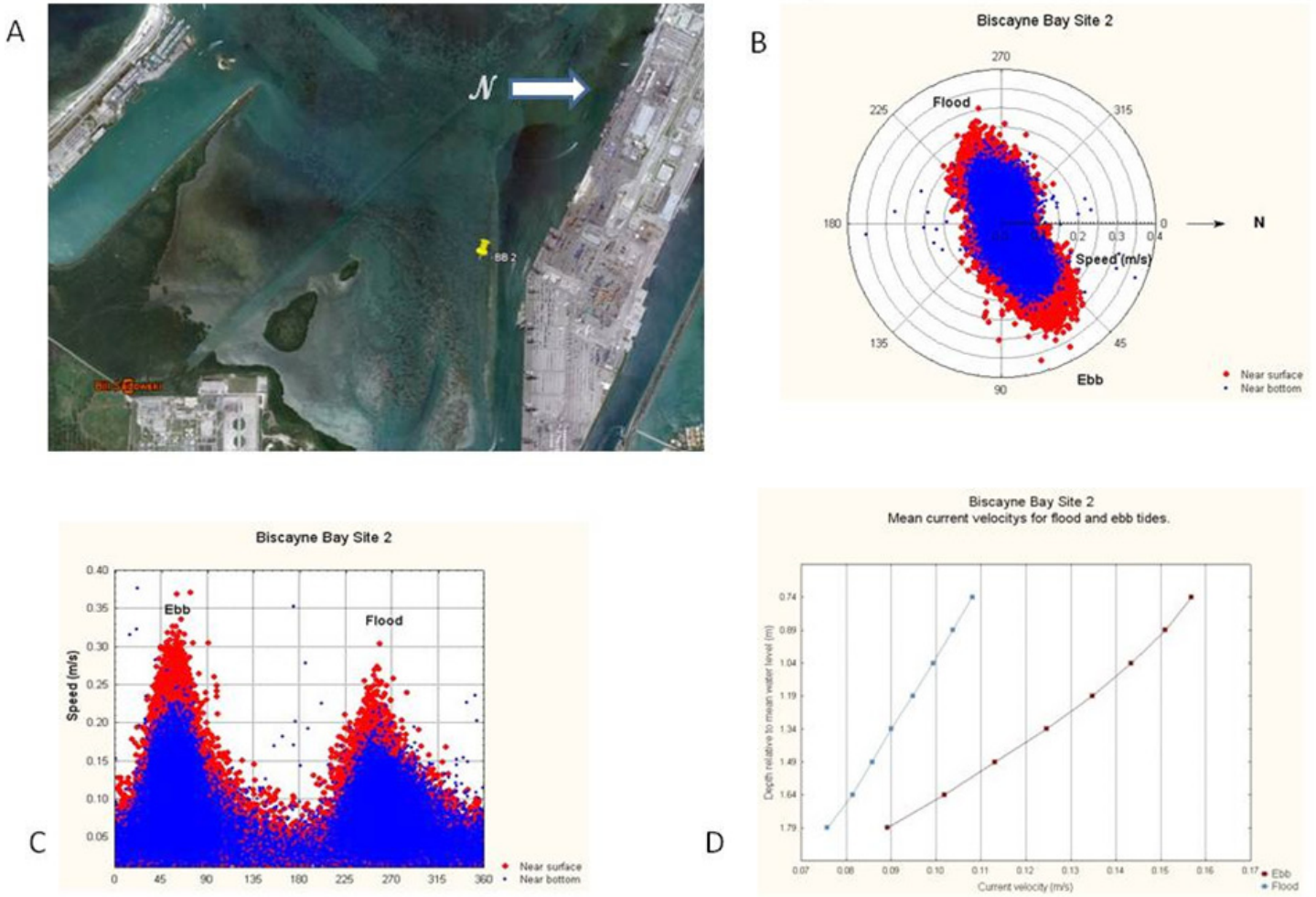
Figure 17. Currents at site 2: (A) the location of site 2; (B) a polar plot showing the velocity versus direction for near-bottom and near-surface currents; (C) a rectangular plot of current velocity versus direction for near-bottom and near-surface currents; and (D) a profile of average velocities with depth for the flood and ebb tides.

Table 7. Site 2 current velocities.

Site 2	Near Bottom	Near Surface
Ebb tide—average speed (m/s)	0.10	0.14
Ebb tide—typical maximum speed (m/s)	0.17	0.30
Flood tide—average speed (m/s)	0.08	0.09
Flood tide—typical maximum speed (m/s)	0.15	0.25
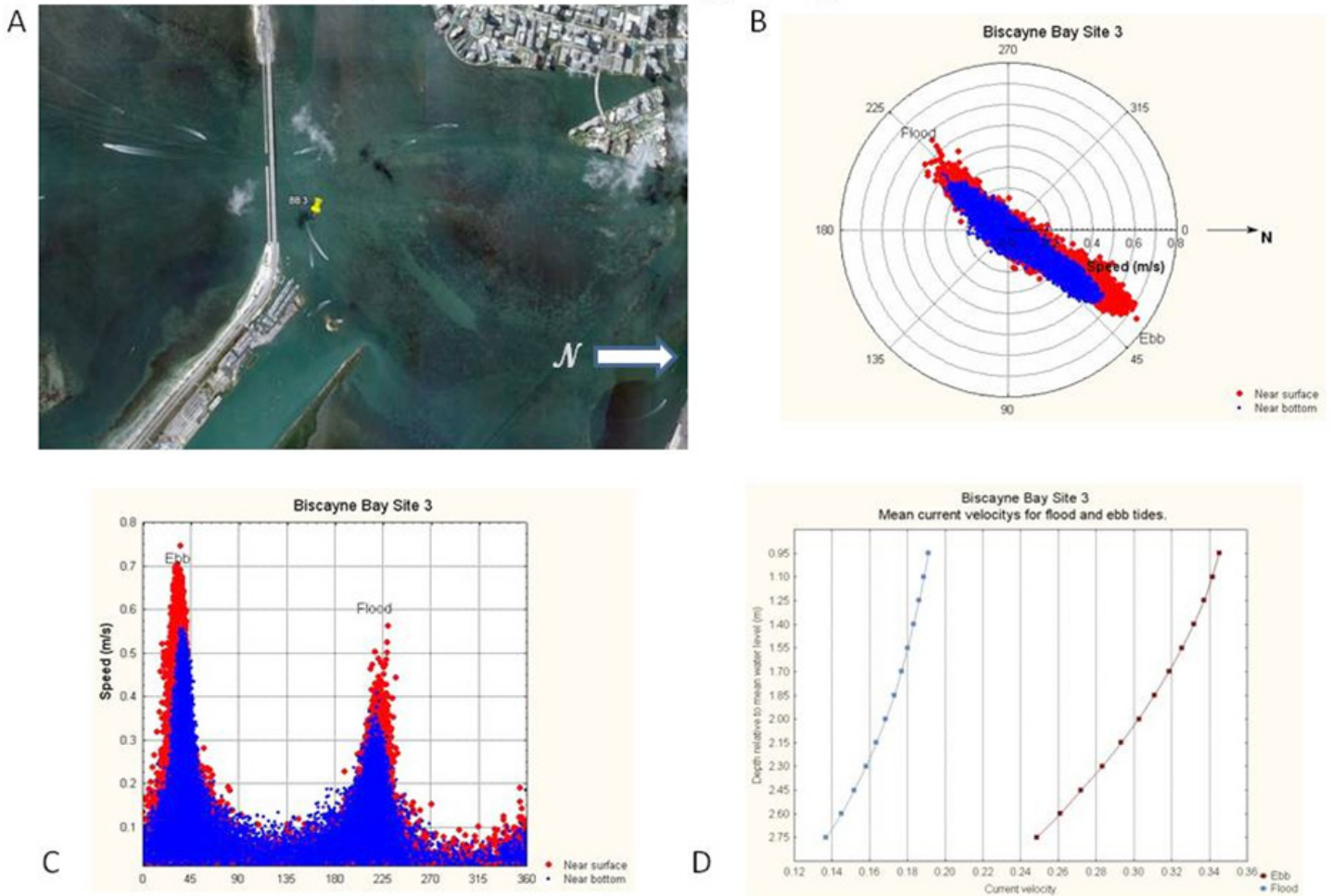
Figure 18. Currents at site 3: (A) the location of site 3; (B) a polar plot showing the velocity versus direction for near-bottom and near-surface currents; (C) a rectangular plot of current velocity versus direction for near-bottom and near-surface currents; and (D) a profile of average velocities with depth for the flood and ebb tides.

Table 8. Site 3 current velocities.

Site 3	Near Bottom	Near Surface
Ebb tide—average speed (m/s)	0.26	0.30
Ebb tide—typical maximum speed (m/s)	0.50	0.70
Flood tide—average speed (m/s)	0.15	0.17
Flood tide—typical maximum speed (m/s)	0.30	0.42
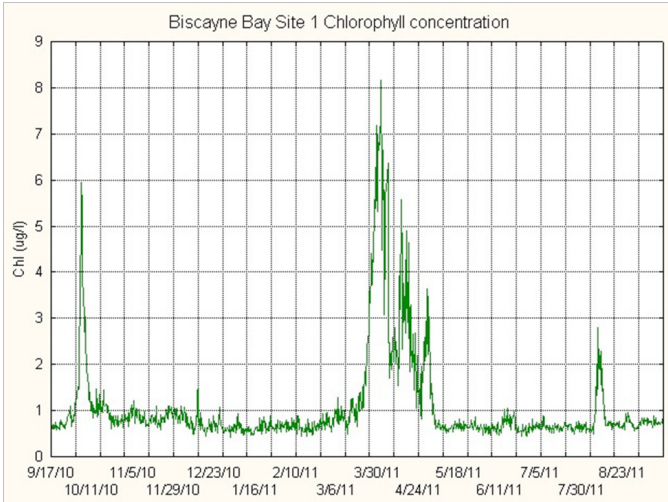
Figure 19. Chlorophyll-*a* concentrations at site 1. Several significant phytoplankton blooms occurred during the study period.
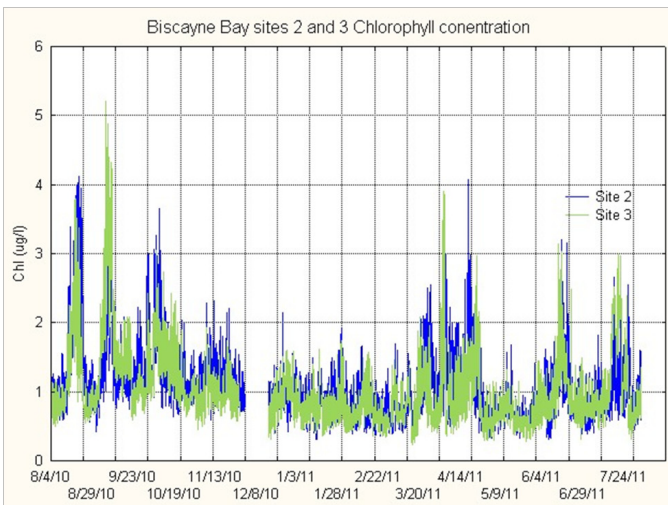
Figure 20. Chlorophyll-*a* concentrations at sites 2-3.

in less than 1% of the available data being marked as bad for site 1, less than 5% of the data being marked bad for site 2, and less than 20% of the data being marked bad for site 3 (site 3 had several deployments that were impacted by sensor fouling and one deployment where a battery prematurely failed, causing a loss of data). Descriptive statistics for the three sites and for the data processed in this manner are presented in Table 9. From this point forward, unless otherwise noted, all references to the turbidity data will be for the one-year period processed as described above. To demonstrate that the choice of the one-year period did not

significantly affect the calculations of the mean statistics for turbidity, the mean values were calculated for the one-year periods and also for all data collected. These results are given in Table 10. Histograms of the turbidity data for each of the sites are shown in Figure 21. Figure 22 shows cumulative histograms of the turbidity data for each of the sites.

3.4.1 Sources of Error in Turbidity Data

The C6 platform is equipped with a shade cap to help eliminate effects from stray light impinging on the sensors. To examine the effects of stray sunlight on the turbidity data, two groups of quality-controlled turbidity data as described in section 3.4 were formed. The "night" group was data collected between the hours of 21:00 Eastern Standard Time (EST) and 05:00 EST the following day. The "daytime" data group was comprised of data collected between 09:00 and 17:00 EST. To control for winds, only data which had an associated wind speed of 3 m/s or less were used in the analysis. The turbidity data, when organized in this way, showed no statistical difference in the means at the p = 0.05 level for sites 1 and 3. Site 2 did show a statistically-significant difference. However, upon examination it was discovered that high turbidity values occurred during daylight hours that appeared to be associated with actual turbidity events. It is felt, therefore, that stray light did not significantly affect the measurements.

During the winter months, there was an abundance of drifting red algae present in the water (possibly *Polysiphonia* sp., Lirman, personal communications) that collected on the instruments and the mountings. Site 3 was particularly plagued by this drifting algae collecting on the sensor platform. It is quite probable, given the abundance of the algae, that filaments or pieces of algae interfered with the optical backscatter measurement. It was observed that the turbidity data would sometimes "spike" up an order of magnitude or more but then immediately return to previous levels. This may be attributable to this algae collecting on the sensor or to objects in the water such as small fish or crabs blocking the sensor, both of which were observed inside the C6 instrument at times. By eliminating data with a value of 25 NTU or higher, many of these transient events were eliminated from the data set. In some cases, the turbidity data would rapidly shift to a high value and remain at an elevated level. These data were identified and flagged as bad. In a few instances, the wiper mechanism of the C6

Table 9. Turbidity data statistics for a one-year period. The number of observations (N), arithmetic mean, geometric mean, median value, minimum and maximum observed values, 10% and 90% values, and the standard deviation are given.

Site	N	Mean	Geo Mean	Median	Min	Max	10%	90%	SD
1	34756	0.881755	0.528883	0.510720	0.000488	24.87080	0.179760	1.778448	1.418570
2	33333	4.140746	3.487601	3.322152	0.196600	24.98488	1.748220	7.471820	2.835089
3	28229	3.074456	2.741325	2.677072	0.558620	24.87140	1.578929	4.842384	1.813572

Table 10. Mean value of turbidity for one year of data and for all data.

Site	Mean of Turbidity for All Data	N for All Data	Mean of One Year of Turbidity Data	N for One Year of Data
1	0.886	39722	0.882	34756
2	4.175	36964	4.141	33333
3	3.119	33307	3.075	28229
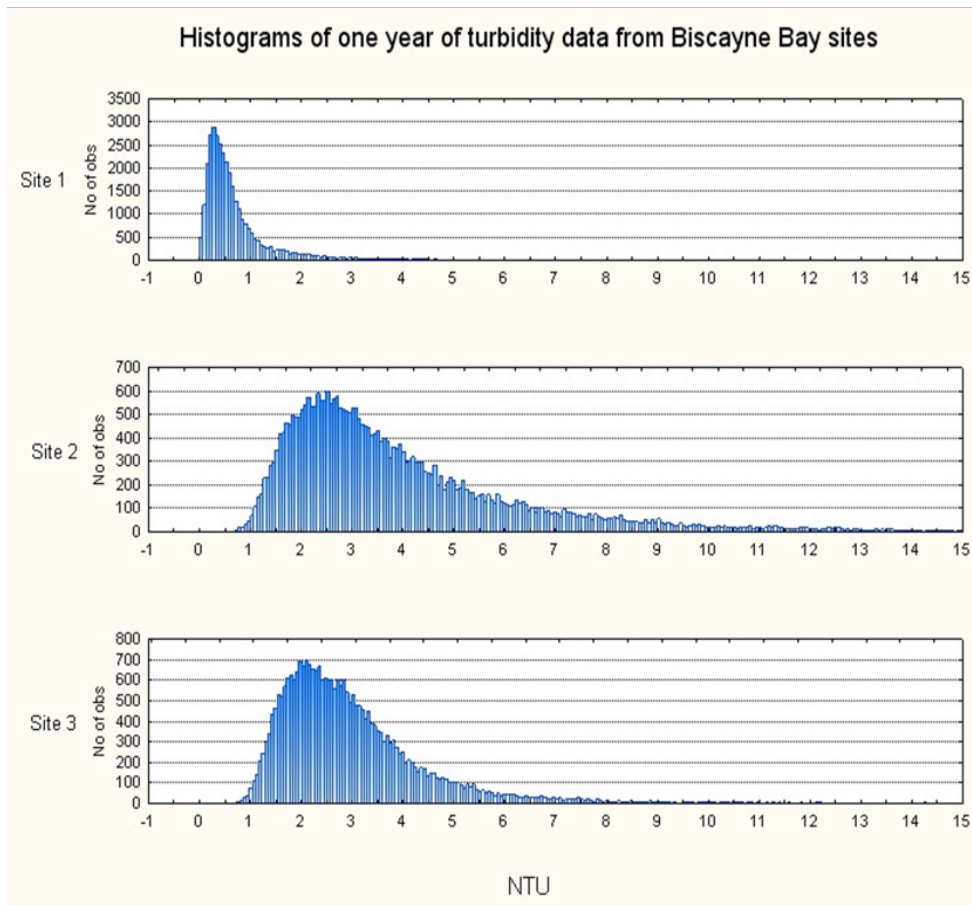
Figure 21. Histograms of turbidity at the three study sites. These histograms suggest that the turbidity data may be lognormal distributed.
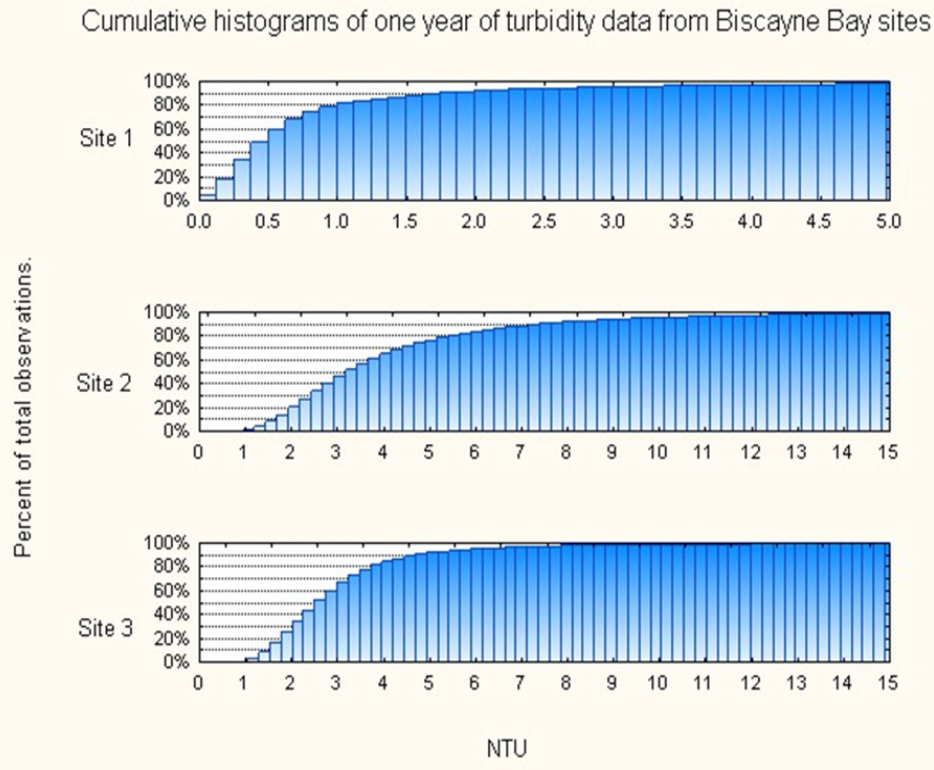
Figure 22. Cumulative histograms of turbidity data collected at the three study sites.

platform stopped in front of the turbidity sensor. The turbidity data in these cases were at an extremely high value and were flagged as bad.

3.4.2 Turbidity at Site 1

For the one-year study period, the mean value of turbidity at site 1 was 0.88 NTU, the 90th percentile value was 1.78 NTU, and the standard deviation was 1.42 NTU (Table 9). Wanless *et al.* (1984) described sources of turbidity in this area as shallow dredged bottom, turbidity advected from adjacent basins, benthic diatoms, seagrasses and calcareous algae, and resuspension of flocculent bottom materials during winter storms. Wanless *et al.* (1984) also described sinks of turbidity in this basin as the trapping and filtering of turbidity by seagrasses and calcareous algae and trapping of suspended sediment in deep dredged troughs. A deep dredged trough exists along the southern margin of this basin parallel to the Rickenbacker Causeway. This trough is located 500 m to the south of site 1. During this study period, the highest turbidity levels were recorded

concurrently with high chlorophyll levels associated with phytoplankton blooms (see section 3.4.9).

3.4.3 Turbidity at Sites 2 and 3

For the one-year study period, the mean value of turbidity at site 2 was 4.14 NTU, the 90th percentile value was 7.47 NTU, and the standard deviation was 2.84 NTU. The mean value of turbidity at site 3 was 3.08 NTU, the 90th percentile value was 4.84 NTU, and the standard deviation was 1.81 NTU (Table 9). The bottom coverage at sites 2 and 3 was sparse in comparison with site 1. Current velocities at sites 2 and 3 were higher than at site 1. Wanless *et al.* (1984) reported that the Miami River was a significant source of turbidity in this basin (although conditions in the river have changed since this publication); other sources of turbidity were boat wake resuspension along the Intracoastal Waterway and Fisherman's Channel, tidal resuspension of fine or flocculent bottom materials, and bottom materials resuspended in the shallow areas along the west side of Virginia Key during winter storms. Visual observations

made during the winter of 2009, before the study began, recorded many such turbidity fields moving off the shallow areas along the west side of Virginia Key; these events were not observed as frequently during the winter of 2010.

3.4.4 Turbidity Distribution

The turbidity distributions shown in Figure 21 suggest that the turbidity data collected may have a lognormal distribution. To examine this, the natural log of the turbidity data was taken, and histograms of these data are presented in Figure 23 with curves for a normal distribution parameterized by the mean and standard deviation of the log-transformed data, superimposed over the histogram. From this it can be seen that the assumption of a lognormal distribution is reasonable.

3.4.5 Descriptive Statistics of Turbidity Data

Table 9 gives several statistics that describe the turbidity data from the study sites. The arithmetic mean describes the average value of the data. The geometric mean describes the average value of the data when a log transformation is applied to the data before averaging. The median value represents that value for which 50% of the data are above the median and 50% of the data are below the median. Any of these aforementioned statistics can be used to describe the central tendency of the data. To describe the extreme values of the data, the 90th percentile value of the non-transformed data is nearly equal to the antilog for the 90th percentile of the log-transformed data for all three sites and can be used to describe the extreme values of the data.

3.4.6 Turbidity Data Grouped by Month

Tables 11, 12, and 13 give statistics for the turbidity data for sites 1, 2, and 3 when grouped by month. The mean values of the turbidity data when grouped by month indicate that a seasonal change in turbidity is present at sites 2 and 3. The months of May, June, and July show lower turbidity levels with higher turbidity values present during the winter months. Site 1 does not show as large a seasonal variation in turbidity (Figure 24). The large increase in turbidity in April at site 1 is attributable to a phytoplankton bloom (see section 3.4.9).

3.4.7 Turbidity and Wind

To examine the effect of wind speed and direction on turbidity levels, the mean and standard deviation for the turbidity data measured under wind conditions segregated as in Table 5 were calculated and are shown in Figure 25. Table 14 gives the mean values for the turbidity data segregated by wind velocity. While there are some distinct patterns in Figure 25 and Table 14, on average, changes in the average turbidity levels attributable to the winds are less than 1 NTU. It may be the case that one year of data may not be sufficient to describe a relationship between wind speed, wind direction, and turbidity at these sites. While this analysis does not show large changes in the average turbidity value with higher than average wind speed, events were noted where higher than average turbidity values and higher than average wind speeds were apparently correlated.

On March 30, 2011, visual observations from the Powell Bridge revealed the appearance of "streaks" of apparently turbid water in the site 2-3 area. Figure 26 shows a time series of wind and turbidity data at site 2 for the time period. From this graphic it can be seen that the wind does apparently effect turbidity levels but in a somewhat unpredictable manner. Figure 26 shows that, at times, the appearance of higher turbidity levels are accompanied by higher winds (e.g., March 31, 2011 at 18:00 UT, "A"), but there are also periods of higher winds without accompanying high turbidity levels (e.g., March 30, 2011 at 18:00 UT, "B") and periods where turbidity levels increase without an increase in the wind speed (e.g., April 2, 2011 at 19:15 UT, "C"). These observations suggest that while elevated winds may cause turbidity increases in the Bay waters, these increases are not necessarily uniform. Data recorded on an instrument fixed in one location had turbidity levels fluctuate significantly during these periods.

On April 5, 2011, visual observations revealed water that appeared to be very turbid. A strong wind from the south and the presence of waves propagating to the north under the Powell Bridge were also observed. Figure 27 shows the turbidity at site 3 and the north component of the wind; turbidity exceeded 14 NTU and remained elevated for several hours. Winds blowing from the south have a significantly longer fetch to blow over than do winds from other directions, and this may allow waves to develop and propagate into the site 2-3 basin. It may be the case that the
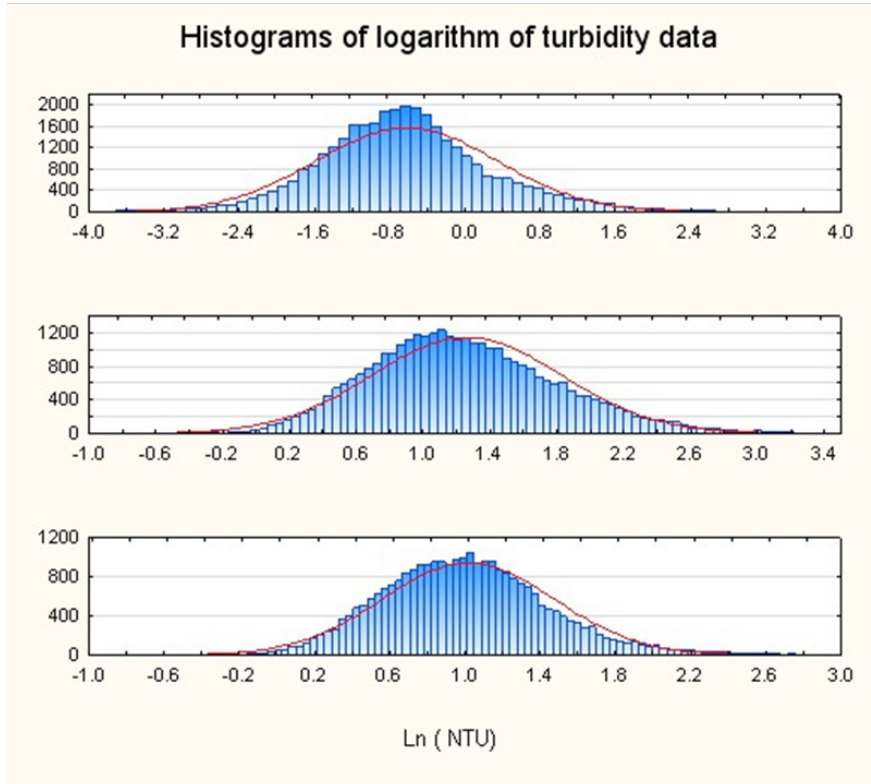
Figure 23. Log-transformed turbidity data for the three study sites plotted as histograms. The curve for a normal distribution parameterized by the mean and standard deviation of the log-transformed data is drawn over the histograms. The reasonably good fit of the data to the normal distribution curves supports the assumption that the data are approximately lognormal distributed.

Figure 24. Mean values of the turbidity data at the three study sites when grouped by month.

Table 11. Statistics of site 1 turbidity data by month.

Month	N	Mean	Geo Mean	Median	10%	90%	SD
Jan	2975	0.660685	0.515842	0.492236	0.253044	1.044852	0.877862
Feb	2661	0.581803	0.354689	0.397116	0.111736	0.926464	1.134626
March	2973	1.023566	0.689768	0.737220	0.212256	2.055780	1.193093
April	2872	1.911499	1.229089	1.289608	0.363708	3.937140	2.127092
May	2966	0.732540	0.475506	0.483260	0.176660	1.306700	1.128944
June	2878	0.721474	0.530680	0.506160	0.237444	1.219080	0.989732
July	2975	0.626089	0.419849	0.390440	0.167820	1.129396	0.951260
Aug	2837	0.828847	0.528518	0.474060	0.210408	1.646024	1.349321
Sept	1276	0.805067	0.619894	0.551020	0.364700	1.175740	1.368733
Oct	2874	0.860866	0.429809	0.505200	0.084720	1.772400	1.442765
Nov	2875	0.820444	0.437948	0.411148	0.130460	1.624088	1.462134
Dec	2969	0.763509	0.435590	0.440568	0.132456	1.377480	1.422775

Table 12. Statistics of site 2 turbidity data by month.

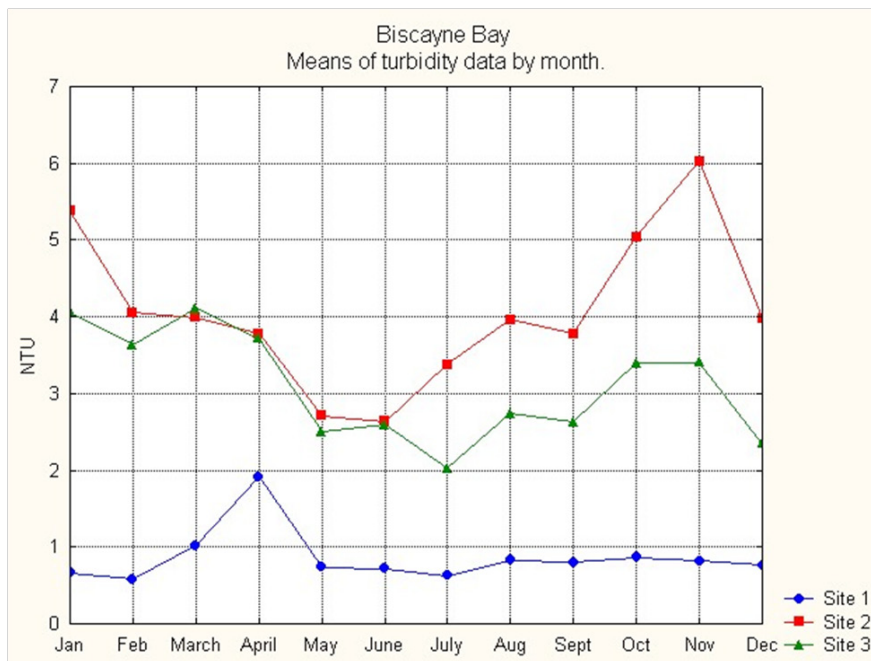| Month	N	Mean	Geo Mean	Median	10%	90%	SD
Jan	2952	5.377738	4.636724	4.611902	2.356192	9.274604	3.210109
Feb	2675	4.055728	3.537265	3.406412	1.935660	6.525528	2.627036
March	2968	3.991623	3.493049	3.363000	1.931520	6.800532	2.359278
April	2870	3.778900	3.286774	3.198100	1.719154	6.368950	2.323245
May	2972	2.709617	2.342718	2.234888	1.310236	4.430024	1.906334
June	2698	2.637873	2.360075	2.286800	1.381080	4.118480	1.577793
July	2974	3.373457	2.962692	2.861736	1.670584	5.467456	2.099757
Aug	2905	3.959884	3.407981	3.204036	1.811652	6.995796	2.562668
Sept	2877	3.782663	3.369267	3.181204	1.987788	6.244924	2.157230
Oct	2968	5.036724	4.361302	4.197882	2.296058	8.689922	3.068980
Nov	2097	6.026685	5.249740	4.965780	2.831260	10.40844	3.545855
Dec	1466	3.981081	3.410539	3.243560	1.782100	7.359980	2.559768

Table 13. Statistics of site 3 turbidity data by month.

Month	N	Mean	Geo Mean	Median	10%	90%	SD
Jan	2929	4.059682	3.741433	3.640552	2.393704	5.901816	2.036657
Feb	1761	3.635629	3.241160	3.049116	2.046984	5.573004	2.330549
March	1622	4.113330	3.675477	3.462166	2.128540	6.874540	2.262112
April	1658	3.718013	3.285818	3.041780	1.985808	5.986984	2.342532
May	2971	2.498768	2.299511	2.247312	1.462428	3.614760	1.259812
June	2129	2.589423	2.263075	2.101640	1.406260	3.895428	2.015390
July	2242	2.028455	1.935649	1.880096	1.403564	2.726612	0.751308
Aug	2915	2.736054	2.525658	2.457232	1.590288	4.075956	1.273198
Sept	2880	2.624803	2.347635	2.242588	1.383964	4.222748	1.548133
Oct	2966	3.398179	3.123829	3.083592	1.954504	5.064688	1.623630
Nov	2658	3.407954	3.205762	3.086470	2.253820	4.804144	1.416690
Dec	1437	2.348219	2.118513	2.067856	1.201276	3.601440	1.243012
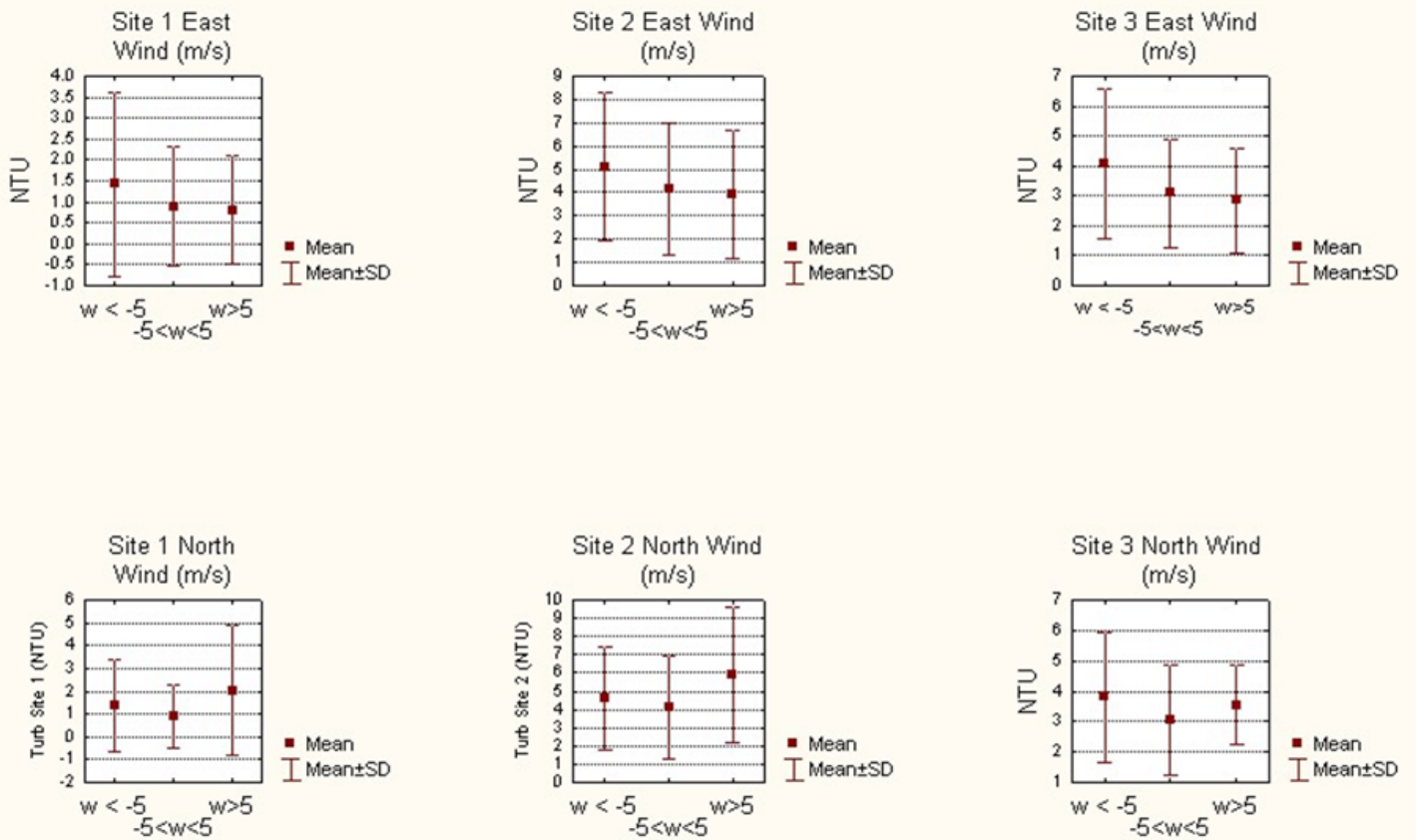
Figure 25. Box plots showing the mean and standard deviation for turbidity data categorized by east and north wind components less than -5 m/s, between -5 m/s and 5 m/s, and above 5 m/s. Wind data were recorded at the Virginia Key (VAKF1) weather station.

Table 14. Turbidity as a function of wind velocity. The mean value of the turbidity data is given when categorized by east and north wind velocities less than -5 m/s, those between -5 m/s and 5 m/s, and those above 5 m/s. The number of observations (N) for each category is also given.

	East < -5	-5 < East < 5	East > 5	North < -5	-5 < North < 5	North > 5
Site 1 turbidity	1.43	0.88	0.81	1.36	.86	2.03
N	667	28715	5309	1259	33364	66
Site 2 turbidity	5.11	4.17	3.94	4.62	4.12	5.87
N	429	27063	5844	1260	32019	55
Site 3 turbidity	4.08	3.1	2.87	3.8	3.05	3.56
N	359	22993	4880	995	27191	44
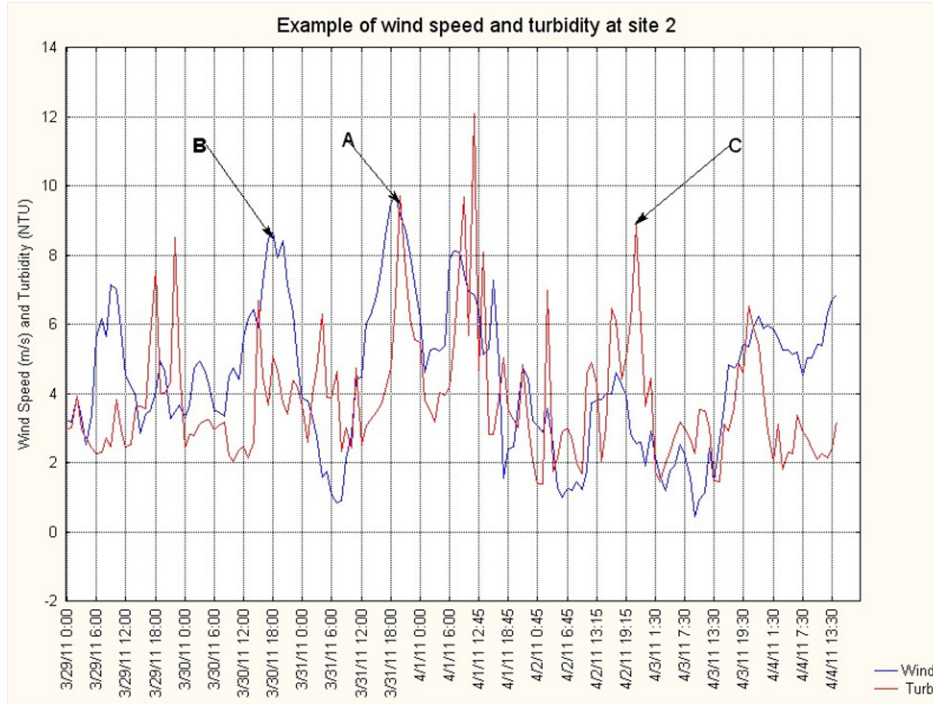
Figure 26. Wind speed from the Virginia Key (VAKF1) weather station and a 96-point running average of turbidity at site 2 for March 29-April 4, 2011. Point (A) shows a time when both turbidity and wind speeds are elevated, Point (B) shows a time when only wind is elevated, and point (C) shows a time when only turbidity is elevated.
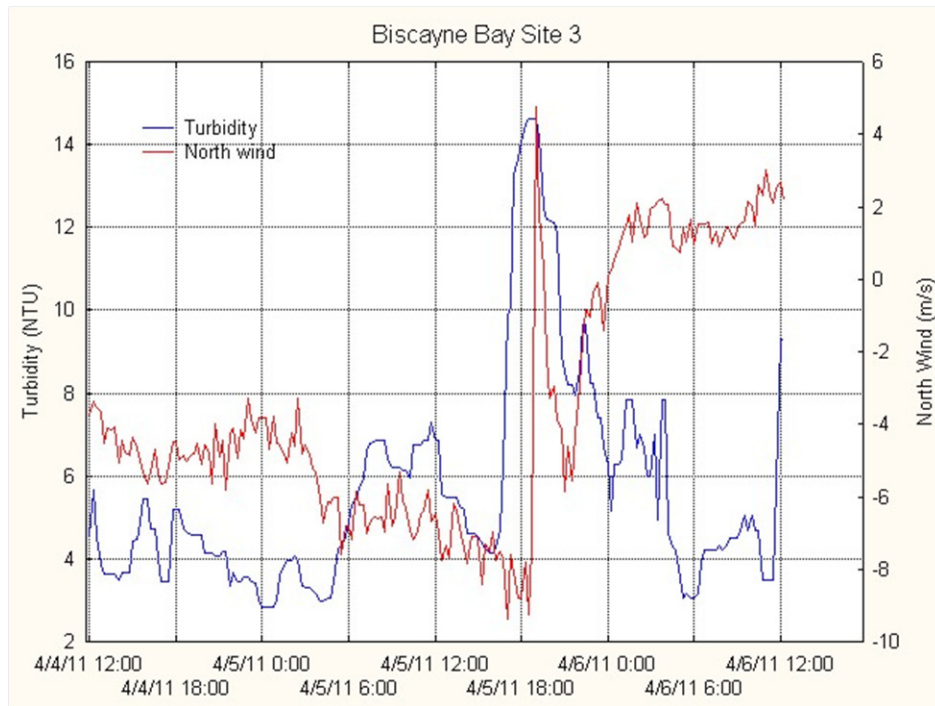
Figure 27. 96-point running averages of turbidity levels at site 3 with the north component of the wind recorded at the Virginia Key (VAKF1) weather station for April 4-6, 2011. As the north component reaches its maximum negative value (winds from the south) on April 5, 2011 at 18:00 UT, the turbidity levels increase significantly. After this time, the wind shifts direction and the turbidity levels are quickly reduced.

south wind was able to develop waves of a sufficient size to resuspend bottom sediments. In Figure 27, the north component of the wind changed sign at approximately 18:00 UT on April 5, 2011, and turbidity levels fell soon after this occurred (Figure 27).

3.4.8 Turbidity and Current Velocities

To examine the effect of currents on turbidity, chlorophyll-*a,* and CDOM, the currents were segregated into flood and ebb tidal phases. This was done as the flood and ebb tides may advect water masses with unique properties over the study sites. Certainly at site 2 it would be expected that on the flood tide, the influence of the oceanic water being advected into the bay would be noticeable. In all cases, there was a statistically-significant difference (p = 0.05) in the means of these variables when comparing the flood and ebb tidal phases; however, the differences were not large. Table 15 gives statistics of the current velocity and direction at each of the three sites segregated into flood and ebb tides. Tables 16, 17, and 18 give statistics of the turbidity, chlorophyll-*a*, and CDOM for all data at sites 1, 2, and 3 during the one-year period, the data during flood and ebb tides, and the data during the times when the currents exceeded the 75th percentile of the ebb and flood velocities. Segregating these parameters by the 75% percentile of the current velocity was done to show the effects of higher current velocities and to also isolate times when the water masses advecting over the study sites were more likely to possess the unique characteristics of a particular tidal phase.

Table 15. Currents during flood and ebb tidal phases.

	Directions Considered for Analysis	Mean Direction (°)	Mean Velocity (m/s)	Upper Quartile of Velocity (m/s)
Site 1 ebb	90-270	183	0.03	0.04
Site 1 flood	320-90	23	0.04	0.05
Site 2 ebb	15-115	65	0.1	0.13
Site 2 flood	225-325	268	0.08	0.1
Site 3 ebb	20-70	45	0.27	0.35
Site 3 flood	180-250	220	0.14	0.18

3.4.8.1 Turbidity and currents at site 1

At site 1, a small increase in turbidity was seen during the flood tide. This may be attributable to higher turbidity waters being advected from the southern margin of the basin, or possibly from the Intracoastal Waterway.

3.4.8.2 Turbidity and currents at site 2

At site 2, turbidity values were lower during the flood tide. This is consistent with less turbid oceanic water being advected across site 2 during the flood tide.

3.4.8.3 Turbidity and currents at site 3

At site 3, the turbidity levels were not significantly different between tidal phases.

3.4.9 Turbidity and Chlorophyll

During periods of high chlorophyll concentration, data from the turbidity sensors were elevated as well. The linear correlation (R) between chlorophyll and turbidity and turbidity at sites 1, 2, and 3 was 0.35, 0.28, and 0.14, respectively. All of these correlations are statistically significant (p = 0.05). Figure 28 shows the chlorophyll and turbidity levels at site 1 during a chlorophyll bloom. Visual observations of the water at site 1 during chlorophyll blooms revealed that the water was more visibly opaque. Table 18 indicates that chlorophyll values at site 3 are higher during an ebb tide, suggesting that chlorophyll values in the Bay waters south of site 3 are higher than those in the sites 2-3 basin.

3.4.10 Comparison with Other Turbidity Data Sets

The Miami-Dade County Department of Regulatory and Economic Resources (DRER) has maintained a program of turbidity monitoring in Biscayne Bay which extends back several decades. This extensive record was examined for comparison with the data collected during the present study. It should be noted that turbidity data from the present study were measured near the bottom of the water column, while the DRER measurements were made from water samples drawn from near the surface. Additionally, although the

Table 16. Turbidity, chlorophyll, and CDOM categorized by tidal phase and velocity at site 1. The mean value and standard deviation of turbidity, chlorophyll-*a*, and CDOM are calculated for the flood and ebb tidal phases and for the times when the current velocities are above the 75% velocity for that tidal phase.

Site 1	N	Mean Value	Standard Deviation
All data—turbidity (NTU)	34756	0.8818	1.4186
All data—chlorophyll (µg/l)	34756	1.0702	1.0173
All data—CDOM (ppb)	34756	14.2769	5.3279
Ebb tide—turbidity (NTU)	16938	0.8240	1.39765
Ebb tide—chlorophyll (µg/l)	16938	1.0381	0.96424
Ebb tide—CDOM (ppb)	16938	14.1557	5.28524
Flood tide—turbidity (NTU)	14665	0.96983	1.4656
Flood tide—chlorophyll (µg/l)	14665	1.13770	1.1087
Flood tide—CDOM (ppb)	14665	14.22687	5.4080
Ebb tide—velocity >75% turbidity (NTU)	4246	0.8463	1.46915
Ebb tide—velocity >75% chlorophyll (µg/l)	4246	1.0455	0.95857
Ebb tide—velocity >75% CDOM (ppb)	4246	13.9480	5.49672
Flood tide—velocity >75% turbidity (NTU)	4246	1.07169	1.61651
Flood tide—velocity >75% chlorophyll (µg/l)	4246	1.31920	1.29425
Flood tide—velocity >75% CDOM (ppb)	4246	13.53961	5.47794

Table 17. Turbidity, chlorophyll, and CDOM categorized by tidal phase and velocity at site 2. The mean value and standard deviation of turbidity, chlorophyll-*a*, and CDOM are calculated for the flood and ebb tidal phases and for the times when the current velocities are above the 75% velocity for that tidal phase.

Site 2	N	Mean Value	Standard Deviation
All data—turbidity (NTU)	33333	4.1407	2.8351
All data—chlorophyll (µg/l)	33333	1.0430	0.7547
All data—CDOM (ppb)	33331	7.0626	4.4174
Ebb tide—turbidity (NTU)	15836	4.25022	2.77094
Ebb tide—chlorophyll (µg/l)	15836	1.05874	0.91345
Ebb tide—CDOM (ppb)	15834	6.90647	4.09521
Flood tide—turbidity (NTU)	14230	3.9699	2.87027
Flood tide—chlorophyll (µg/l)	14230	1.0148	0.58245
Flood tide—CDOM (ppb)	14230	7.2619	4.87340
Ebb tide—velocity >75% turbidity (NTU)	4192	4.62200	2.92262
Ebb tide—velocity >75% chlorophyll (µg/l)	4192	1.08024	0.66554
Ebb tide—velocity >75% CDOM (ppb)	4191	7.28358	4.30022
Flood tide—velocity >75% turbidity (NTU)	3970	3.8317	2.73379
Flood tide—velocity >75% chlorophyll (µg/l)	3970	1.0250	0.48239
Flood tide—velocity >75% CDOM (ppb)	3970	7.5038	5.28851

Table 18. Turbidity, chlorophyll, and CDOM categorized by tidal phase and velocity at site 3. The mean value and standard deviation of turbidity, chlorophyll-*a*, and CDOM are calculated for the flood and ebb tidal phases and for the times when the current velocities are above the 75% velocity for that tidal phase.

| Site 3	N	Mean Value	Standard Deviation
All data—turbidity (NTU)	28229	3.0745	1.81357
All data—chlorophyll (µg/l)	28229	1.1681	3.35093
All data—CDOM (ppb)	28228	8.5941	4.91754
Ebb tide—turbidity (NTU)	12765	3.07497	1.78344
Ebb tide—chlorophyll (µg/l)	12765	1.07064	3.24558
Ebb tide—CDOM (ppb)	12764	8.34975	4.57568
Flood tide—turbidity (NTU)	11074	3.0484	1.89294
Flood tide—chlorophyll (µg/l)	11074	1.2732	3.60115
Flood tide—CDOM (ppb)	11074	8.9048	5.53132
Ebb tide—velocity >75% turbidity (NTU)	3375	3.57475	2.11960
Ebb tide—velocity >75% chlorophyll (µg/l)	3375	1.08395	2.96626
Ebb tide—velocity >75% CDOM (ppb)	3374	8.15345	4.18253
Flood tide—velocity >75% turbidity (NTU)	2980	3.1814	1.857881
Flood tide—velocity >75% chlorophyll (µg/l)	2980	1.4240	5.266785
Flood tide—velocity >75% CDOM (ppb)	2980	8.2561	5.346051
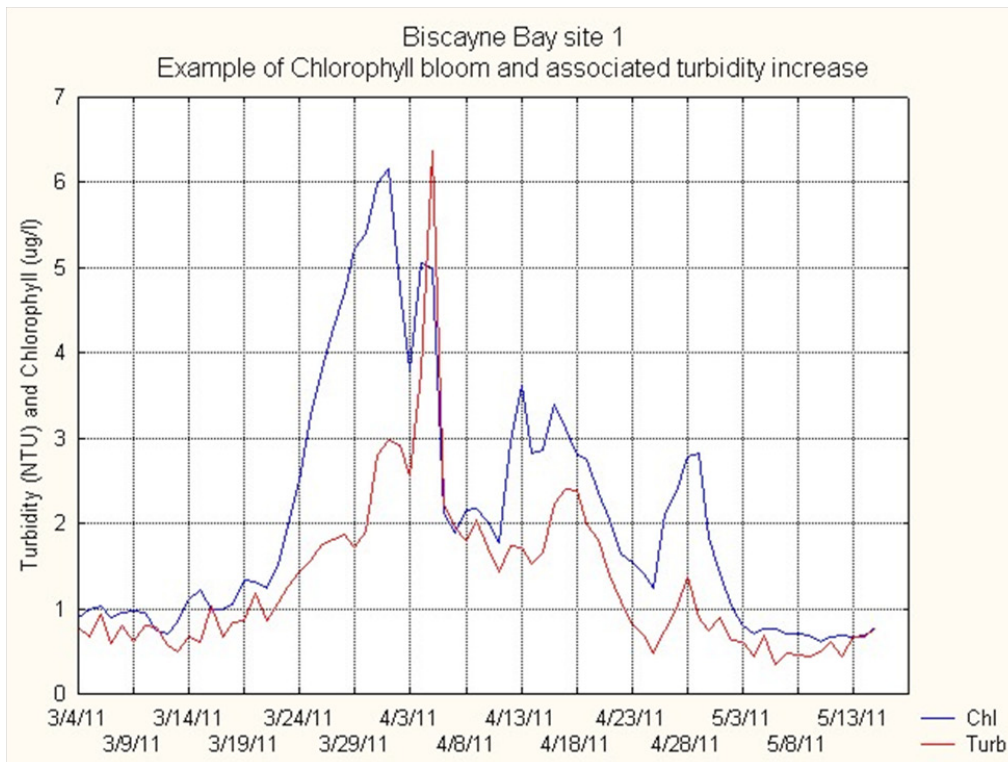
Figure 28. Chlorophyll-*a* and turbidity levels (both traces are 96-point running averages) at site 1 for the period March 4-May 15, 2011. A chlorophyll bloom is observed during this period, and turbidity values are also elevated.

DRER samples were taken at locations near the sites occupied for the present study, if persistent gradients in turbidity exist across the study areas, small differences in the two data sets would be expected. DRER data from 1979 through 2011 are presented with turbidity data greater than 25 NTU excluded from the analysis, as was done with the data from the present study. Table 19 gives statistics about the DRER data, i.e., the location of the three DRER sites chosen for comparison and the distance separating the DRER stations from the three sites in the present study. The mean and standard deviation for the DRER turbidity data collected between 1979 and 2011 are presented in Figure 29.

Figure 29. Mean and standard deviation of DRER turbidity data collected at three sites between 1979 and 2011. DRER site 14 is in the vicinity of study site 1. DRER sites 22 and 26 are located in the basin where sites 2 and 3 are located. Note the DRER data were collected near the surface, whereas turbidity data for the present study were collected near the bottom. Turbidity values greater than 25 NTU are excluded.

3.5 Total Suspended Solids

During visits to the monitoring sites, water samples were collected near the surface and at the depth of the sensor platform. These water samples were analyzed for TSS concentration, expressed in milligrams per liter. The mean, standard deviation, and minimum and maximum values for TSS are shown in Figure 30 and given in Table 20. The differences between the surface and bottom samples are not large, with the bottom values being 8%, 12%, and 5% higher for sites 1, 2, and 3, respectively. TSS at sites 2 and 3 are similar in value, with the average top TSS value at site 2 being 2% higher than at site 3 and the average TSS bottom value at site 2 being 9% higher than at site 3.

3.5.1 TSS and Turbidity

Turbidity data from the bottom-mounted instruments recorded at the time closest to the collection of the TSS samples show similar trends and features (Figure 31). Figure 31 shows that top and bottom TSS measurements are typically similar in value. The linear correlations between
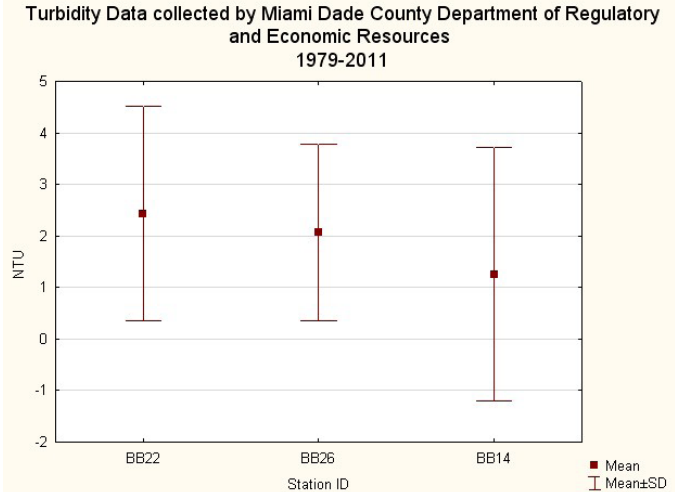
TSS and turbidity at sites 1, 2, and 3 are R = 0.95, R = 0.71, and R = 0.74, respectively. For each of the measurements, the ratio of turbidity to TSS was calculated. These ratios are presented with the statistics for the TSS and turbidity recorded at each site and for the combined data from sites 2 and 3 (Table 20) and shown graphically in Figure 32. To examine the relation between TSS and turbidity, TSS is plotted as a function of turbidity with a line drawn on the graph that represents the mean of the ratios of TSS to turbidity. This is done for site 1 (Figure 33) and for the combined data from sites 2 and 3 (Figure 34). It must be remembered that turbidity is an optical property of the water based on the scattering of light from particles, whereas

Table 19. Turbidity data collected by the Miami-Dade County Department of Regulatory and Economic Resources from 1979 to 2011. Turbidity values greater than 25 NTU are excluded.

Site ID	Mean Turbidity (NTU)	N	Standard Deviation	Distance from Site 1 (km)	Distance from Site 2 (km)	Distance from Site 3 (km)
BB14	1.26	240	2.45	1.3	NA	NA
BB22	2.44	326	2.08	NA	1.46	1.0
BB26	2.07	327	1.71	NA	2.9	0.5

Table 20. TSS from water samples and turbidity data. Shown are TSS from water samples at the surface and bottom and the turbidity values measured by the bottom-mounted instruments at the time of sample collection.

Sample Location	Mean Turbidity (NTU)	Standard Deviation of Turbidity	Mean TSS (mg/l)	Standard Deviation of TSS	Mean Ratio of NTU/TSS	Number of Samples
Site 1 top	na	na	0.953	0.0848	na	21
Site 1 bottom	0.905	1.237	1.029	1.107	0.8075	18
Site 2 top	na	na	2.420	1.200	na	23
Site 2 bottom	3.924	2.032	2.704	0.944	1.364	22
Site 3 top	na	na	2.373	0.985	na	22
Site 3 bottom	3.185	1.094	2.487	1.089	1.346	22
Sites 2-3 top	na	na	2.397	1.088	na	45
Sites 2-3 bottom	3.554	1.656	2.596	1.036	1.355	44
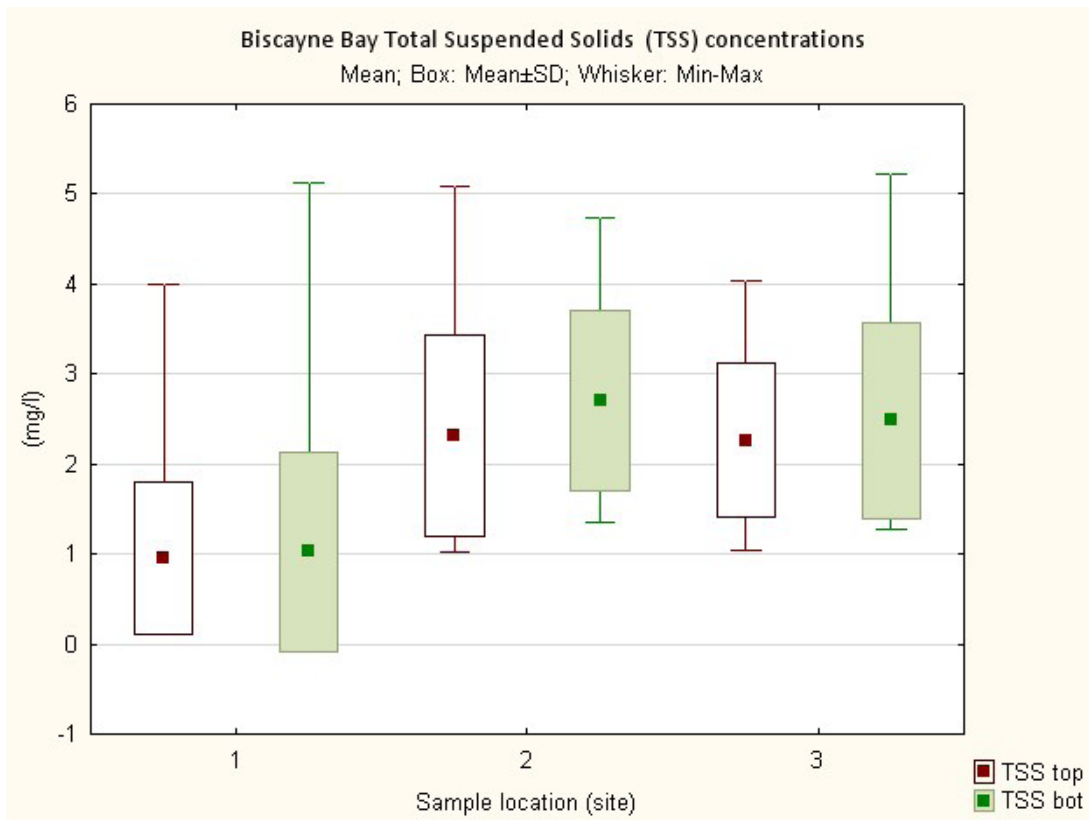
Figure 30. Mean, standard deviation, and minimum-maximum values from surface and bottom TSS samples from the three study sites.
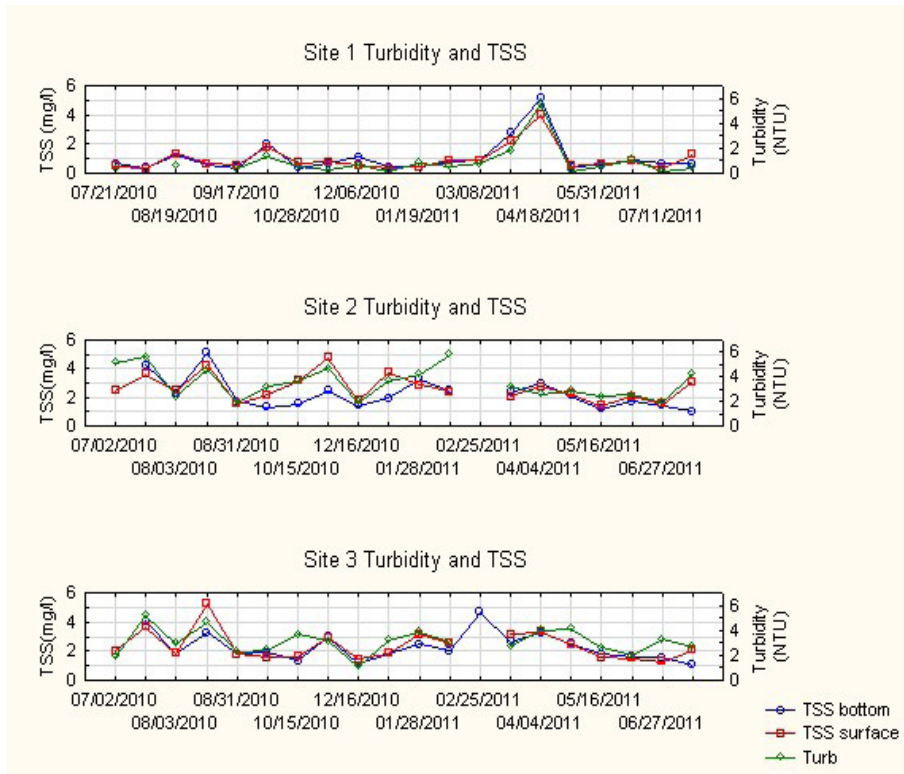
Figure 31. Time series of TSS concentrations from water samples at the bottom and surface with turbidity from the bottom-mounted sensor.
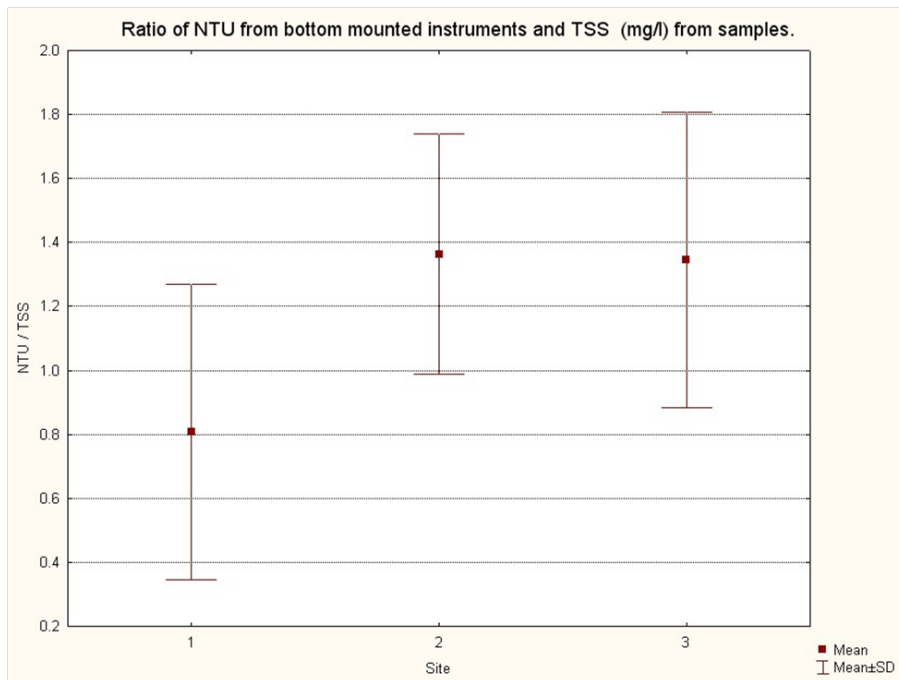

Figure 32. For each of the bottom TSS samples collected during the study, the corresponding turbidity value from the bottom-mounted instruments was extracted. The ratio of NTU/TSS was calculated. The mean and standard deviation of NTU to TSS ratio for the three study sites are shown.
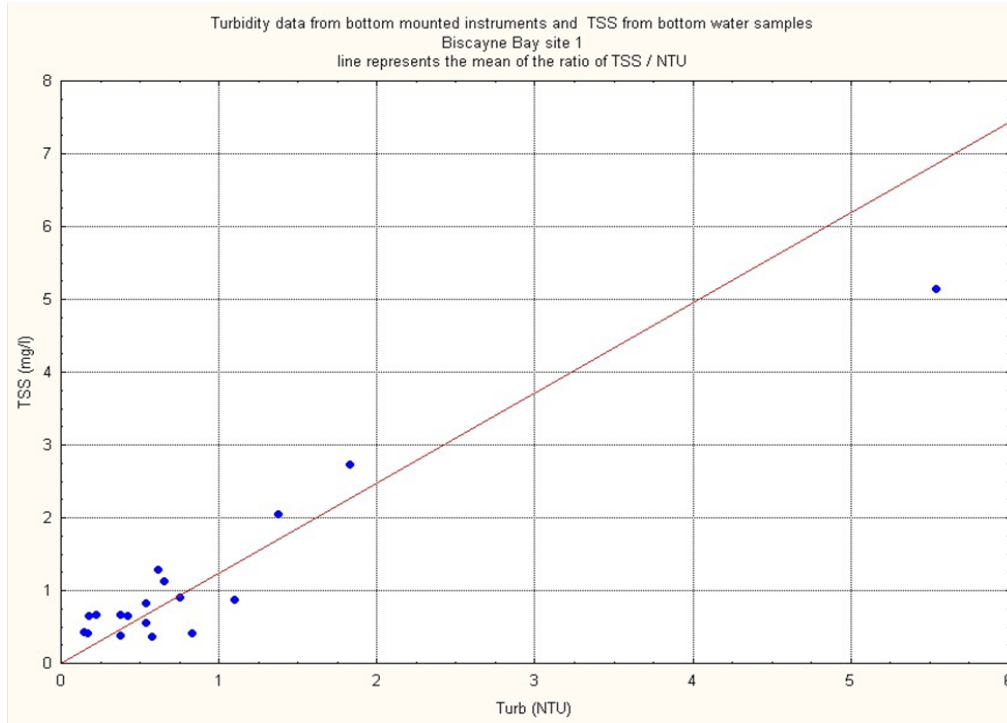
Figure 33. Scatter plot of TSS versus NTU with a line representing the mean of the ratios of TSS/NTU for all data collected at site 1.
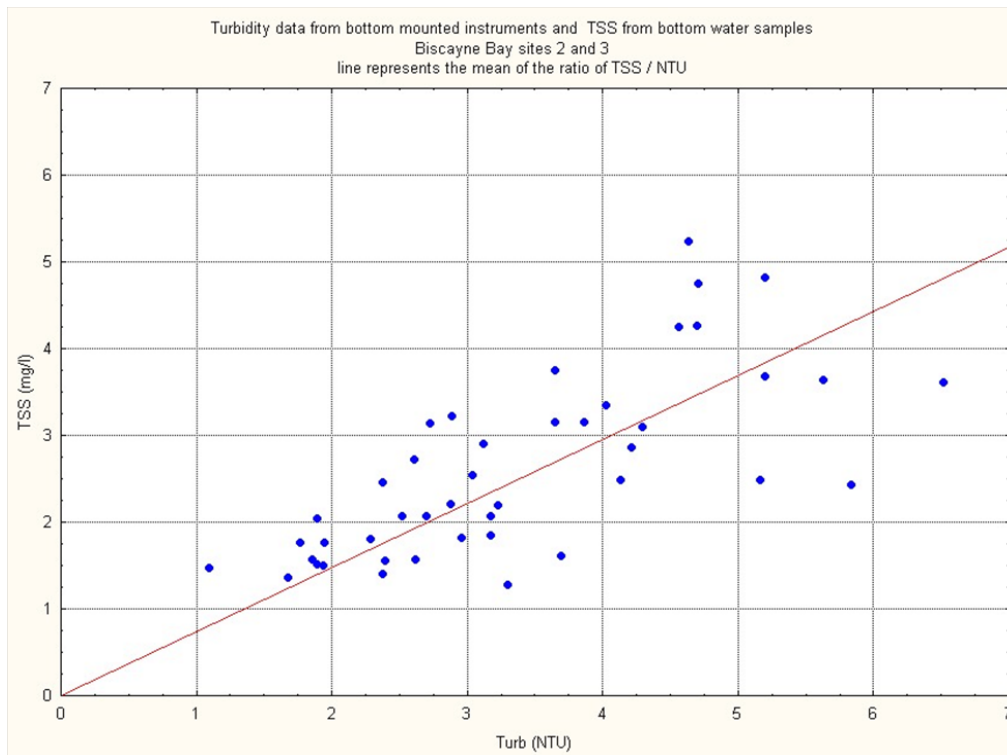

Figure 34. Scatter plot of TSS versus NTU with a line representing the mean of the ratios of TSS/NTU for all data collected at sites 2 and 3.

TSS is the weight of the suspended particles in the water per unit volume. There is no presumption that TSS and turbidity have any intrinsic relationship. Previous studies have observed that the relationship between turbidity and TSS in Biscayne Bay is variable (Wanless *et al.*, 1984).

3.6 Salinity

Unfortunately, several difficulties were experienced using the conductivity sensor. Unrealistic values of conductivity were seen during the first deployments of the instruments. After conversations with the manufacturer, it was determined that the manner in which the instrument was mounted needed to be changed. This was done, and data quality improved immediately. Data quality was also affected by fouling of the sensor. The manufacturer adamantly advised against placing any anti-fouling materials or barriers near this instrument. Fouling of the sensor (particularly at site 1 where it was suspected that small fish and crabs inhabited the sensor) was a persistent problem, and much of this data had to be flagged as bad. To generate a data product that illustrates the salinity levels at the study sites, the salinity data were edited and smoothed. Figure 35 shows the salinity levels at site 1, and Figure 36 shows the salinity levels for sites 2 and 3. As the site 1 location is somewhat isolated from oceanic water, freshwater input from precipitation might be expected to lower salinities in this basin. Figure 37 shows the salinity levels at site 1 with the cumulative precipitation recorded at Miami International Airport (12 km inland) for the site 1 analysis year. From Figure 36 it can be seen that precipitation does lower salinity levels at site 1.

3.7 Colored Dissolved Organic Matter

CDOM levels during the analysis year for site 1 are shown in Figure 38. At all three sites, CDOM and salinity showed statistically-significant ($p = 0.05$) (anti) correlations ($R = -0.82$, $R = -0.80$, and $R = -0.73$ for sites 1, 2, and 3, respectively). It is thought that during rain events freshwater runoff from inland areas brings CDOM-laden water into the site 1 basin. Figure 39 shows CDOM and salinity at site 1, plotted for the analysis year. CDOM levels for the analysis year at sites 2 and 3 are presented in Figure 40.
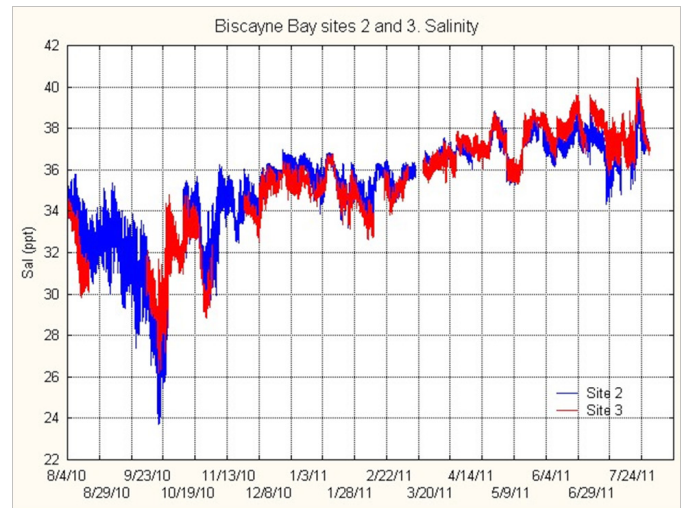

Figure 35. Salinity at site 1.

Figure 36. Salinity at sites 2 and 3.

3.8 Temperature

Figure 41 shows the temperature for the analysis year at site 1. Bay water at this site responded rapidly to changes in air temperature and reached a minimum temperature of 12.5°C during December 2010. Figure 42A shows the temperature for the analysis year at sites 2 and 3. These data are from the CT sensor, except for the period at site 3 when the CT sensor was not functioning. For this period, the data from the C6 temperature sensor were used. The water temperature at site 1 showed a more rapid response to the changes in air
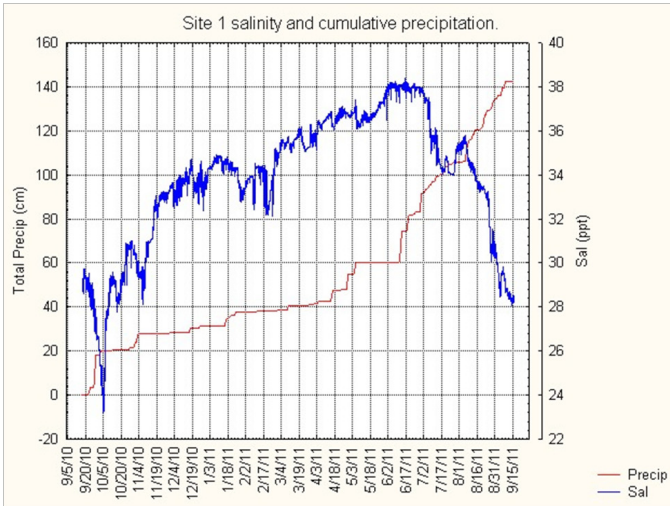
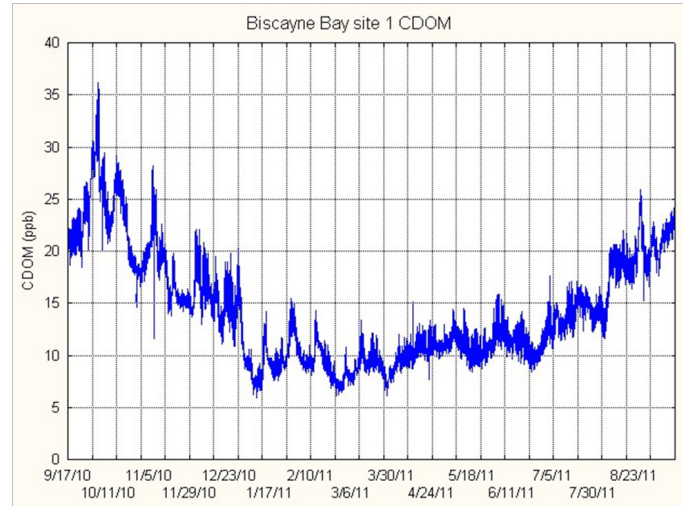**Figure 37.** Salinity at site 1 and cumulative precipitation at Miami International Airport.
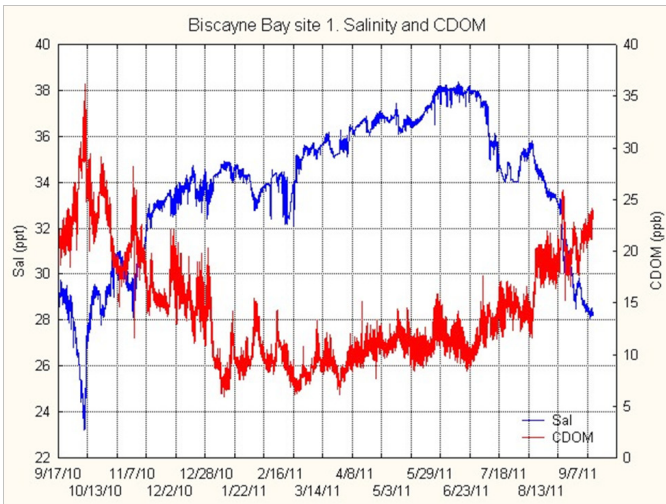

Figure 38. CDOM at site 1.

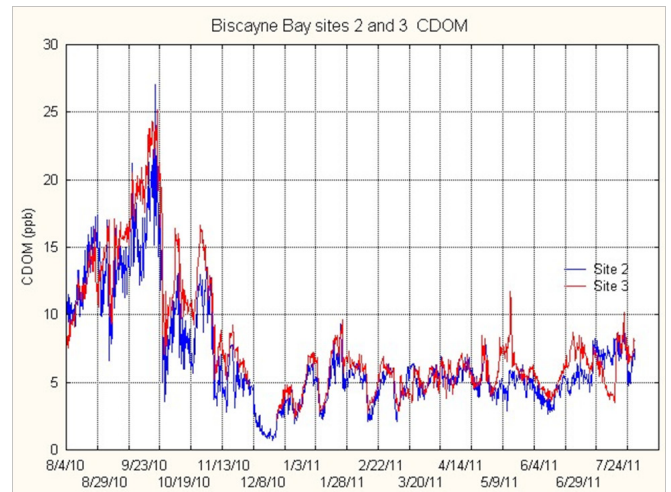**Figure 39.** CDOM and salinity at site 1. Salinity and CDOM are correlated at R = -0.83.

Figure 40. CDOM at sites 2 and 3.
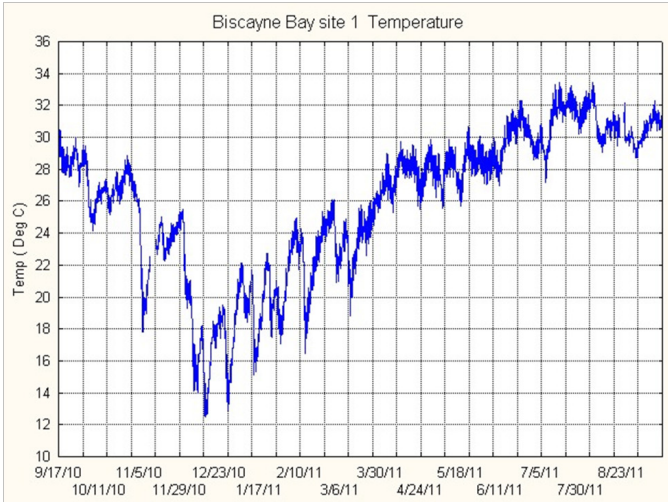
Figure 41. Temperature at site 1.

Figure 42A. Temperature at sites 2 and 3.

temperature during the passage of cold fronts. This is attributable to the shallow water depths and the relative isolation of site 1 from oceanic waters as compared to sites 2-3 (Figure 42B).

3.9 Scanning Electron Microscopy Particulate Analysis

SEM analysis of water samples collected at the surface and bottom during the visits was accomplished by manual (particulate identification) and automated (Image-J) analysis of the SEM images. Estimates of particle loading in MPL, average particle areas, and the distribution of the particle areas into seven size classes were conducted (see section 2.6.3). Although over 20 identification categories were observed, only selected particulate categories were compared for the purposes of this study. These included the relative abundance of centric diatoms, centric fragments, pennate diatoms, fecal pellets, fecal fragments, and dinoflagellates. Additional detailed species identifications are presented for selected images. These assessments were compared to measurements taken with the bottom-mounted instruments and meteorological data related to the study area. Specifically, the chlorophyll-*a* fluorescence and turbidity measurements from the bottom-mounted sensors were used to estimate the onset, magnitude, and cessation of the phytoplankton blooms and to examine the relationship between the SEM observations and turbidity levels.
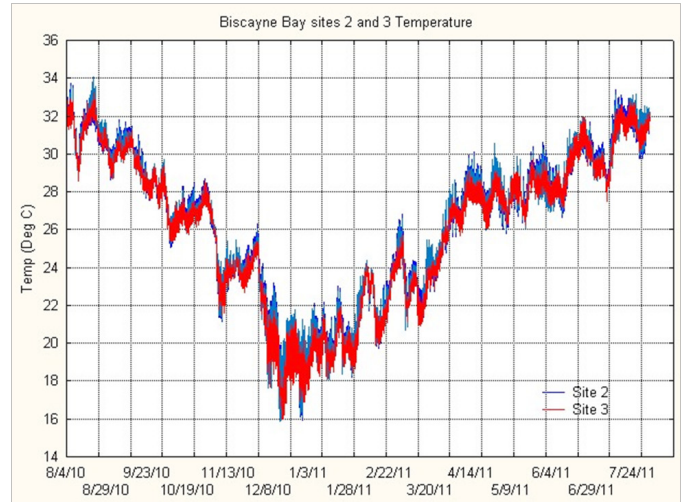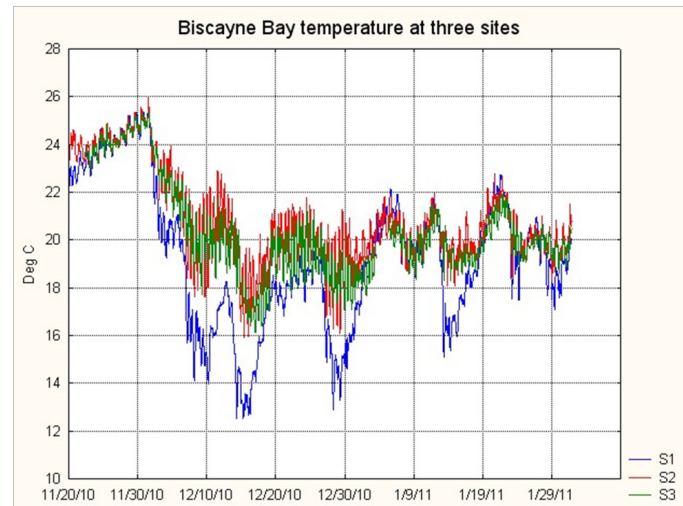

Figure 42B. Subset of temperature data from the three study sites showing more rapid cooling at site 1 after the passages of cold fronts.

Although site 1 is physically separated from the sites 2 and 3 basin, SEM analysis suggests that, despite differences between the two basins, many of the trends observed occur concurrently in both basins, indicating these phenomena are not site specific.

3.9.1 SEM Data Overview

This section presents the results of the SEM analysis and selected data from other sources (Figures 43-58). These results and data illustrate trends and specific events that are subsequently discussed in detail. The combined turbidity
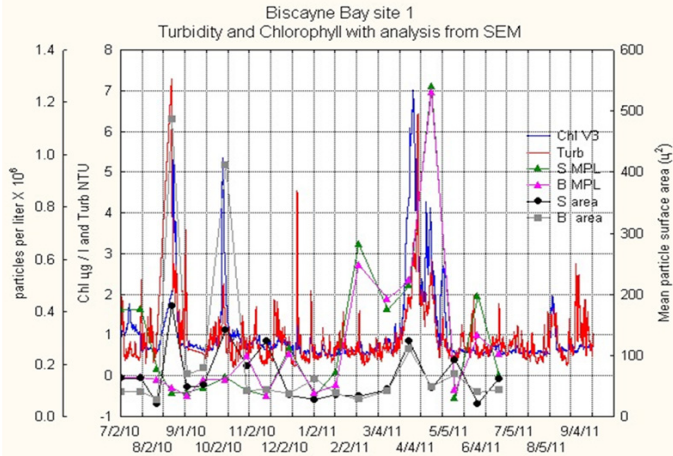
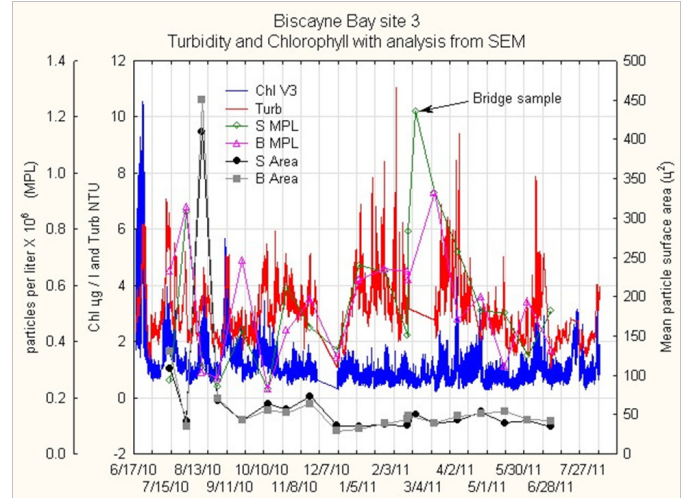**Figure 43.** Chlorophyll, turbidity, and particulate analysis at site 1.

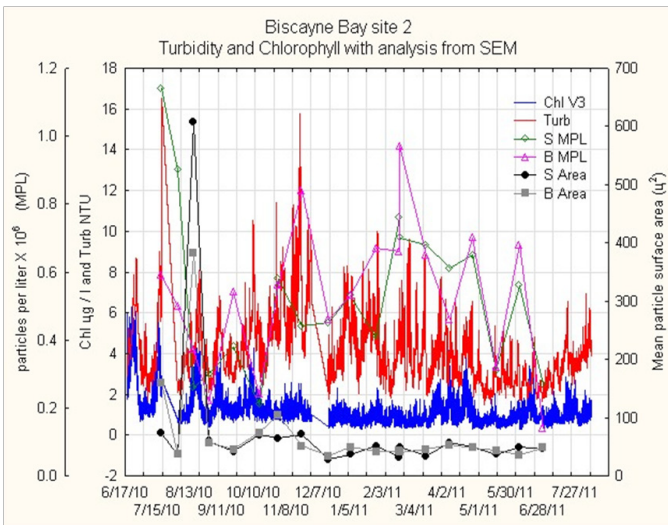**Figure 44.** Chlorophyll, turbidity, and particulate analysis at site 2.

Figure 45. Chlorophyll, turbidity, and particulate analysis at site 3.

and chlorophyll data from the bottom-mounted sensors with the mean particle area and MPL estimates are shown (Figures 43-45). Presented next are the particle size class distributions for the sample data (Figures 46-48). The distribution data are presented in two ways. First, the absolute number of particles in each size class for a particular sample is presented. Secondly, the number of particles in each size class is normalized by the total number of particles in that sample so that a relative particle size distribution could be generated. Examples of the images created by the SEM are shown in Figures 49 and 50. The results of the particulate identification for the surface samples are shown

in Figures 51-56. Chlorophyll concentrations from the bottom water samples are presented in Figure 57, and the cumulative rain precipitation data recorded at Miami International Airport are presented in Figure 58.

Chlorophyll-*a* and turbidity data from the bottom-mounted instruments (Figures 43-45) showed periods of elevated chlorophyll and turbidity that were largely synchronous with a higher than average number of particles and/or higher than average particle loading. Chlorophyll-*a* concentrations from water samples at the three study sites showed four distinct peaks (Figure 57). These peaks occurred in the July 16, 2010 sample at sites 2 and 3, the August 19, 2010 and August 17, 2010 samples at sites 1, 2, and 3, respectively, the October 18, 2010 sample at site 1 (with a broader elevation in chlorophyll at sites 2 and 3), and the March 28, 2011 and April 4, 2011 samples at site 1 and sites 2-3, respectively.

At site 1, particulate size distribution data confirmed the presence of larger particles in the surface and bottom water during the chlorophyll peaks observed on August 19, 2010, October 8, 2010, and March 28, 2011 (Figure 46). Particle characterization of these samples revealed a high concentration of large centric diatoms (Figure 49). Centric diatoms comprised from 18-55% of the particulates over three intervals of bloom conditions (Figure 51). The turbidity extremes recorded at site 1 were clearly associated with diatom blooms.
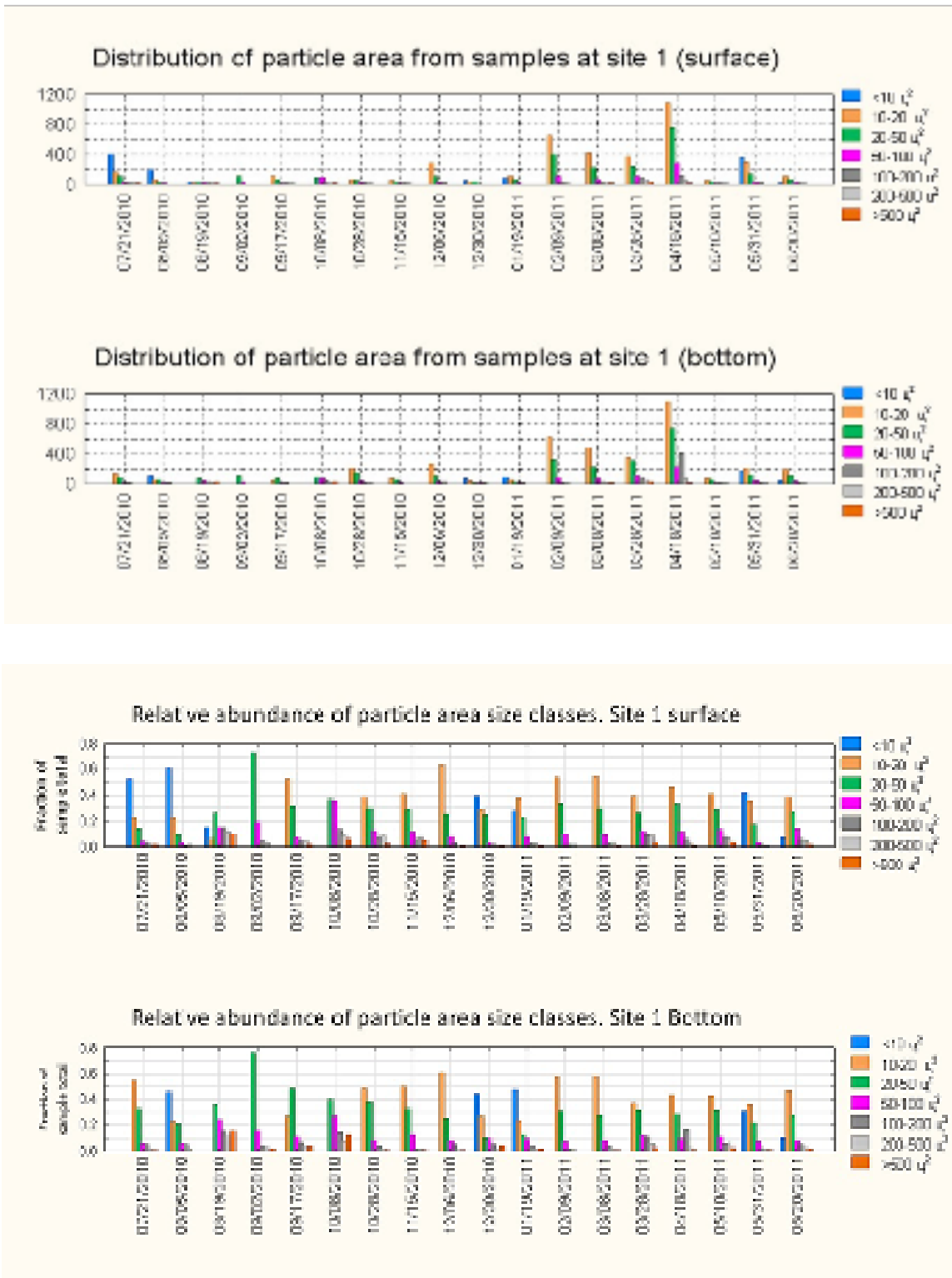
Figure 46. Absolute and relative size class abundances for site 1 during July 2010-June 2011.
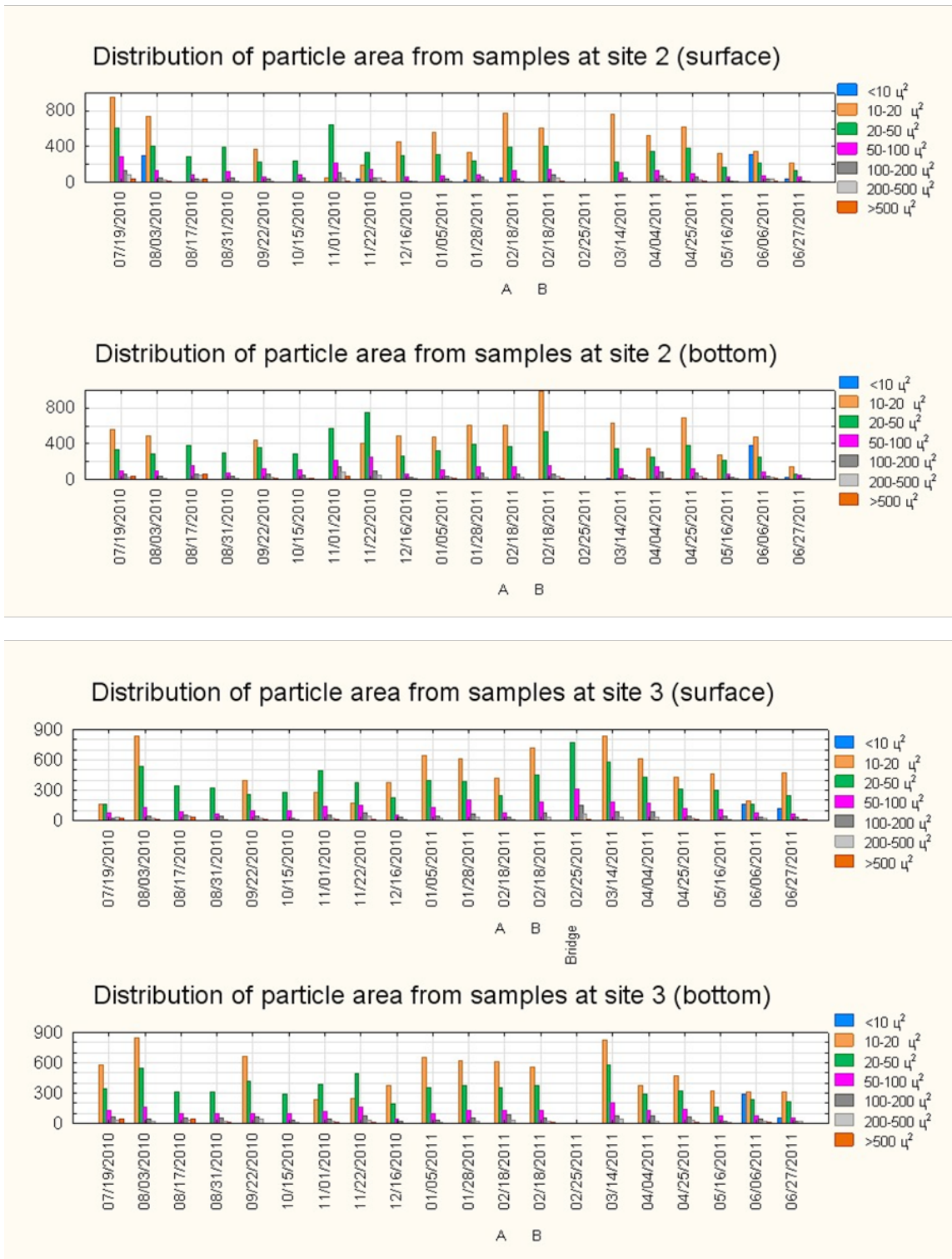
Figure 47. Distribution of particle area in surface and bottom samples for sites 2 and 3 during July 2010-June 2011.
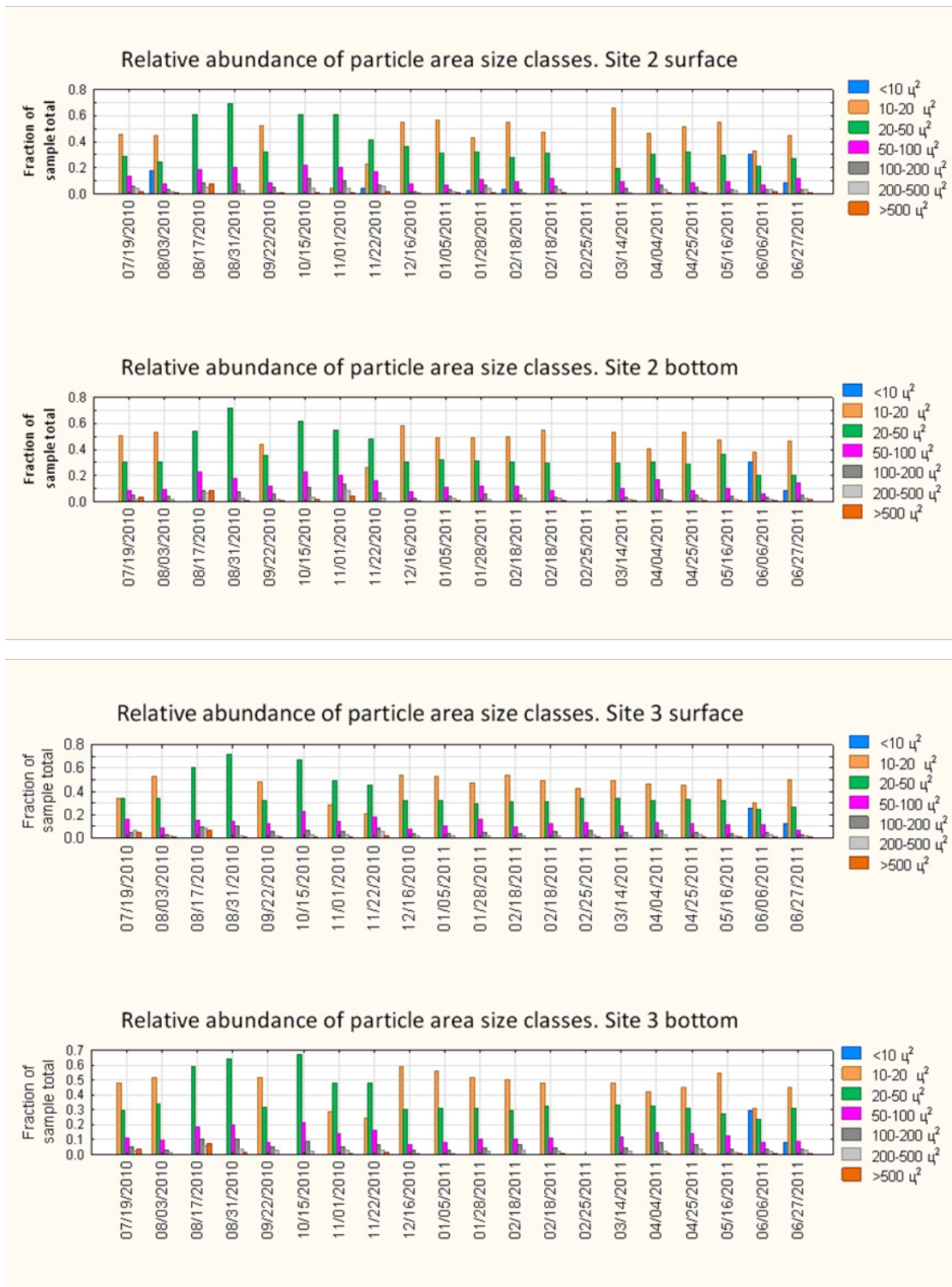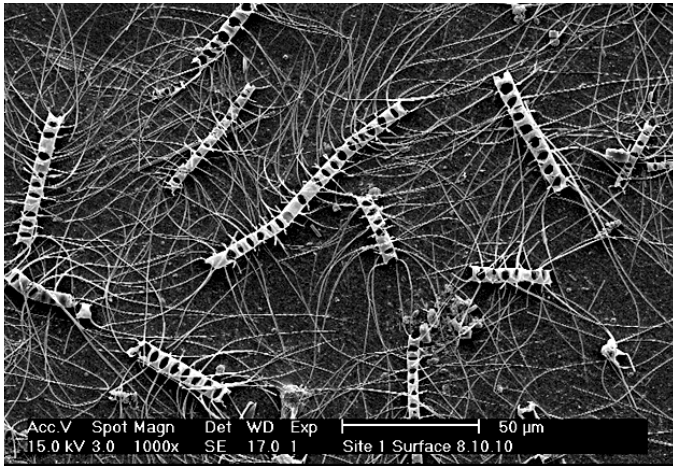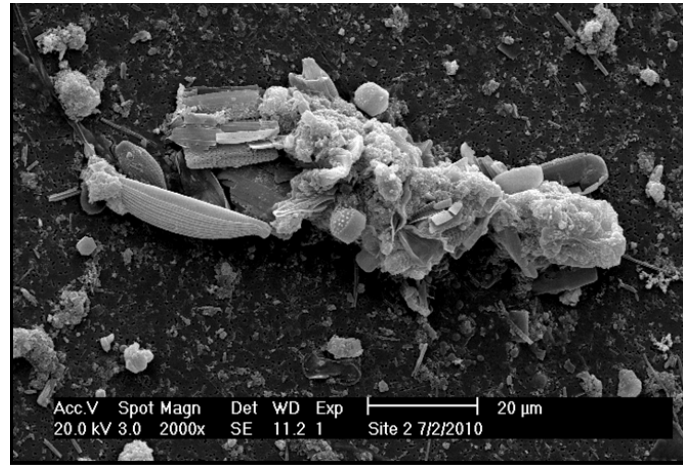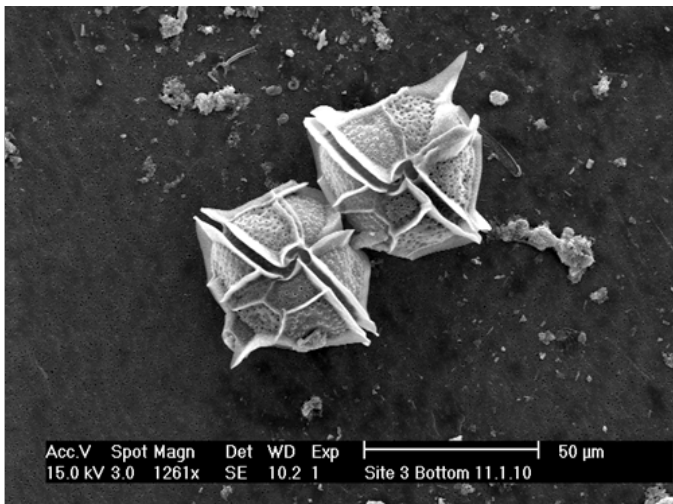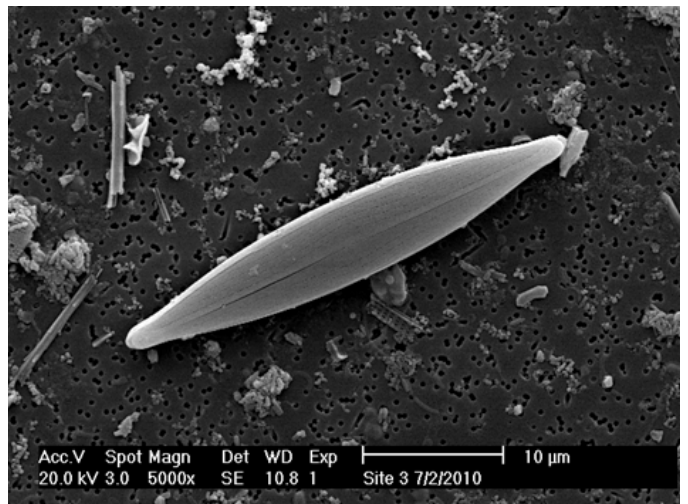
Figure 48. Relative abundance of particle area in surface and bottom samples for sites 2 and 3 during July 2010-June 2011.

Centric diatom *Chaetoceras* sp.

Fecal pellet

Figure 49. Examples of centric diatoms and fecal pellets.

A fully-developed dinoflagellate (*Pyrodinium bahamense*)

Pinnate diatom

Figure 50. Examples of dinoflagellates and pinnate diatoms.

At sites 2 and 3, the samples collected on August 17, 2010, April 4, 2011, and April 25, 2011 contained a large number of centric diatoms coincident with the diatom blooms observed at site 1. The peak in chlorophyll observed at sites 2 and 3 in the July 19, 2010 samples and a broad peak in chlorophyll and turbidity observed during October and November 2010 were not as clearly associated with the data at site 1. Site-specific differences in particulate loading over time were evident with average turbidity levels at sites 2 and 3 higher than at site 1. Site 1 particulate distributions appeared to be in-situ productivity related. In contrast, sites 2 and 3 contained a subset of particulates likely not produced

on site. Water velocities at sites 2 and 3 were significantly higher than at site 1, and resuspension of bottom sediment due to higher water velocities would be expected as a result.

The results for sites 2 and 3 are generally similar in terms of mean particle size, size distribution and particle loading (Figures 44, 45, 47, and 48), and particle identification (Figures 51-56), although some differences were seen. These differences may be explained by the differing depths at the two sites, the proximity of site 2 to the open ocean, and the differing tidal velocities present at the two sites. In addition, although samples from sites 2 and 3 were collected on the same day and usually within one hour of each other, the
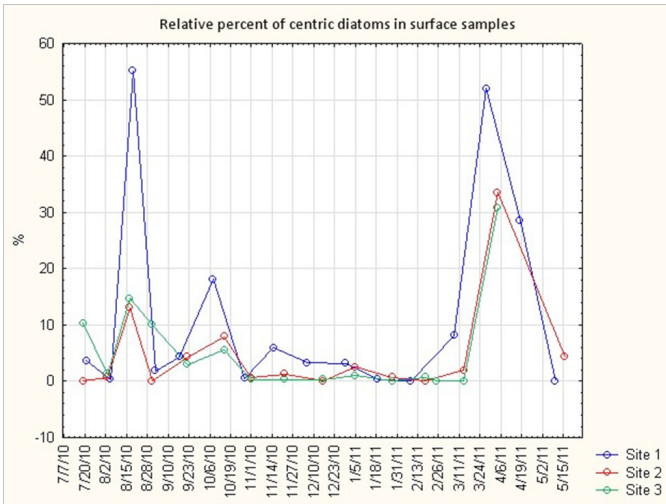
Figure 51. The relative abundance of centric diatoms collected in surface samples.
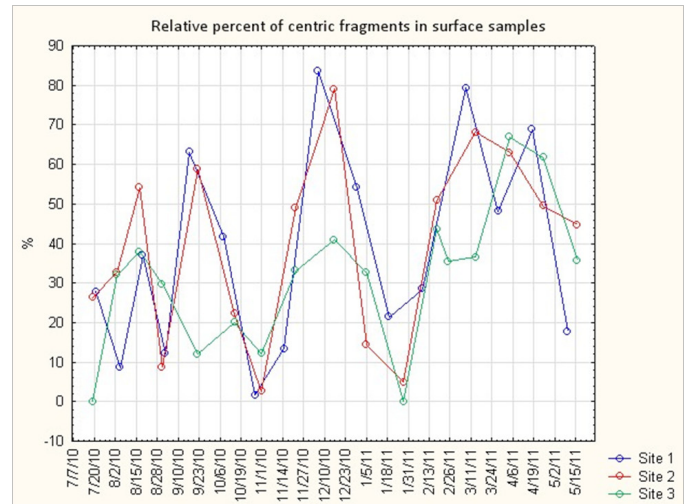
Figure 52. The relative abundance of centric fragments collected in surface samples.

Figure 53. The relative abundance of fecal pellets collected in surface samples.

Figure 54. The relative abundance of fecal fragments collected in surface samples.

Figure 55. The relative abundance of pennate diatoms collected in surface samples.

Figure 56. The relative abundance of dinoflagellates collected in surface samples.
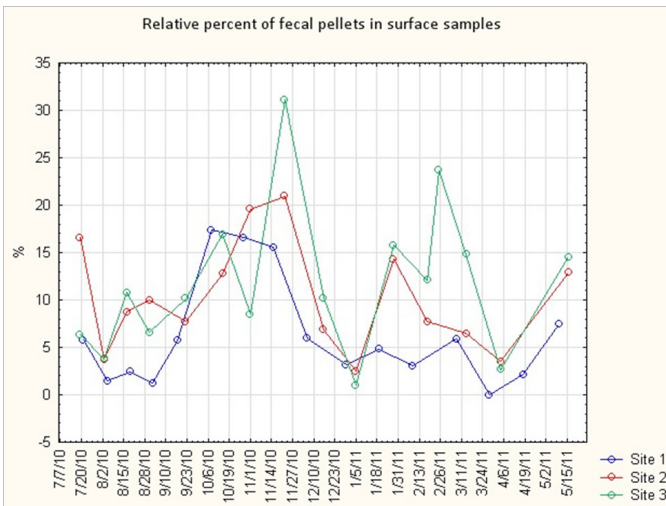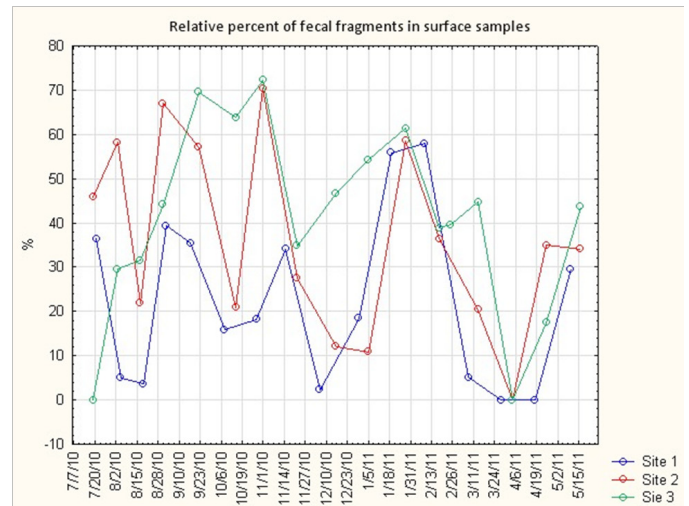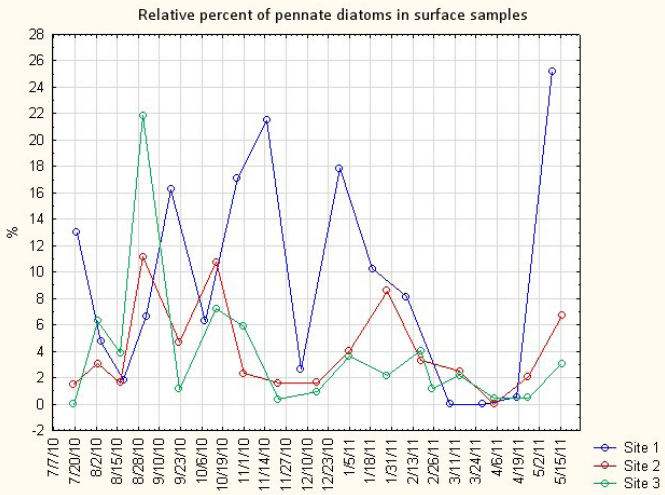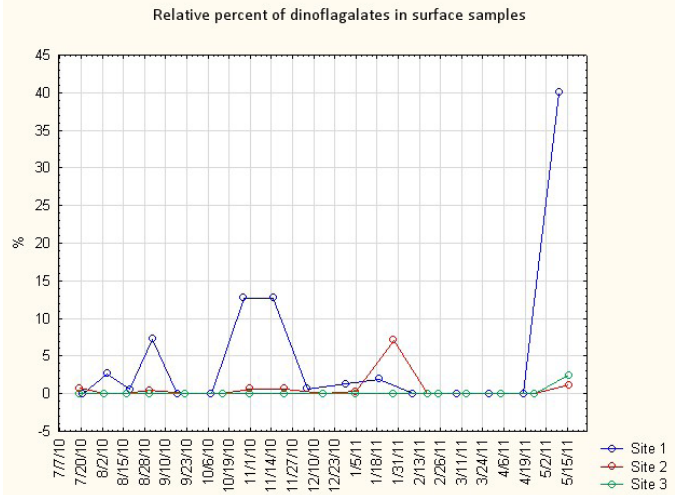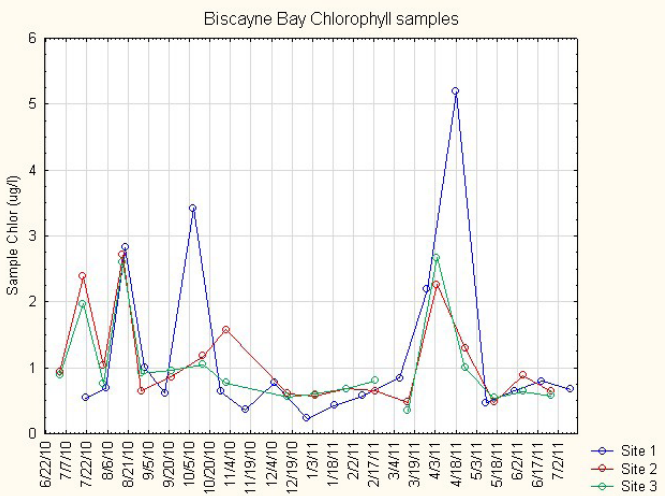

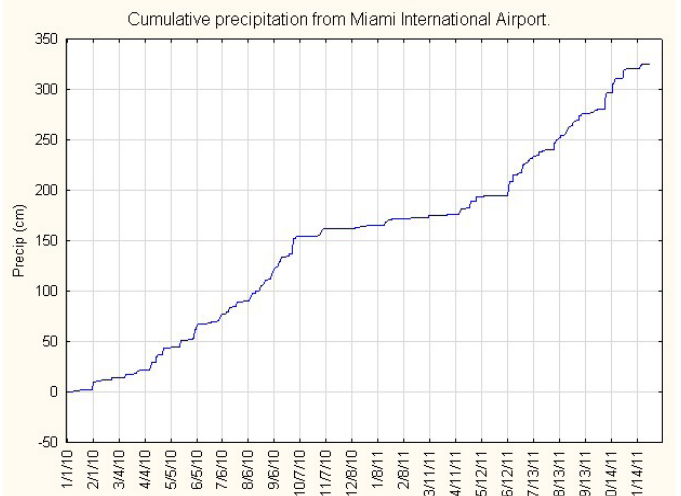**Figure 57.** Chlorophyll concentrations from water samples.

Figure 58. Cumulative precipitation rates recorded at Miami International Airport.

site 3 samples were typically collected at the slack of the tide. This was done to enhance safety during the instrument exchange. Therefore, water was collected from site 2 at some other point in the tidal cycle.

It has been observed that eutrophication from freshwater runoff is a likely cause of higher abundances of phytoplankton in northern Biscayne Bay (Brand *et al.*, 1991). In particular, runoff after the first significant rain following a dry period can initiate a phytoplankton bloom. This appears to be confirmed in the April 2011 samples which show a bloom developing at all three sites shortly after rainfall at the end of the dry season (Figures 58 and 51). Sampling in 2010 began after the onset of the rainy season, and significant rain events were observed to precede the onset of the major 2010 diatom bloom. The following is a discussion of specific samples of particular interest.

3.9.2 Specific Examples

July 19, 2010 (sites 2 and 3): The SEM data suggest that sites 2 and 3 were likely experiencing the end of a diatom bloom on July 19, 2010. This conclusion is based on the trend of the chlorophyll signal, the high percentage of centric and fecal fragments contained in the samples (Figures 52 and 54), and the observation that the setae of the centric diatoms in the images were broken or missing in some cases, suggesting that the diatoms were no longer living when sampled (Figure 59). The number of particulates in the surface and bottom water at site 2 was 1.14 and 0.59 MPL, respectively (Figures 47 and 48). The number of particles in the surface water sample at site 2 on this date contained the highest concentration in the site 2 data set. The size distributions for sites 2 and 3 at the surface were quite different. The site 2 surface sample had 954 particles in the 10-20 μ^2 class, whereas the site 3 surface sample had 156 particles in the 10-20 μ^2 class.

At this time, the surface water at site 3 contained approximately 25% fewer particles (0.26 MPL) than did site 2 (1.14 MPL). As is evident in the SEM images (Figure 59), there appears to be a difference in the number and size of centric diatom fragments in these samples. The size distributions for sites 2 and 3 at the surface were also quite different. As mentioned above, the site 2 surface sample contained many more particles in the 10-20 μ^2 class than did site 3. Interestingly, the bottom water at sites 2 and 3

contained a similar number of particles (0.59 and 0.65 MPL, respectively). The overall distribution of these size classes and number is confirmed by the SEM images (Figure 59) and appears to be related to the size and number of the centric diatom population. Chlorophyll-*a* and turbidity levels were significantly above the baseline at both sites 2 and 3 (Figures 44 and 46), coincident with the observation of centric diatoms visible in the SEM images of the collected particulates. The rainfall data from Miami International Airport showed that 8.6 cm of rain fell between the dates of July 4-14, 2010.

July 21, 2010 (site 1): The surface sample at site 1 on July 21, 2010 had more particles (396) with an area <10 μ^2 than any other site 1 sample, although the surface area distribution (Figure 46) and SEM images (Figure 60) show that particles of other size classes were present as well. The distribution in the bottom sample was quite different, and no particles were found in the <10 μ^2 size class. Turbidity was above average at this time (2.8 NTU), and chlorophyll was not elevated. The wind had been blowing moderately hard in the days preceding this sample. The elevated turbidity may be attributable to bottom resuspension in addition to biological activity.

August 2010 (sites 1, 2, and 3): From August 8-10, 2010, 7.5 cm of rain fell at Miami International Airport. On about August 14, 2010, the chlorophyll data show an increase that suggests the beginning of a bloom. The August 17, 2010 images from sites 2 and 3 all show a high number of centric diatoms. In one case, an image revealed what appears to be a copepod containing a large dinoflagellate ingested by the copepod (Figure 61). Particulate numbers (MPL) are similar for the surface and bottom at sites 2 and 3 (site 2 = 0.26 and 0.37; site 3 = 0.31 and 0.29, respectively). The chlorophyll signal suggests that these samples were taken just before the peak of the bloom. Elevated turbidity levels mirror the chlorophyll signal and suggest that these diatoms were a principal driver of turbidity levels during this period.

Site 1 on August 19, 2010 was dominated by centric diatoms (*Chaetoceras* sp., Figure 62). Turbidity levels were well above the baseline during this period, and there was a distinct chlorophyll signal associated with this event. The number of particles/liter (MPL) in the surface and bottom water was 90,000 and 110,000, respectively. The mean particle surface area at the bottom was significantly larger (487 μ^2) compared to the surface sample (181 μ^2). The comparison of surface
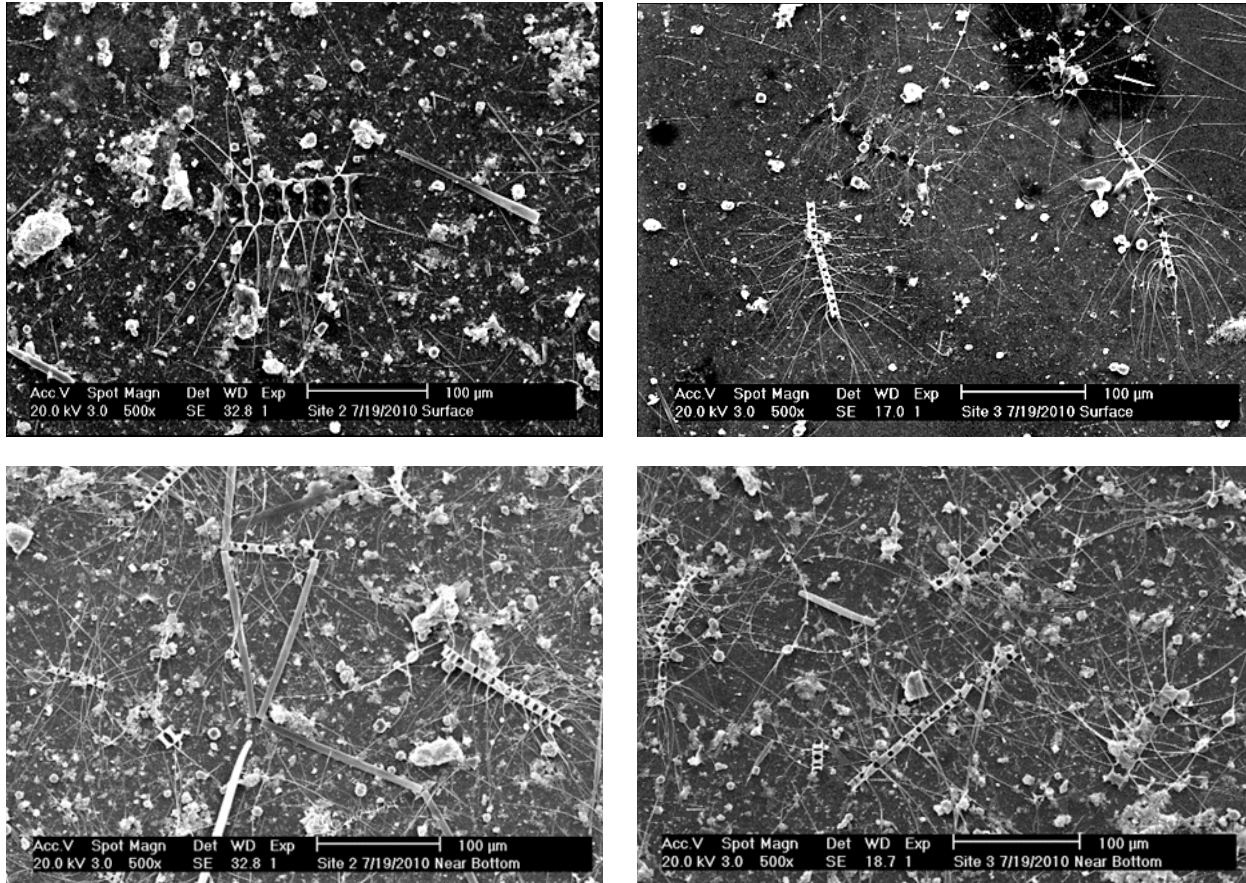
Figure 59. Surface and bottom samples from sites 2 and 3 on July 19, 2010. This sample was likely taken near the end of a diatom bloom.
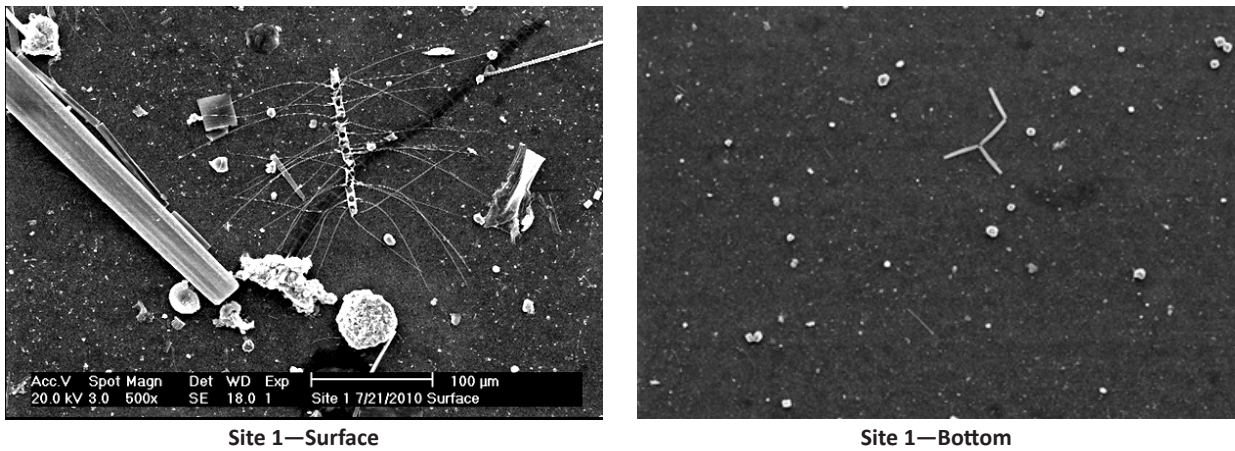
Site 1—Surface	Site 1—Bottom

Figure 60. Images of surface and bottom samples at site 1 on July 21, 2010. Note the very small particulates.

Figure 61. Images of surface and bottom samples at sites 2 and 3 on August 17, 2010. Note the abundance of centric diatoms and a copepod containing an ingested dinoflagellate in the site 3 bottom image.

Figure 62. Images from site 1 on August 19, 2010.

Figure 63. Images from site 1 on October 8, 2010. The chlorophyll data suggest that this sample was collected at the end of a diatom bloom.

and bottom water samples indicates a shift from smaller to larger particulates, perhaps reflecting a large centric diatom population in the near bottom water (Figure 50).

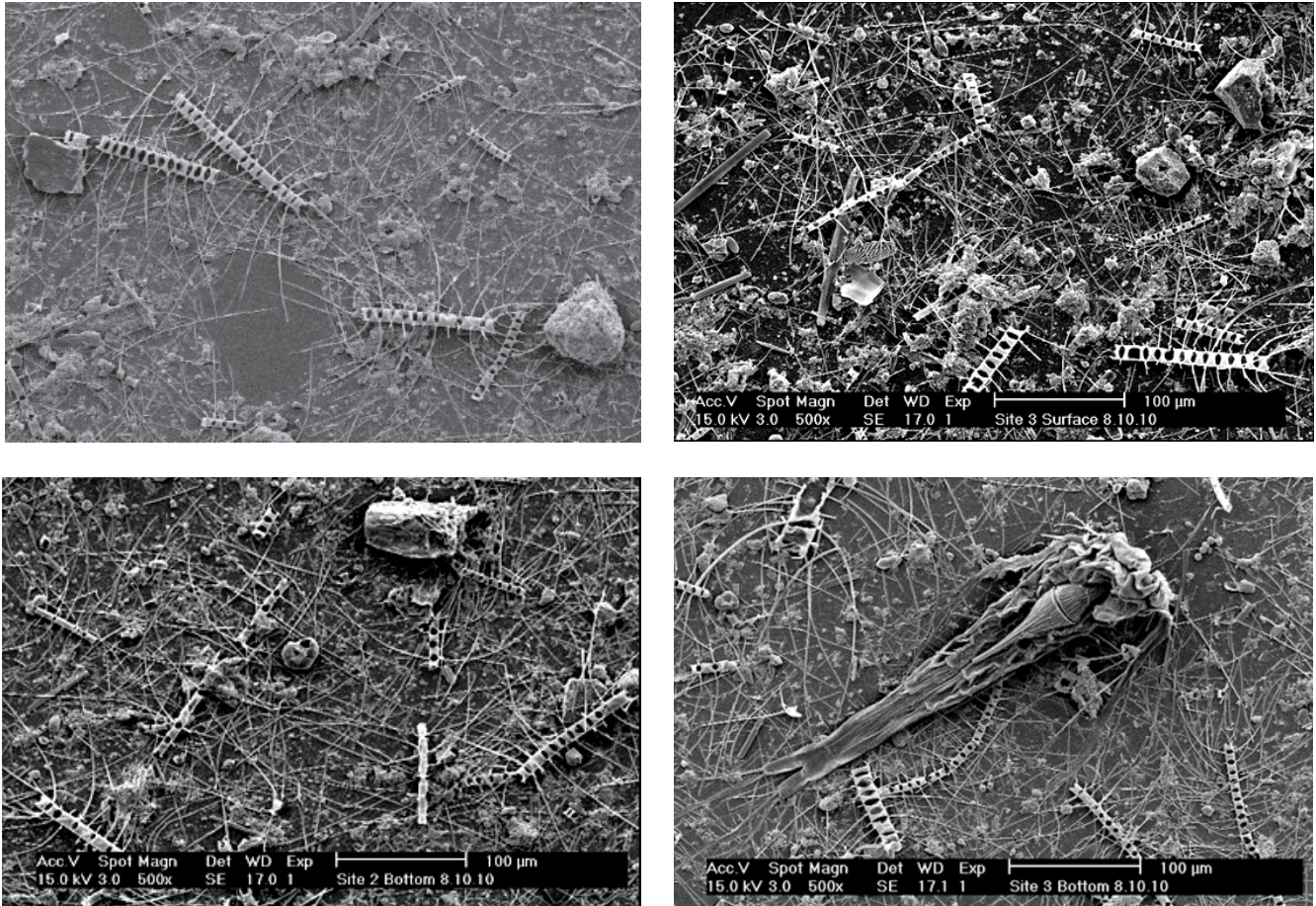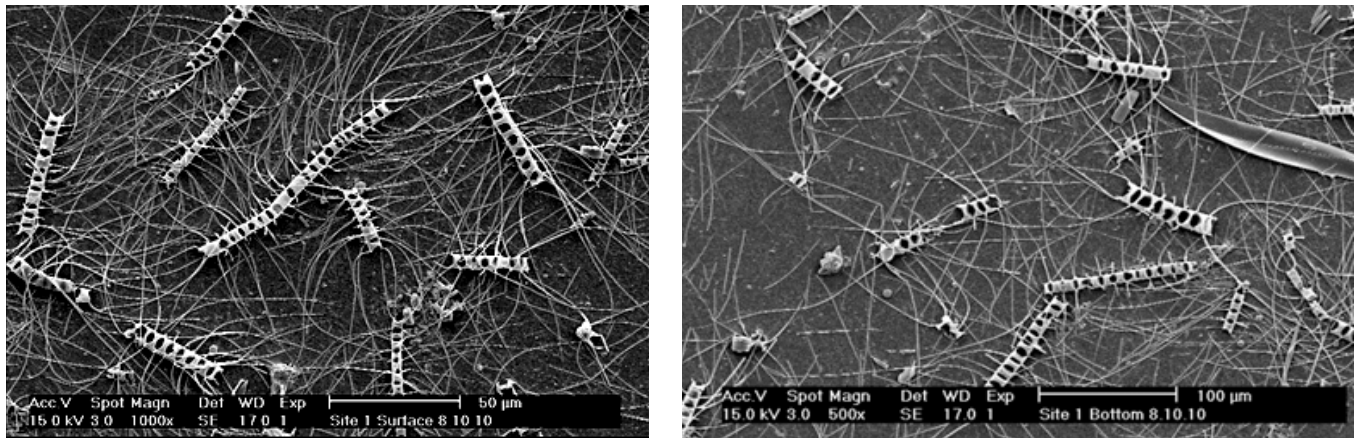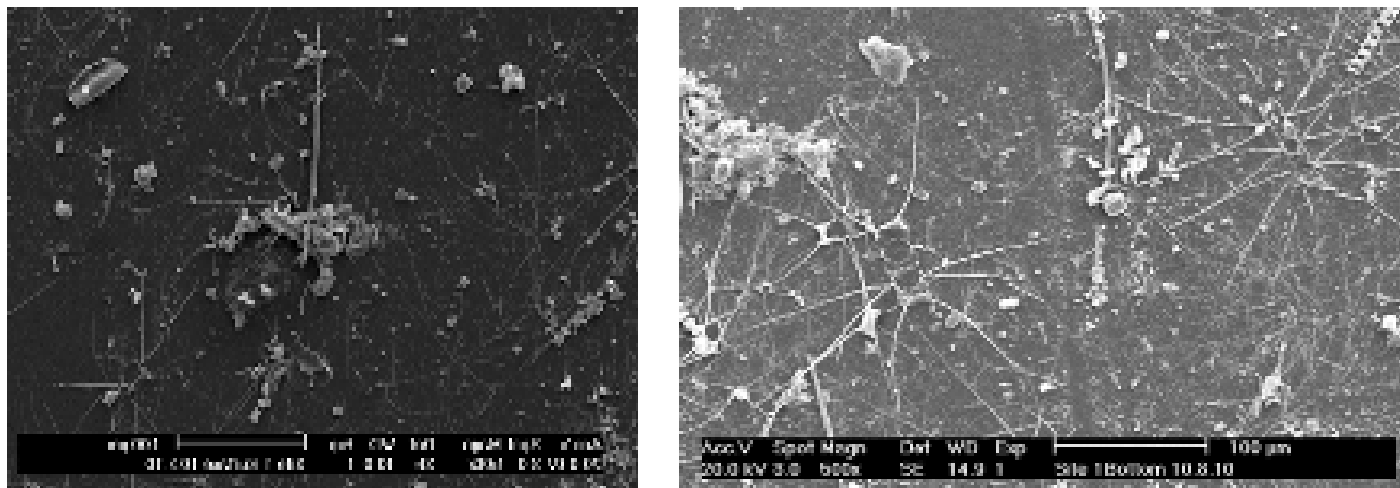***October 2010 (site 1):*** The chlorophyll data and degraded condition of the diatoms seen in the SEM images (Figure 63) suggest that the October 8, 2010 site 1 collection captured the end of a bloom of centric diatoms. The number of particles (MPL) for the surface and bottom was similar at 150,000 and 140,000, respectively. However, the mean particle area is different (142 μ^2 and 412 μ^2, respectively). This can also be seen in the particle area distributions in which there was half the number of particles of an area greater than 500 μ^2 at the surface compared to that area class at the bottom. Particulate characterization estimates found that 18% of the surface sample was comprised of centric diatoms and 42% of the surface sample was comprised of centric fragments.

November 2010 (sites 2 and 3): Turbidity levels were elevated at sites 2 and 3 during the November 1, 2010 and November 22, 2010 sample collection. Site 2, in particular, exhibited some of the highest turbidity levels of the record. Chlorophyll levels were not particularly elevated during this period (Figures 44, 45, and 57). The particle size distributions (Figures 47 and 48) showed that the particles in the 2050 μ^2 class were elevated, with the November 22, 2010 site 2 bottom sample having the largest number of particles in that size class (753) of any of the site 2 bottom samples. The relative percentage of fecal pellets identified at all three sites during this period was one of the highest observed at each of

the sites (Figure 53). At site 2, the relative percentage of fecal pellets had a linear correlation with turbidity of R = 0.67.

January-February 2011 (sites 1, 2, and 3): During the winter dry season, centric diatom concentration was quite low at all three sites. Chlorophyll-*a* levels remained low as well, suggesting that this was a period of low biological activity. Turbidity levels, however, were often elevated during this period with fragments of centric diatoms and fecal pellets comprising a significant fraction of the samples (Figures 52 and 54).

One site 3 surface sample, identified as the "bridge sample," was collected from the old Rickenbacker Causeway Bridge on February 25, 2011. The collection of this sample was motivated by the visual observation that the water was particularly turbid that day. A location on the bridge closest to site 3 near the surface was selected to collect a surface sample. The bridge sample contains the greatest number of particles of any sample collected during the study (1,220,000 particles per liter). It was taken on a windy day with waves present. The source of turbidity is thought to be resuspension, and there are no associated elevated chlorophyll levels. The particle area distributions indicate the majority of the particles are in the 20-50 μ^2 class. It should be remembered that this sample was taken at the bridge and not at site 3, although they are in proximity. The SEM images (Figure 64) show fecal pellets, fecal fragments, and centric fragments comprising 24%, 40%, and 36% of the particles identified in this sample, respectively.
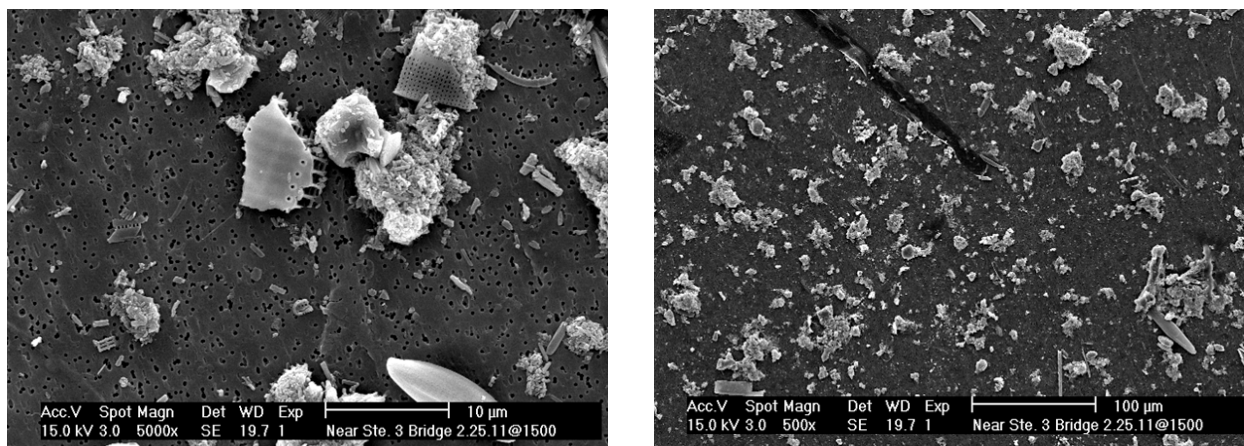
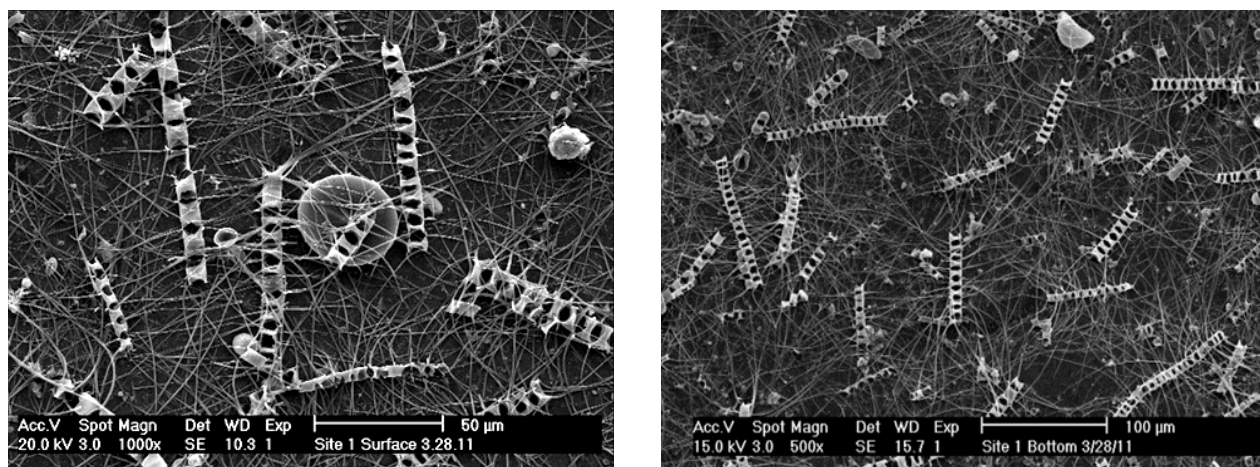**Figure 64.** Images of Rickenbacker Causeway bridge sample of February 25, 2011.

Figure 65. Images of site 1 surface and bottom samples collected on March 28, 2011 during a centric diatom bloom of *Chaetoceras* sp.

March-April 2011 (Beginning of the rainy season): In the latter part of March 2011, chlorophyll levels began to increase at all three sites. Large blooms of centric diatoms then developed and evolved at all the study sites. At site 1, chlorophyll-*a* values reached a maximum on April 1, 2011. Concurrent with the increase in chlorophyll was an increase in turbidity. The peak turbidity signal occurred later in the data record on April 5, 2011 and is associated with a secondary peak in the chlorophyll (Figure 28). During this period, turbidity levels were quite variable, typically elevated 3-4 NTU above the yearly mean value.

The March 28, 2011 site 1 sample contained a large number of centric diatoms in the surface and bottom water samples with *Chaetoceras* sp. present (Figures 51 and 65). The mean

area of particulates in the surface and bottom water was 123 μ^2 and 110 μ^2, respectively, and the number of particulates in surface and bottom water samples was 500,000 and 520,000 particles per liter, respectively (Figure 43). The particle size distributions in both the surface and bottom water for the March 28, 2011 sampling exhibited a shift to larger particles from the previous sampling (Figure 46).

The chlorophyll and turbidity data (Figure 43) suggest that the April 18, 2011 site 1 sample was collected near the end of a secondary peak in the bloom. The mean particle area at the surface and bottom is similar (46 μ^2 and 49 μ^2, respectively) (Figure 43) and is significantly smaller than particulates recovered on March 28, 2011. The smaller centric diatom *Bacteriostrum* sp. replaced *Chaetoceras* sp. as
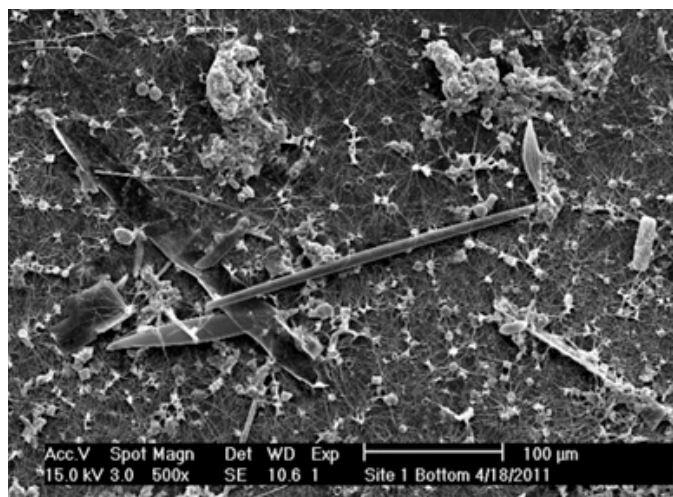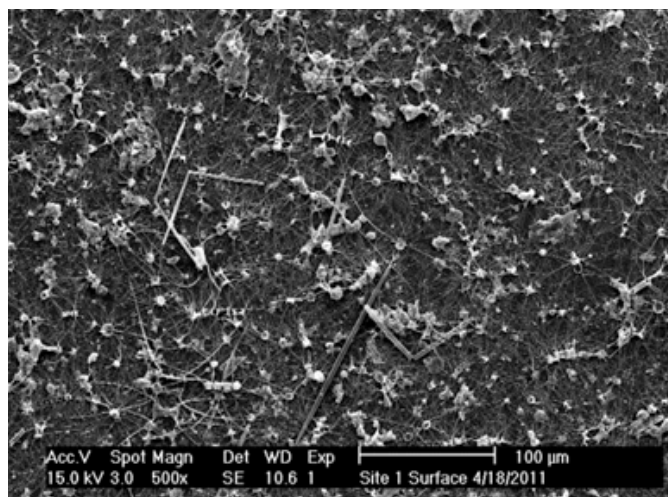
Figure 66. Images of surface and bottom samples at site 1 collected on April 18, 2011. The phytoplankton population is dominated by the centric diatom *Bacteriostrum* sp.
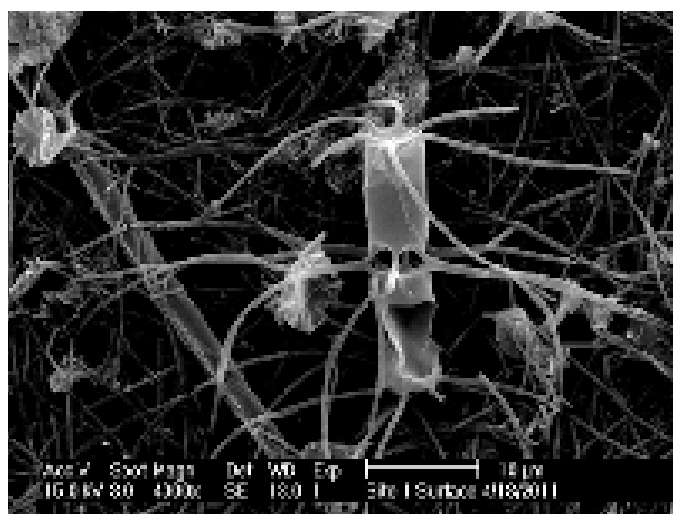

Figure 67A. High magnification view of *Bacteriostru*m sp.
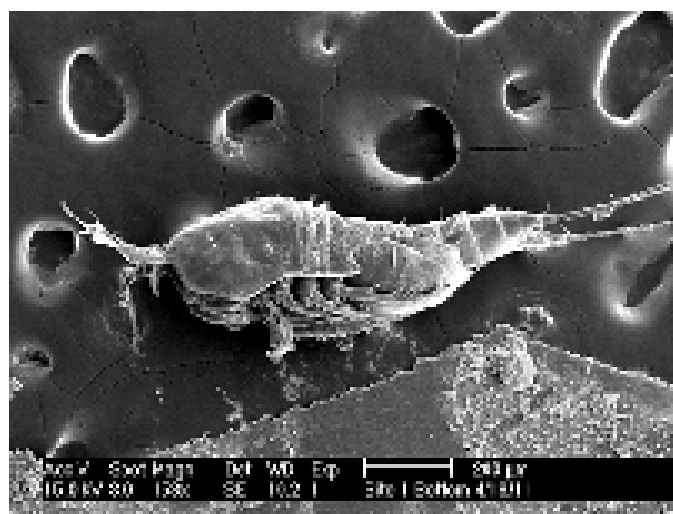
Figure 67B. Copepod collected in the April 2011 sampling.

the dominant species (Figure 66). The number of particulates in the surface and bottom water was the highest seen in the site 1 data set (1,260,000 and 1,240,000 per liter, respectively). Particle size data (Figure 46) indicate particles were in the 10-20 μ^2 and 20-50 μ^2 area classes, as well as a large number of particles in the 100-200 μ^2 area class in the bottom sample (411 particles). This is the highest number of particles seen in that area size class for the site 1 data set and is likely a reflection of the contribution of *Bacteriostrum* sp. centric diatoms (Figure 67A).

At sites 2 and 3, the April 4, 2011 and April 25, 2011 samples exhibited high concentrations of centric diatoms (Figures 68 and 69). The chlorophyll-*a* and turbidity data from site 2 (Figure 44) suggest that the April 4, 2011 sample was taken near a peak in this bloom and that the April 25, 2011 sample may have occurred at some time after a secondary peak. This is further supported by the apparent condition of the diatoms captured in the samples. In the April 4, 2011 sample, the diatoms are relatively intact. The diatoms in the April 25, 2011 sample exhibit missing setae

Figure 68. Images of surface and bottom samples from sites 2 and 3 collected on April 4, 2011.
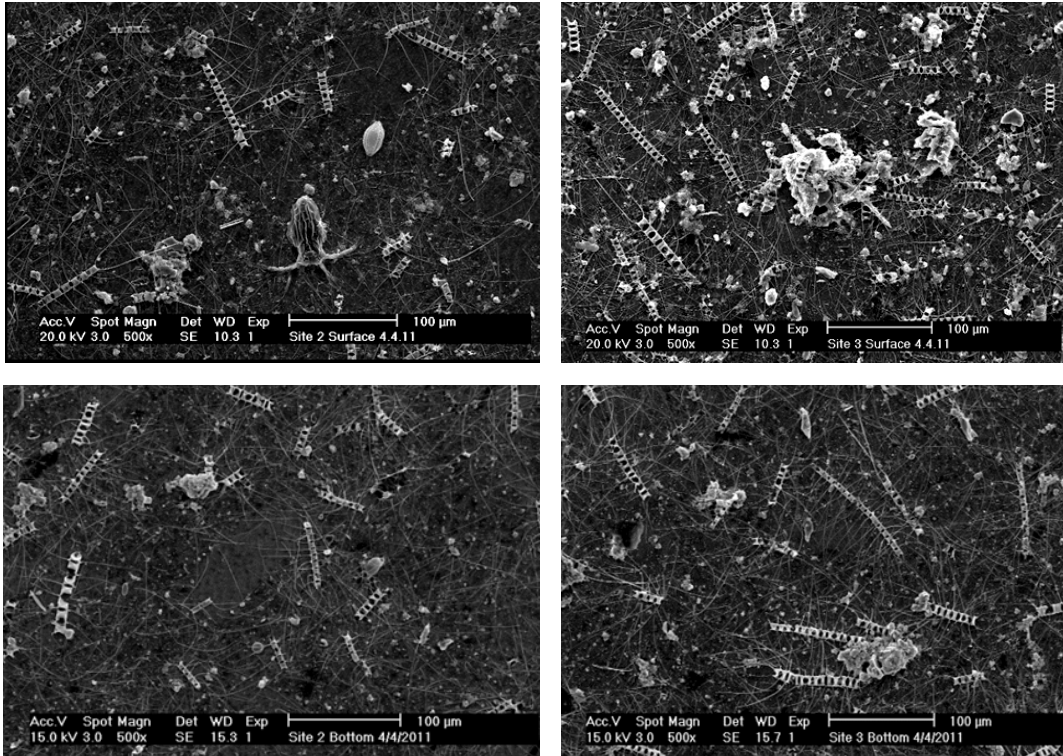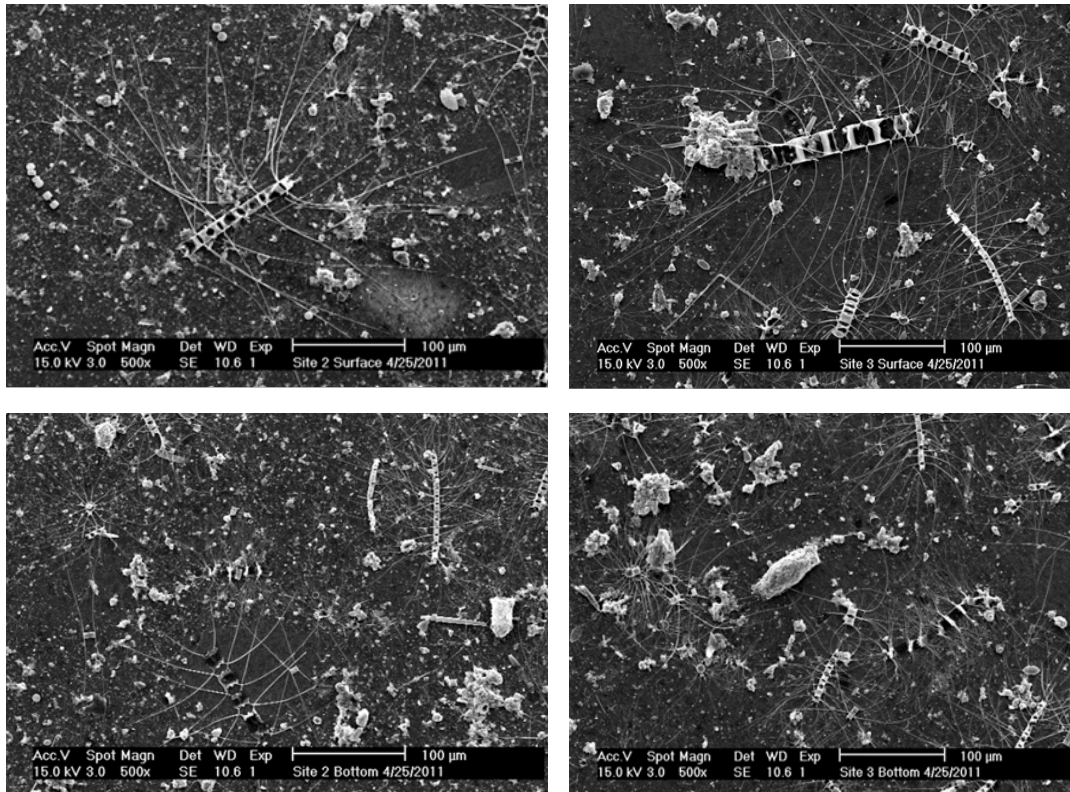

Figure 69. Images of surface and bottom samples at sites 2 and 3 collected on April 25, 2011.

and other signs of degradation, suggesting that these diatoms were dead when collected.

3.9.3 SEM and TSS

As was observed with turbidity, elevated levels of TSS were often associated with blooms of diatoms. At site 1, the linear correlation between TSS and the relative abundance of centric diatoms in the bottom samples was R = 0.74. The correlation of TSS in the bottom samples with chlorophyll-*a* from discrete water samples was R = 0.91. At site 1, all of the observed peaks in TSS were associated with peaks in chlorophyll (Figure 70). During these events, whole or fragments of centric diatoms were observed in the SEM images (Figure 71). During the large diatom bloom observed in the March 28, 2011 and April 18, 2011 samples (Figures 65, 66, and 71), TSS concentrations at the surface and bottom at site 1 were the largest observed in the site 1 data. These concentrations are significantly above the mean values at the surface and bottom (0.95 and 1.03, respectively).

At sites 2 and 3, the relationship between diatom blooms and TSS levels was also evident (Figures 72 and 73). Chlorophyll and bottom TSS samples were correlated at sites 2 and 3 (R = 0.64 and R = 0.72, respectively). Chlorophyll levels were also correlated to the relative abundance of centric diatoms at sites 2 and 3 (R = 0.72 and R = 0.78, respectively). At sites 2 and 3 during periods when blooms were not occurring, excursions in the TSS levels were associated with an abundance of fecal pellets, centric fragments, and fecal fragments (Figures 52 and 54). On February 25, 2011, Bay waters were observed to be particularly turbid. Strong winds and the presence of waves were also observed. A sample was collected near the surface from the old Rickenbacker Causeway Bridge at the location closest to site 3. SEM analysis showed this sample to contain a significant fraction of fecal fragments, centric diatoms, and centric diatom fragments (39.6%, 35.5%, and 23.7%, respectively). For this sample, the TSS values were the highest seen during this study (4.7 mg/l). The particle loading was also the highest recorded at site 3 (1.22 million particles per liter). No intact diatoms were seen in the SEM images, and chlorophyll levels were not elevated (Figure 64). When controlling for centric diatoms and centric fragments, the partial correlation of fecal pellets with surface TSS at sites 1-3 was 0.55, 0.58, and 0.64, respectively.

3.9.4 SEM Conclusions

It is apparent from this analysis that the diatom populations at the study sites contributed significantly to the turbidity and TSS levels measured. At site 1, all the major periods of elevated turbidity and TSS were associated with an increase in centric diatom populations. At sites 2 and 3, there were certainly periods where elevated levels of turbidity and TSS could be associated with diatom population dynamics, although there were also elevated periods not attributable to living diatoms.

3.10 Microbiological Analysis

Water samples were collected on many of the site visits to assess the concentrations of several microbial species. Over the course of the study, nine samples were collected at site 1, seven samples were collected and site 2, and seven samples were collected at site 3. *Enterococci* are a fecal indicator bacteria used as a marker for human sewage and fecal contamination of fresh and marine waters. Current regulatory limits for public health are set at 104 colony-forming units (CFU)/100 ml for a single grab sample or 35 CFUs/100 ml as a geometric mean for serial samples. *S. aureus* is typically a human skin pathogen, which may be spread and acquired through physical contact. Its presence in marine waters may be associated with bather shedding during swimming or other recreational activities and with contamination from untreated shower or other "gray" waters. Currently, there are regulatory standards or public health recommendations for *S. aureus* and methillin-resistant *S. aureas* (MRSA) in coastal marine waters. None of the *Enterococci* mEI plates for the three study sites ever exceeded 5 CFUs/100 ml, well below the regulatory limits. Additionally, no *S. aureus*, either methicillin-sensitive *S. aureus* or MRSA, were cultured from any of the samples.

3.11 Light Attenuation

Light attenuation (K_t) in the study region was remarkably consistent both temporally and spatially (Figure 74), ranging from 0.220 to 0.809. These values are considerably lower than typically observed in western Florida Bay (Kelble *et al.*, 2005); however, the depths of these stations are greater than those in Florida Bay. Equation 1 (section 2.7) was solved to determine the K_t value that would result in 10% and 15.4%
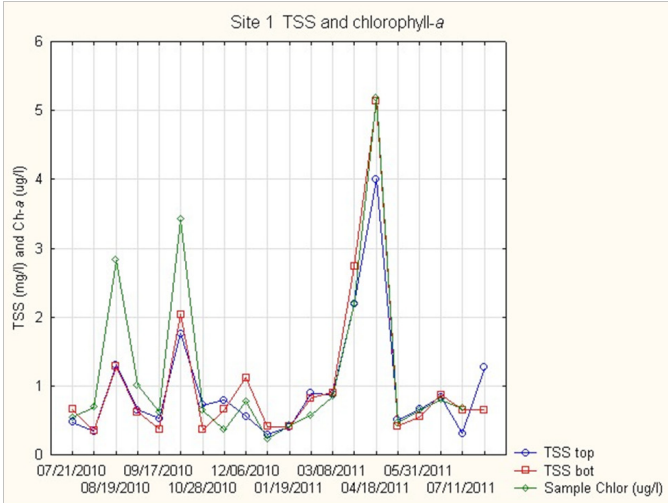
Figure 70. TSS and chlorophyll-*a* from water samples at site 1.
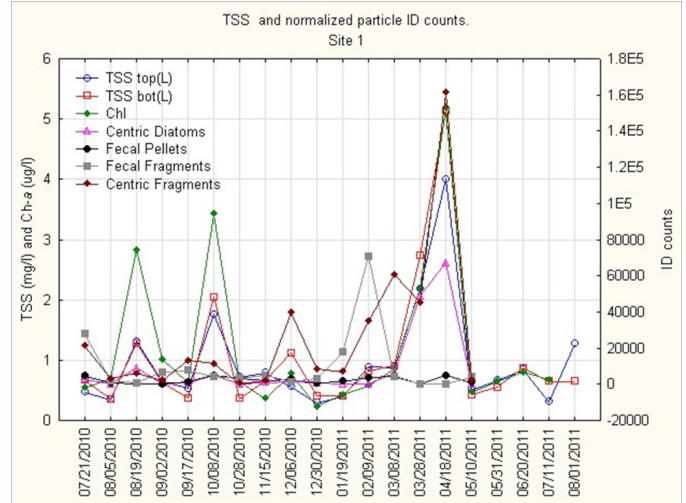

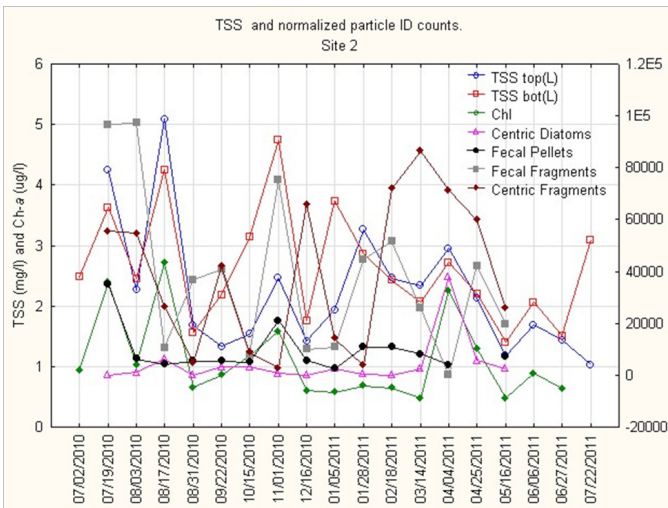**Figure 71.** TSS and SEM particle analysis from water samples at site 1.

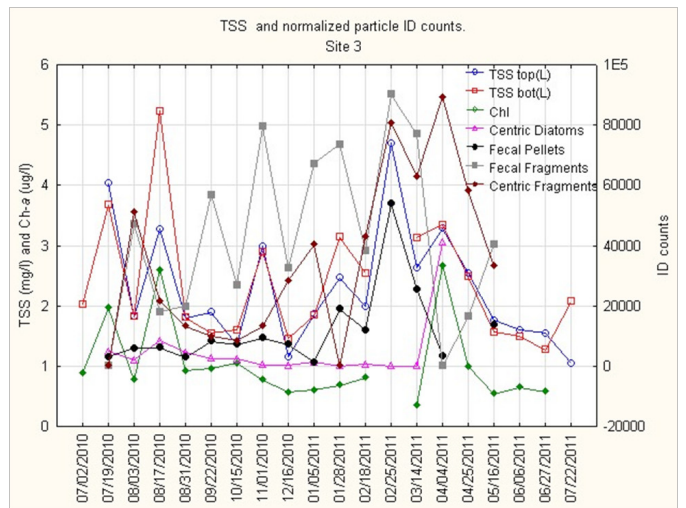**Figure 72.** TSS and SEM particle analysis from water samples at site 2.

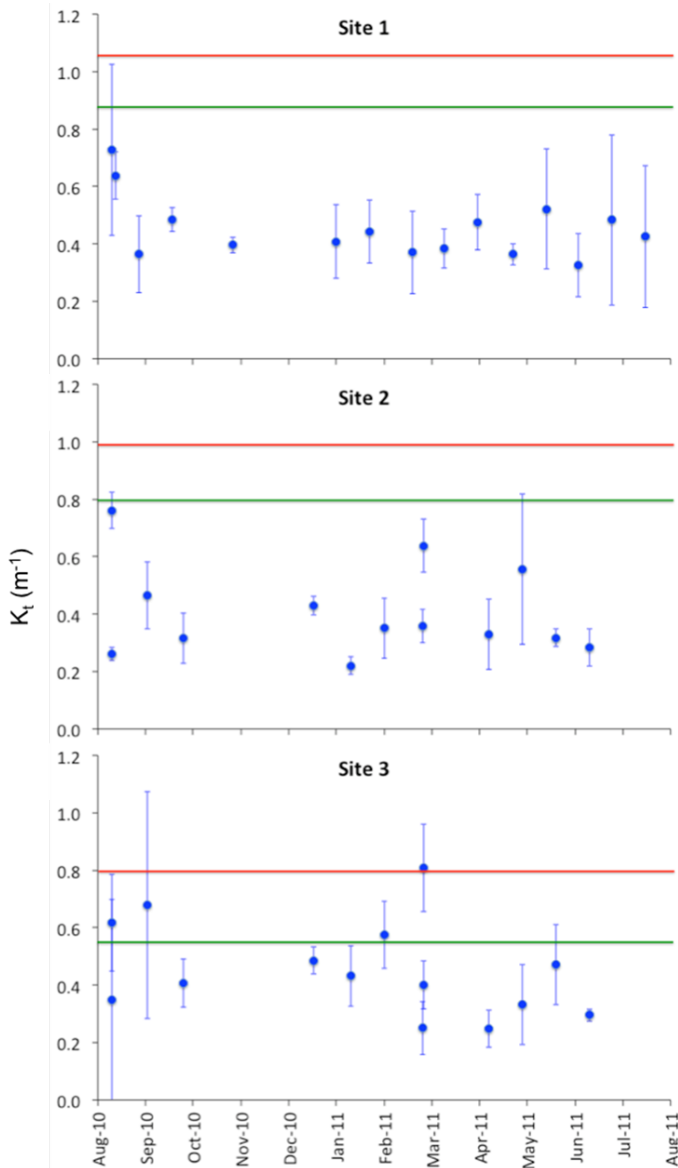**Figure 73.** TSS and SEM particle analysis from water samples at site 3.

Figure 74. The light attenuation coefficient, K_t, for all three study sites. The green and red lines indicate the K_t value above which seagrass would be light limited. The red line is specifically for *Thalassia testudinum,* and the green line is based on a worldwide review of all seagrass species.

of the surface irradiance reaching the bottom to examine the potential for light limitation of seagrass beds under current conditions. K_t values above the 15.4% threshold (shown in green in Figure 74) would be light limiting for the majority of seagrass species, as determined by a review of global seagrass data (Duarte, 1991). K_t values above the 10% threshold (shown in red in Figure 74) would be light limiting for *Thalassia testudinum*, a dominant seagrass species in

south Florida (Zieman *et al.*, 1999). The data suggest that sites 1 and 2 consistently had K_t values below both thresholds, suggesting seagrass in these areas was not subject to light limitation (Figure 74). However, site 3 had intermittent periods where the more protective 15.4% threshold was exceeded, suggesting seagrass in this area is subject to intermittent light limitation. This is likely a contributing factor as to why seagrass was sparsest at this location.

It is important to note that K_t values at all three locations were near these thresholds despite very low turbidity values. This suggests that care must be taken to ensure increases in turbidity are not large enough to push any of these sites over the thresholds for extended periods and potentially cause seagrass senescence due to a lack of sufficient light at the benthos.

3.12 Photographic Images

The images taken from the vantage point of the Four Seasons Hotel in downtown Miami provide the opportunity to compare the visual appearance of the sites 2-3 basin with data from the bottom-mounted instruments and to identify sources of turbidity.

The large turbidity signal associated with the strong south winds presented in Figure 25 was captured in the photographic images from April 5, 2011 at 12:16 and 14:05 Eastern Daylight Time (EDT). The wind streaks from the strong wind were seen in the photographs, as well as the resultant turbid water (Figure 75). Later in the day after the winds had subsided, a rain event occurred in the area. Photographs show a plume of water (possibly from the Miami River) appearing to emanate from the shipping channel and the Intracoastal Waterway (Figure 76). The bottom-mounted instrument data record was examined for evidence of this water, but none was found. This would be consistent with fresher, less dense rainwater occupying the surface of the water column but not present at the depth of the instruments. Vessels passing through the area were seen to cause plumes of turbidity that were visible on the images for several hours (Figure 77). The Miami Marine Stadium basin was often seen to be visibly more turbid than surrounding water, and this "whiter" water was seen to exit the basin and be advected towards the site 2 area (Figure 78).

Figure 75. Two images from April 5, 2011 at 12:16 (top) and 14:06 (bottom) EDT showing the development of a significant turbidity plume (bottom image) after the occurrence of a strong south wind. Note the wind streaks present in the top image.

Figure 76. Development of a plume after a strong rain on April 5, 2011. Top image is at 18:11 EDT, and the bottom image is at 19:06 EDT. Arrows indicate the expansion of the plume.
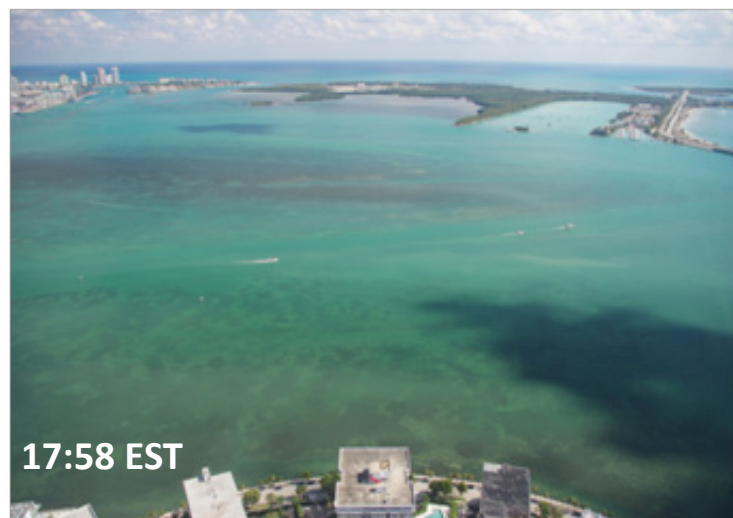
Figure 77. Three images from January 15, 2011 showing a turbidity plume generated by a vessel. The plume was visible for nearly two hours.

Figure 78. Two images from January 2011 that show the development of a plume of turbid water in the Miami Marine Stadium basin (top) which then moved north (bottom).

3.13 Acoustics

3.13.1 Bottom-Mounted 2 MHz Profilers

The mounting structures that held the acoustic Doppler current profilers (ADCPs) were constructed so that the first measurement bin of the profiler would coincide with the depth of the turbidity sensor. The bottom TSS measurements were also taken at this depth. The ADCPs operated at a frequency of 2 MHz. If the speed of sound is taken to be 1500 m/s, the wavelength at this frequency is 0.00075 m. The optimal backscattering occurs when $ka \geq 1$, where k is the wavenumber and a is the radius of the particle being scattered (Clay and Medwin, 1977). At 2 Mkz with a sound speed of 1500 m/s, the particle radius for which $ka = 1$ is 0.199 mm.

Previous studies have shown that the logarithm of acoustic backscatter intensity from Doppler profilers can be proportional to the logarithm of the turbidity or TSS levels present in the water column (Stamates, 2002). The acoustic backscatter data from the bottom-mounted instruments were examined for correlation with the logarithm of the turbidity and TSS measurements made during the study. The correlation between the acoustic backscatter and the logarithm of turbidity at sites 1, 2, and 3 was $R = 0.23$, $R = 0.40$, and $R = 0.34$, respectively. The correlation between the acoustic backscatter and the logarithm of TSS at sites 1, 2, and 3 was $R = 0.46$, $R = 0.59$, and $R = 0.78$, respectively. Changes in the distribution of particle sizes during the study period (possibly attributable to the changing abundances and species of phytoplankton) likely inhibited the development of a more robust relationship between the acoustical backscatter and the TSS and turbidity.

3.13.2 Acoustical Data from the Small Boat Transects

During the small boat transects, a 1200 kHz RD Instruments ADCP was operated to measure the backscatter return from the water column. These data are presented in section 3.14 to help visualize the relative concentrations of suspended materials in the water column.

3.14 Small Boat Transects

Attempts to calibrate the turbidity, CDOM, and chlorophyll-*a* data from the small boat flow-through system were unsuccessful. Although this severely limits the usefulness of the data, the trends shown by the raw values do give some insight into the relative values of these parameters at different locations in the study area. These data are presented here without units.

Transect example 1—March 15, 2011 (16:43-17:30 UT): During this transect, the boat traveled from site 3 westward to the end of the Powell Bridge and then north along the Intracoastal Waterway to the mouth of the Miami River. The tide was beginning to rise, and the Miami River was flooding. The path of the vessel is given in Figure 79, the acoustic backscatter from the ADCP is given in Figure 80, and the data from the flow-through system are given in Figure 81. Moving from site 3 (point A) to point B near the bridge, turbidity rose slightly, as did salinity, and chlorophyll-*a* values decreased. As the boat transected westward along the north side of the Powell Bridge (points B-C), CDOM levels rose significantly, turbidity levels fell significantly, and salinity was seen to drop from near 36 ppt at point B to 34.7 ppt at point C. This suggests that the water on the western side of the basin may be of a somewhat different character than water on the eastern side of the bridge. This finding is consistent with the observation that water from the south side Virginia Key is transported along the east side of the bridge during an ebb tide.

Along the west end of the bridge (before point C), the water becomes deeper and the chlorophyll-*a* levels rise. As the vessel approached point D, chlorophyll-*a* levels rose significantly and then fell as the vessel proceeded north to the Miami River. This may be due to the effects of the Intracoastal Waterway or Miami River water, which are seen in the photographic images to be transported along the eastern side of the basin during ebb tide (which had just ended). As the vessel transected north along the Intracoastal Waterway (points C-F), turbidity levels rose somewhat, making small-step increases as the boat passed point E.

Transect example 2—July 12, 2011 (15:40-16:25 UT): During this transect, the vessel traveled eastward from the mouth of the Miami River to the confluence of Fisherman's Channel and Government Cut. The tide was approaching slack low, and the Miami River outflow was near its maximum. The path of the vessel is given in Figure 82, the acoustic backscatter from the ADCP is given in Figure 83, and the data from the flow-through system are given in Figure 84. There was a steady decrease in chlorophyll-*a* and CDOM and an increase in salinity and turbidity as the boat

Figure 79. Transect path of March 15, 2011 (16:43-17:50 UT).

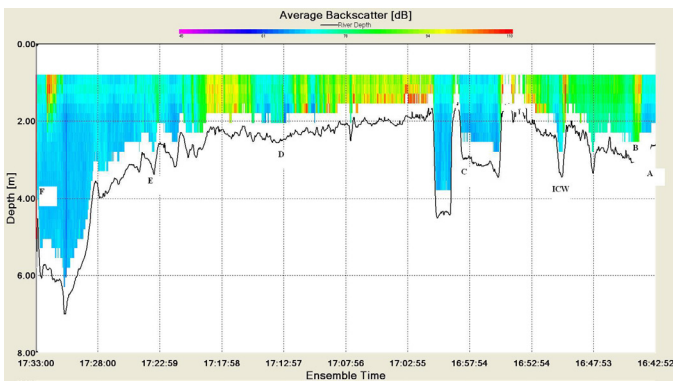**Figure 82.** Transect path of July 12, 2011 (15:40-16:25 UT).

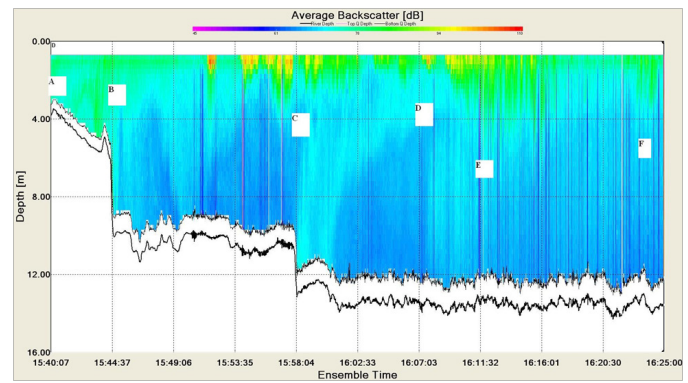**Figure 80.** Acoustic backscatter transect for March 15, 2011 (16:43-17:50 UT).

Figure 83. Acoustic backscatter transect from July 12, 2011 (15:40-16:25 UT).
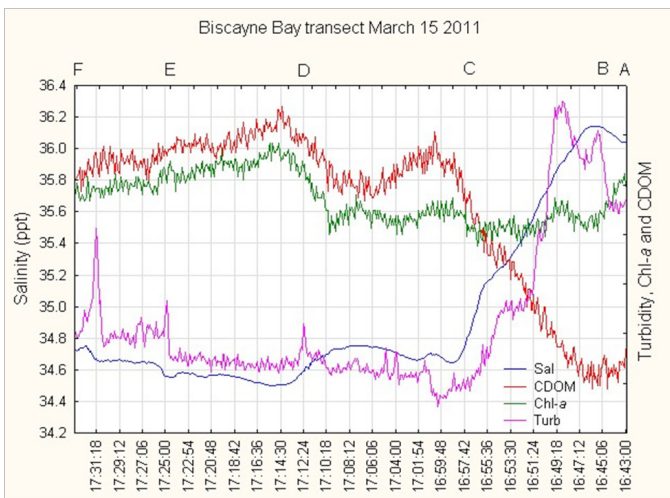

Figure 81. March 15, 2011 transect (16:43-17:30 UT). Salinity is in parts per thousand (ppt). Chlorophyll-*a,* CDOM, and turbidity are on an uncalibrated scale.
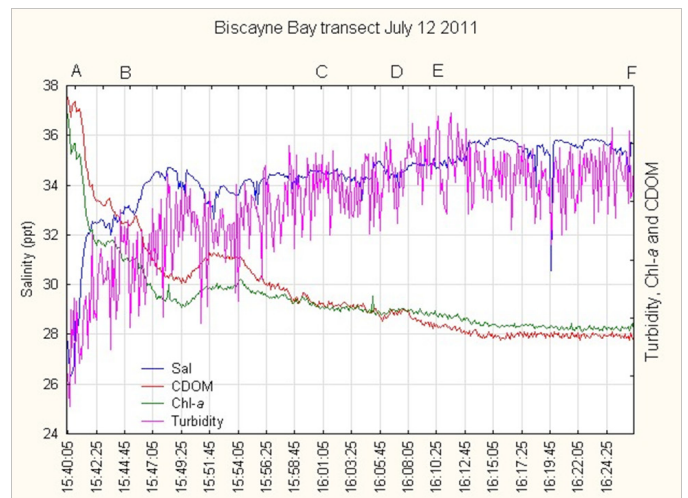

Figure 84. July 12, 2011 transect (15:40-16:25 UT). Salinity is in parts per thousand (ppt). Chlorophyll-*a,* CDOM, and turbidity are on an uncalibrated scale.

moved away from the Miami River. At point E where we left the turning basin, there was a small increase in salinity and drop in turbidity. Although the turbidity levels could not be determined with significant accuracy to warrant the display of the values, the turbidity levels near the mouth of the Miami River were estimated to be approximately 1 NTU. At point C, the turbidity levels had risen to approximately 3 NTU. The backscatter return suggests that there were larger concentrations of suspended materials at depth along the western side of the turning basin. Turbidity levels during this transect were at their highest levels at point E, and the backscatter plot indicates scatterers distributed down into the water column at this location.

Transect example 3—March 15, 2011 (18:26-18:57 UT):
This transect was from site 2 to site 3. The path of the vessel is given in Figure 85, the acoustic backscatter from the ADCP is given in Figure 86, and the data from the flow-through system are given in Figure 87. The tide was rising during this period and, therefore, flow was southwesterly across the transect path. Salinity increased as the vessel proceeded from site 2 to site 3, while CDOM and chlorophyll-*a* levels generally decreased. At point B, there was an increase in turbidity and chlorophyll-*a* with a decrease in CDOM. A possible explanation is that there is a channel that crosses the basin at this point which is significantly deeper than the surrounding area. This channel may be a conduit for water from the shallow, densely-vegetated area inside the Bill Sadowski Critical Wildlife Area that reaches the more central portions of the basin. Turbidity levels showed a distinct peak as the vessel passed point D, and backscatter levels were higher in the vicinity of points C, D, and E. This may be the effect of water exiting the Miami Marine Stadium basin. A photograph for a time near the end of this transect showed what appears to be bands of turbid water moving from north to south across the basin (Figure 88). These bands are seen in Figure 88, and the spikes in turbidity seen in Figure 87 illustrate the turbidity variability present in this basin. Although the absolute value of the turbidity taken during the transects was not determined, an estimate of the magnitude of the turbidity spikes seen in Figure 87 was made. In Figure 87 at 18:42:07 UT, a turbidity spike occurred. The magnitude of this spike over the levels that preceded it was estimated to be 0.3 NTU. An increase in turbidity was also seen at 18:47:15 UT. The magnitude of this increase was estimated to be 0.15 NTU.

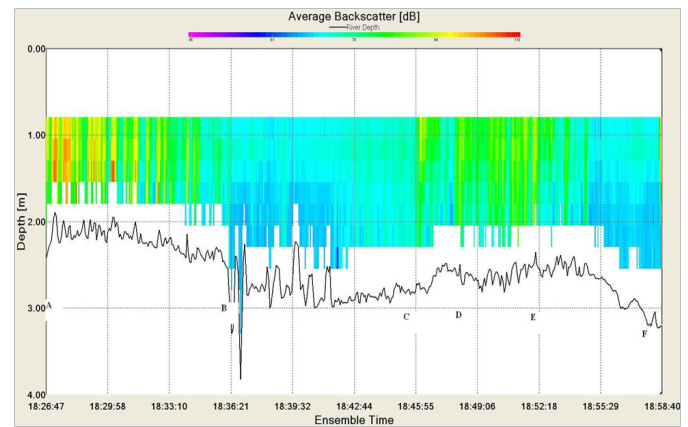**Figure 85.** Transect path of March 15, 2011 (18:26-18:57 UT).

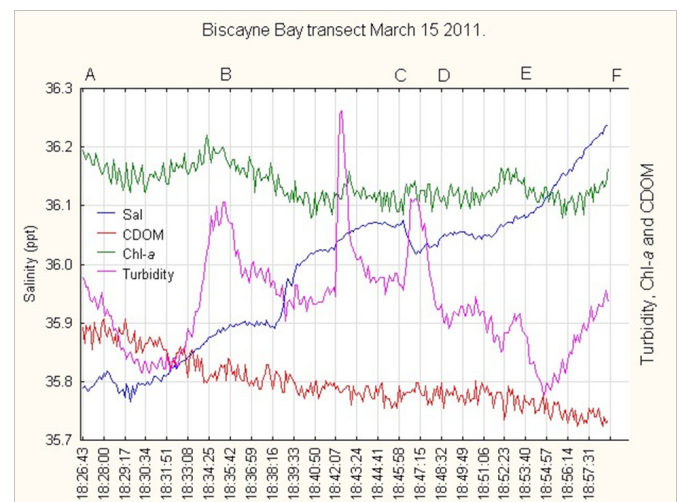**Figure 86**. Acoustic backscatter transect for March 15, 2011 (18:26-18:57 UT).

Figure 87. March 15, 2011 transect (18:26-18:57 UT). Salinity is in parts per thousand (ppt). Chlorophyll-*a,* CDOM, and turbidity are on an uncalibrated scale.

Figure 88. Image from March 15, 2011 (20:12 UT). Note the streaks of turbidity.

4. Summary

Mean turbidity levels at the three study sites over a one-year period were all less than 5 NTU. Site 1, which is located in a somewhat isolated basin, had mean turbidity levels less than 1 NTU. These results are consistent with previous observations of northern Biscayne Bay waters. Variability in the turbidity levels during this study was principally attributed to phytoplankton populations and to meteorological events.

Phytoplankton blooms were observed to elevate turbidity levels for periods as long as a month. Chlorophyll-*a* concentrations were well correlated to phytoplankton concentrations and could possibly be used as an indicator of elevated turbidity levels due to high phytoplankton concentrations. Meteorological events during the study period were observed to elevate turbidity levels for periods lasting, typically, less than a day.

Photographic images showed short-term elevations in apparent turbidity in the wake of vessels, and streaks of apparently turbid water are seen crossing the site 2-3 area in these images. These images show plumes of apparently turbid water exiting the Bill Sadowski Critical Wildlife Area and the Miami Marine Stadium basin. The images and data from the small boat transects suggest that spatially variable turbidity levels existed across the site 2-3 basin.

A correlation between TSS and turbidity at the study sites was examined and found to be reasonably robust. Light attenuation measurements indicate that benthic light levels at the study sites were typically above the value where seagrasses could become light limited but not by a large margin.

5. References

Boyer, J.N., C.R. Kelble, P.B. Ortner, and D.T. Rudnick, 2009: Phytoplankton bloom status: An indicator of water quality condition in the southern estuaries of Florida, USA. *Ecological Indicators,* 9s: s56-s67.

Brand, L.E., M.D. Gottfried, C.C. Baylon, and N.S. Romer, 1991: Spatial and temporal distribution of phytoplankton in Biscayne Bay, Florida. *Bulletin of Marine Science,* 49(1-2): 599-613.

Clay, C.S., and H. Medwin, 1977: *Acoustical Oceanography.* New York, John Wiley and Sons, 544 pp.

Davies-Colley, R.J., and D.G. Smith, 2001: Turbidity suspended sediment and water clarity: A review. *Journal of the American Water Resources Association*, 37:1085-1101 (doi:10.1111/j.1752-1688.2001.tb03624.x).

Duarte, C.M., 1991: Seagrass depth limits. *Aquatic Botany,* 40(4): 363-377.

Kelble, C.R, P.B. Ortner, G.L. Hitchcock, and J.N. Boyer, 2005: Attenuation of photosynthetically available radiation (PAR) in Florida Bay: Potential for light limitation of primary producers. *Estuaries,* 28(4):560-571.

Kirk, J.T.O., 1994: *Light and Photosynthesis in Aquatic Ecosystems.* Cambridge University Press, 509 pp.

Shoaf, W.T., and B.W. Lium, 1976: Improved extraction of chlorophyll a and b from algae using dimethyl sulfoxide. *Limnology and Oceanography,* 21(6):926-928.

Stamates, S.J., 2002: Predicting total suspended matter concentrations in the Chesapeake Bay estuary using a calibrated acoustic Doppler current profiler. M.S. thesis, University of Miami, 54 pp.

Tester, L.A., and K.A. Steidinger, 1979: Nearshore marine ecology at Hutchinson Island, Florida: 1971-1973. VII. Phytoplankton. Florida Marine Research Publication, 34:16-61.

Tomas, C.R., 1997: *Identifying Marine Phytoplankton.* Academic Press, 858 pp.

Turner Designs, 2012: Colored dissolved organic matter (CDOM) calibration procedures and performance data (available at http://www.turnerdesigns.com/t2/doc/appnotes/S-0081.pdf), 3 pp.

Van de Kreeke, J., and J.D. Wang, 1984: Hydrography of north Biscayne Bay. Part I: Results of field measurements. Report for DERM and Sea Grant. University of Miami, Rosenstiel School of Marine and Atmospheric Science, Miami, FL.

Wanless, H., D. Cottrell, R. Parkinson, and E. Burton, 1984: Sources and Circulation of Turbidity in Biscayne Bay, Florida. Final Report, Florida Sea Grant and Miami-Dade County, Miami, Florida.

Young, R.A., T. Clarke, R. Mann, and D.J.P Swift, 1981: Temporal variability of suspended particulate concentrations in New York Bight. *Journal of Sedimentology and Petrology,* 51: 293-306.

Zieman, J.C., J.W. Fourqurean, and T.A. Frankovich, 1999: Seagrass die-off in Florida Bay: Long-term trends in abundance and growth of turtle grass, *Thalassia testudinum. Estuaries,* 22: 460-470.